AN INVESTIGATION OF PULSED EDDY CURRENTS FOR THE DEVELOPMENT OF A PROFILE GAUGING SYSTEM SUITABLE FOR ALUMINIUM HOT ROLLING MILLS

Betty Kibirige

A thesis submitted to the Faculty of Engineering and the Built Environment, University of the Witwatersrand, Johannesburg, in fulfilment of the requirements for the degree of Doctor of Philosophy.

Johannesburg, July 2011

Declaration

I declare that this thesis is my own, unaided work, except where otherwise acknowledged. It is being submitted for the degree of Doctor of Philosophy to the University of the Witwatersrand, Johannesburg. It has not been submitted before for any degree or examination in any other university.

Signed this ___ day of __________ 20___

____

Betty Kibirige.

Abstract

This study investigates the Pulsed Eddy Current (PEC) technique, as an alternative method, to establish its performance in a profile gauging system for aluminium hot rolling mills. Radiation gauges are the popular choice for profile gauging. However, they present poor accuracy (±0.1%), are not safe, require frequent maintenance and are very expensive. A PEC system model, was developed using analytical methods in order to allow for specimen conditions that could not be easily emulated, to be investigated thus giving a complete assessment of the PEC system. The model was validated against experimental data. The coil probe and specimen were characterised as lumped resistance and inductance and the characterisation gave a good fit between simulated results and results from experiments and was therefore useful to the investigation. Results from experiments and simulations reveal that changes in specimen temperature show a point of crossing in the received signal agreeing with findings made by other researchers, for other parameters. Furthermore, results indicate that relative motion between a small probe and a massive specimen does not affect the signal at the probes and a quasi-static approximation was assumed for the model.

The developed characterisation of the aluminium specimen used in conjunction with the developed system model indicate that differences in thickness of up to 4 microns at the minimum nominal thickness of 2 mm required for the finishing mill could be gauged. The signal processing method described in the study indicates that at a crown and wedge definition of 0.2%, accuracies of ±0.04% were achieved, showing PEC to have better accuracy than radiation gauges. Temperature changes in the specimen were successfully eliminated from the profile measurement.This was achieved by using the relationship observed between the temperature point of crossing (TOC) and specimen thickness for different specimen temperatures. A method for harnessing profile measurements from the PEC signal was also developed. PEC system could therefore have potential in profile gauging systems for aluminiunm hot rolling mills.

Acknowledgements

The journey comes to an end. It has revealed a lot of interesting qualities about myself; some good while others not so good. In trying to understand the whole concept of a PhD, there has always been someone to make a simple statement that carries a well of meaning, and lo and behold, an understanding or a revelation. It has been made clearer to me through the whole process of this study that there are different levels of understanding the same subject; the ultimate being the point when one has understood it so well that they actually can add on to prior knowledge.

Profile gauging in hot rolling mills has taken me through this process. It all started at Hulett Aluminium in Pietermaritzburg, South Africa. I would like to thank them for allowing me to have a first hand glimpse into understanding the intricacies involved in profile gauging and control in aluminium hot rolling mills and also for their financial support. Thanks to Rodney Torr and Tim Hawkins for their assistance in helping me to obtain the literature needed on hot rolling mills and for the time given to make things that much more interesting.

In the process of investigating thickness gauging techniques, it dawned on me that x-rays were never going to give the accuracies required for the finishing gauge! Looking at the industrial environment; dusty and moist, some other technique had to be considered. Pulsed eddy currents, it had to be! This technique ignores the environment and engages with only the specimen. The question was, could it really work? The specimen is moving and its temperatures are changing; have pulsed eddy currents been used in these conditions before? Prof. Dubois of Kingston College Canada, thank you for the part you played in refining my understanding of Eddy Currents and their use in various applications especially in materials evaluation. The simple statement you made, *a specimen with changing temperatures would be an interesting addition*, set me on a quest to understand eddy currents.

Then I needed formers, winders and different copper wire gauges in small amounts. And for this I would like to acknowledge Kuthula Rewind based in Richards Bay, South Africa, for providing me with the various copper wire gauges that I needed for my experiments and for the readiness to assist whenever I needed some advice in the art of winding coils. To the science workshop at the University of Zululand, thank you for the support that was readily given for the various fittings I needed for my setup.

TAGAF Empangeni, you have always been ready to try out anythings! Thank you for the specimens you prepared for me with such dedication.

To friends, Sarah Waswa and her family, the moral support given to me whenever I needed to visit Gauteng, I really thank you. Olivia, your constant check on me has been a good catalyst for my progress. Alice, the bed in Pietermaritzburg and that constant morale booster given when ever needed, were always a welcome addition. Your words of encouragement, have been a gem throughout this study. I have just discovered that men think rather differently from us ladies. *Write up and finish*, this from my dear husband Abiaaza. Probably you are right.

To my children Joshua and Jemimah, whom I have watched grow during the course of this study, the advice you have both given has amazed me and it has become more mature as the years have progressed. *Mummy you only need to do what is required*; what better philosophy than that!

To my supervisor Prof. Gibbon, I would like to thank you for the support and mentorship given throughout the course of this work. The suggestions you have made for me to try out new things sometimes seemed insurmountable, but I stuck in there and I have done my best. Your final statement that, *you are not a student*, made me realise what it was all about. Thank you once again. It has been hard but worth it!

Not forgetting that inner voice that always spoke to me when faced with confusion. In the middle of the night during the course of the day and even when everything around me was noisy and boisterous; a voice that makes you notice reason where you least expect it. I would like to acknowledge that voice, which I know to be God's; it has guided me and brought different people in my path, so that this work may be brought to a completion.

Contents

List of Figures

List of Tables

Chapter 1

BACKGROUND

1.1 Introduction

This study describes an investigation of Pulsed Eddy Currents (PEC) toward the development of a profile gauging system for aluminium hot rolling mills. The main thrust of the work is the development of a method to extract information relevant to profile gauges from the PEC system eliminating environmental, physical, dynamic and material effects. The profile of a sheet is viewed as the measure of the variation in sheet thickness across the sheet width [2]. The profile of the sheet is created and set during the hot rolling process and cannot be readily altered during cold rolling [3]. Therefore, in order to control and achieve the standards required for flatness in subsequent mills, it is crucial to gauge profile accurately in the hot mill. In this chapter, a brief overview of a typical aluminium mill with an emphasis on conditions important to profile measurement is given. Important aspects of profile gauging are explored, described and discussed. Radiation gauges and other thickness probing techniques are also discussed to establish a background for the investigation of Pulsed Eddy Currents (PEC).

1.2 Overview of Aluminium Hot Rolling Mill Operation

Hulett Aluminium Hotline at Camps Drift in the province of KwaZulu-Natal in South Africa was used as a typical example of a hot rolling mill. Information on the mill was compiled by observation, interviews and consultation of manuals stored at the plant[3, 4, 5, 2, 6, 7, 8].

The mill consists of a Roughing Mill and a Finishing Mill [4]. Both mills have a drive side and an operator side. The drive side is connected to alternating current variable speed drives that can provide a maximum roll speed of 180 meters per minute (3 meters per second), while the operator side is free to allow the operators to access the mill. Both mills are four high stand reversing mills [4] with two work rolls that have a diameter of 930 mm and two back-up rolls that have a diameter of 1500 mm (figure 1.1). A force of up to 4500 ton can be applied to the rolls, processing an incoming ingot into flat sheets of a pre-specified thickness. An ingot having a maximum mass of 22620 kg, a

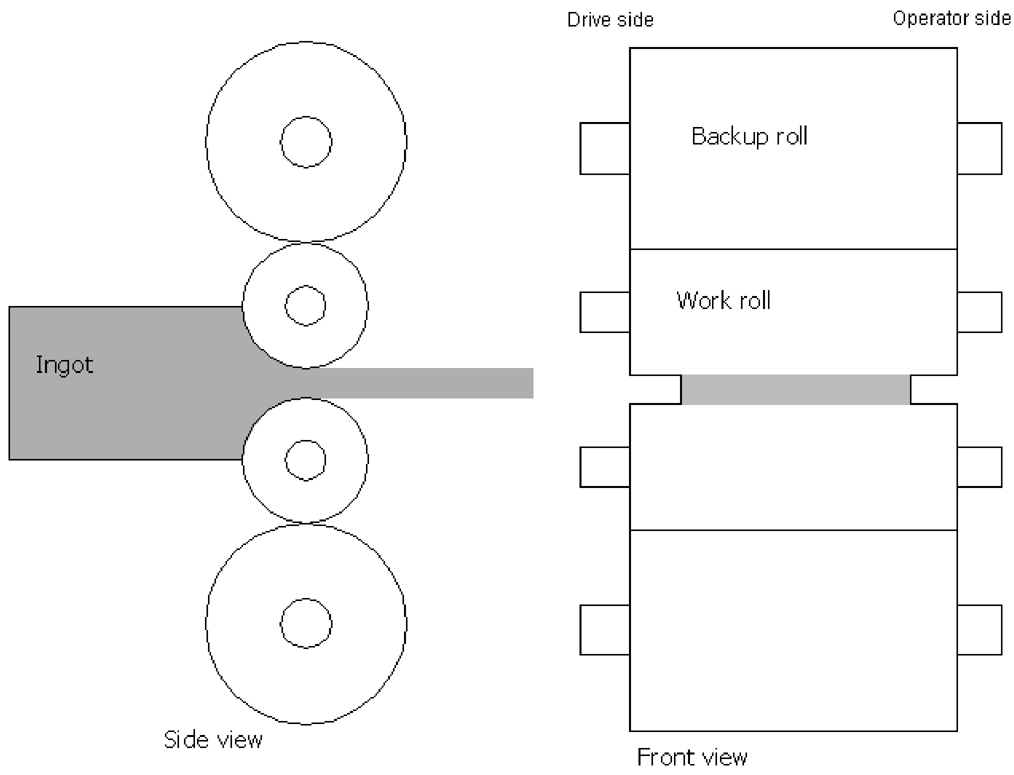

Figure 1.1: Four-high stand reversing mill.

length of 2700 mm to 6000 mm, a width of 900 mm to 2200 mm and a thickness of 460 mm to 630 mm, is heated to a temperature of approximately 560^{o}C. It is transported on rolls to the Roughing Mill, where the rolling process begins. The rolling mill does not have the luxury of running one alloy nor does it roll sheets of the same width. Typical sheet widths fall in the range of 850 mm to 2250 mm.

Model parameters for dynamic control are calculated and set, and a rolling schedule is drawn up for the required sheet thickness [4]. The initial rolling speed is slow ranging from 0.4 to 0.6 m/s and it increases to a higher steady state rolling speed that lies between 1.0 and 1.6 m/s. There is therefore a change in sheet velocity during any specified schedule. The aluminium ingot is rolled from a thickness of approximately 600 mm to a gauge approximately between 20 mm and 30 mm at the roughing mill. The transfer slab has a length of approximately 180 m. When the desired transfer gauge is reached, the aluminium slab is transferred to the Finishing Mill where further reduction is done to obtain a final gauge as thin as 2 mm. The finishing and the roughing mills use the same rolling principle. They have two coilers in order to accommodate the length of the sheet, which goes up to 1770 m. The finishing mill overwrites (changes) the profile of the roughing mill [3] and profile gauging should be precise at this stage.

1.3 Profile - Definitions and Measurement

As mentioned earlier, the profile of a sheet is defined as the measure of the variation in sheet thickness across the sheet width [2]. In a hot rolling mill, the profile of a sheet can be shaped by six major factors: tilt, roll bend, coolant sprays, rolling loads, mechanical camber and thermal crown [3, 4, 5]. The best required sheet profile results from a balance of all the above factors. To control the profile, a feed forward/feedback control technique which requires precise gauging of the profile is ideal and therefore, on line measurement of the profile is necessary for a feedback/feed forward control of the sheet profile.

Quality control requirements [2, 6] dictate that a simple means must be found to identify a small number of parameters which can be used for profile description. One common approach is to measure the thickness at three points across the sheet width [2]:

1. Sheet centre line, a thickness h_o (also coinciding with the mill centreline)
2. At nominal distance more than 100 mm from the drive edge, thickness h_e^+
3. and at nominal distance more than 100 mm from the operator edge, thickness h_e^-.

Profile is then characterised by two main features:

1. Wedge
2. Crown

1.3.1 Wedge

This is the amount of variation in thickness in a profile from one edge of the sheet to the other (see figure 1.2(a)). Wedge [3, 4], h_{wedge}, is expressed as a percentage of the centre line thickness, h_o, in equation 1.1.

$$h_{wedge} = \frac{(h_e^+ - h_e^-)100\%}{h_o} \tag{1.1}$$

If the wedge is more than 0.5% it is a concern [3]. High levels of wedge cause loose edges on the rolled sheet and as a result the system experiences tracking problems [3].

1.3.2 Crown

Crown [3, 5, 2] is the general term used to describe the amount of barrelling in a body such as a sheet profile or a work roll. If the thickness of the centre of the sheet is thicker or thinner than the average of the two edges, the sheet is said to have a positive crown (Figure 1.2(b) or a negative (Figure 1.2(c)) crown respectively. Crown is expressed as a percentage of the centerline thickness h_o [3, 4] as:

$$h_{crown} = \frac{[h_o - (h_e^+ + h_e^-)/2]100\%}{h_o} \tag{1.2}$$

A slight positive crown is the desirable crown but if it becomes excessive, it causes loose centres in the sheet [3]. Excessive negative crown will also cause loose edges subsequently leading to tracking difficulties. The sheet is deliberately rolled with a thicker centre, generally in the range 0.2% - 0.8% [3].

Consider the sheet at the finishing mill which is rolled from a thickness of between 20 mm and 30 mm to 2 mm. For the purposes of this analysis, we look at the three point definition of profile in hot rolling mills (section 1.1). An

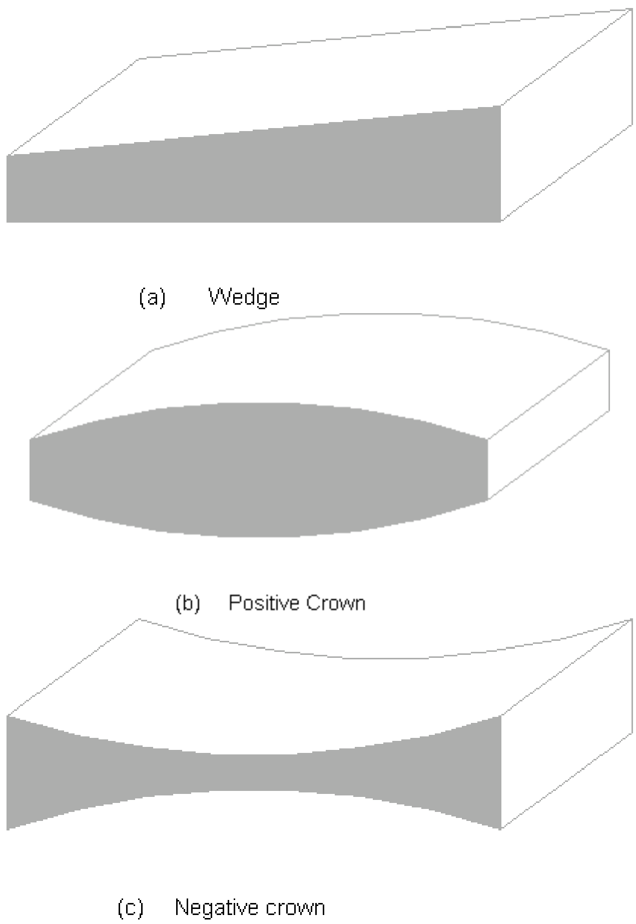

Figure 1.2: Sheet profiles.

acceptable wedge of less than 0.5% implies that at 2 mm nominal thickness, the difference between h_e^+ and h_e^- should be less than 0.01 mm. A deliberate crown of between 0.2% and 0.8% at a nominal thickness of 2 mm implies that the average value of h_e^+ and h_e^- should differ from the centre line thickness h_0 by a typical value that lies between 0.004 mm or 4 μm and 0.016 mm or 16 μm. At a centre line thickness of 20 mm, the acceptable wedge of 0.5% would imply a difference between h_e^+ and h_e^- of 0.1 mm. Therefore, difference between the average value of h_e^+ and h_e^- and the centreline thickness (h_0) should lie between 0.04 mm and 0.16 mm. For a nominal thickness of 2 mm, it is important that the developed profile gauging system gauges differences in profile thickness of up to a minimum of 4 μm.

1.4 Traditional profile gauging methods in hot mills

Radiation methods are the preferred way of gauging profiles in hot mills. It is therefore not surprising that Hulett Aluminium took this route for their profile gauges. However, the installed radiation gauges have not provided satisfactory results that warrant on line profile control. The fundamentals of the physical nature of x-rays applicable to thickness gauging are explored in this section. On the basis of the physical nature of the x-rays, an attempt is made to analyse the problems encountered in an example plant. Reasons for investigating Eddy Currents are made apparent.

1.4.1 X-rays

X-rays are a form of electromagnetic radiation of the same physical nature as visible light and radio waves [9, 10, 11]. They include a fairly wide range of wavelengths of radiation from about 10 nm (Grenz rays or ‘soft’ rays), which penetrates only very small thickness of solid materials, to about 10^{-4} nm (‘hard’ x-rays), which penetrates up to 500 mm of metals like steel [9, 10]. This range of wavelengths allow them to penetrate all materials with partial absorption during transmission. With the industrial conditions described in section 1.3, that include spray coolants and the inevitable dust particles, the x-ray gauges would have to correct for these harsh conditions.

Shortcomnings in x-ray applications

X-ray thickness gauges depend on the basic law of absorption given by [9, 10, 11]:

$$I = I_s e^{-\mu x} \tag{1.3}$$

Where x is the penetrated thickness, I_s is the incident intensity of radiation, I is the transmitted intensity and μ is a constant that depends on the penetrated material and the x-ray wavelength.

This equation is strictly true for mono-energetic radiation and for narrow beam conditions under which the amount of scatter radiation reaching the detector is small enough to be ignored [10]. This requirement is quite stringent and proves to be a problem in some developed gauges [2, 6]. X-rays, like light, travel in straight lines from a source and are therefore projected in a radial manner from the source. To obtain a narrow beam, a collimator is used to prevent all scattered radiation [9, 11].

X-ray generators do not provide mono-energetic radiation [11]. Also the energy content of the beam changes as it passes through the specimen thickness [11]. These two facts make it difficult to determine thickness without uncertainties. Two useful derivations of μ widely used are [10]:

- The half-value thickness (HVT), the thickness of the material required to reduce the intensity by a factor of two

  where $HVT = 0.693/\mu$

- The tenth value thickness ($(1/10)VT$)

  where $(1/10)VT = 2.303/\mu$

For a broad beam, neither *HVT* nor *(1/10)VT* is constant with changes in thickness. Also their values differ from those that are determined using the true narrow beam value. A narrow mono-energetic beam is ideal for the application but it can only be approximated.

The source of the x-ray is never a point source. It is usually a small area of a few millimeters in diameter [10]. This could have implications in the determination of incident intensities at varied source-detector distances. Therefore, it should always be necessary to consider the industrial pass-line distance from the x-ray source in order to make equation 1.3 consistent for all system conditions.

X-rays are harzadous to humans and they have to be used carefully. The production of x-rays is expensive, a single source costing over 20 thousand rands in South Africa.

A summary of the shortcomings of x-rays in the mill

- The constant μ that appears in equation 1.3 depends on the material penetrated by the x-rays, the width of the beam and the wavelength of the x-rays [9]. The hot mill does not have the luxury of rolling one alloy type. This implies that the value of μ changes with a change in the rolled material alloy and could mean higher demands on calibration and/or signal processing.
- Equation 1.3 is strictly true for mono-energetic radiation and for narrow beam conditions under which the amount of scatter radiation reaching the detector is small enough to be ignored [10]. X-ray generators do not provide mono-energetic radiation. The energy content of the beam changes as it passes through the specimen thickness making it difficult to determine thickness without uncertainties.
- The source of the x-ray is never a point source. Pass-line distance and angles from the x-ray source to the tested specimen and the detectors affect the incident intensities, I_s, of the x-rays and ultimately the consistence of equation 1.3.
- Radiation intensity is reduced as it penetrates all materials. Under the

industrial conditions necessary for hot rolling mills (coolant sprays, dust particles and dirty specimen or workpiece surface) gauges using x-rays techniques fail to produce accurate results.

- X-ray sources are very expensive and harzadous.

Hulett Aluminium Hot rolling mill installed multiple x-ray source profile gauges [2]. The three x-ray source gauges installed in the year 2000 did not give results that could support on line control. Other possible causes of poor results also discussed and reported by the manufacturers [12] and Gibbon [13] could include:

1. Dynamic response.
2. Calibration algorithm.
3. Edge distortion.
4. Emulsion on the x-ray source plates.
5. Deterioration of the equipment.

Discrepancies found in the x-ray gauges do not necessarily disqualify the gauges. However, x-rays are cumbersome to use and very expensive [9]. An approach that would give more precise results that are independent of specimen material and of the hostile industrial environment would be a contribution to industry.

Typical specifications of x-rays in thickness gauging

Typical specifications from Radiometrie [14] RM 215 X-Ray Strip Thickness Gauges are given below:

- X-ray source energies: 50 to 225 keV
- Maximum steel thickness: 73 mm

- Maximum aluminum thickness: 200 mm
- Detector sizes: 50 mm to 150 mm Ion chamber or PMT selected to optimize performance
- Accuracy: ±0.1%
- Repeatability: ±0.05%

1.5 Other techniques for thickness gauging

More thickness gauging techniques are described in this section. A brief description of the technique is given and examples of accuracies achieved are included in the discussions.

1.5.1 Optical and Laser thickness gauges

For laser sensor technology, true thickness is measured using two precision laser sensors facing each other [15]. The measuring range of the sensors overlap allowing the material under test to move in the gap while remaining within the measuring range of the sensors. The true thickness of the specimen is determined from the measurement from the two lasers. Typical specification from Oryx systems, Inc [15] are shown below:

- Reference distance: 25 mm / 150 mm
- Measuring range: ±4.5 mm / ±30 mm
- Wavelength: 670 nm
- Spot 30: μm /70 μm
- Linearity: 0.05% FS / 0.05% FS
- Resolution: 0.05 μm / 0.5 μm
- Thickness: up to 20 mm

- Accuracy: 0.5 μm to 5 μm
- Temperature range: 0 to 50^o C

Although high accuracies have been achieved using optical sensors, the major draw back in any optical sensor is the fact that light does not penetrate air born dirt and steam readily and it is refracted by water. Optical components such as lenses and lamps are easily soiled and are mechanically very sensitive. The industrial environment that is common in hot rolling mills would be a hindrance to any measurement accuracy.

1.5.2 Ultrasonic thickness gauges

Ultrasonic thickness gauges widely use the pulsed echo technique [16]. High frequency sound energy is launched into the probed material and the thickness of the evaluated material is calculated by considering the speed of this energy and the time it takes to traverse the material. Typical specifications for ultrasonic gauges [17] are given below:

- Range: 1.0 - 200.0 mm
- Resolution: 0.01 mm
- Temperature Limits:
  - Ambient: -5 to 50^oC
  - Material: -10 to 60^oC

The major draw back for the application of this technique to the industrial scenario described earlier is the need to use a coupling fluid.

1.6 Eddy Currents

Eddy currents are generated in conducting materials by time varying magnetic fields [18]. While optical and radiation gauges are hampered by the harsh industrial environment, eddy currents are oblivious to such media. This characteristic makes them a promising candidate for applications in the harsh non-conducting environment of hot rolling mills.

1.6.1 Conventional Eddy Currents (CEC)

The magnetic field used to generate the eddy currents could be sinusoidal or pulsed and eddy currents generated by these fields are referred to as conventional eddy currents (CEC) and pulsed eddy currents (PEC) respectively[18, 19, 20]. In somewhat simplified terms, for CEC, the material to be measured affects the amplitude and phase change of the electromagnetic field, yielding two parameters. When the response is analyzed, it is difficult to separate the influences due to the properties material from those due to the dimensions of the material[19]. Multiple frequency CEC scans were necessary to be able to inspect a specimen at various depths because the depth to which eddy currents penetrate the tested specimen depends on the frequency of applied field in CEC [18]. Difficulties were also encountered in the use of conventional eddy currents (CEC) for non-destructive evaluation of materials. These difficulties that include the effects of low sensitivity and the presence of high harmonics [19] led to the consideration of PEC.

1.6.2 Pulsed Eddy Currents (PEC)

The use of pulsed eddy currents (PEC) has been considered for non-destructive testing/evaluation of materials since the 1950s [19]. Pulsed waves consist of a continuum of sinusoidal frequencies that add up to present a pulsed waveform [21, 22]. These frequencies are odd number harmonics of the fundamental frequency at which the pulse wave is generated. Pulsed eddy currents have an advantage over conventional eddy currents in that they contain all the information that would be acquired by the use of a multiple frequency CEC scan [20]. Also, the pulse usually has a short duration and can be relatively powerful without excessively heating the test probe [23] as would be the case with CEC.

For a PEC probe in the presence of a conducting material, the measurement of the voltage pulse induced in a pickup coil when the current in a drive coil is suddenly interrupted reflects the magnetic field produced by the eddy current in the conducting material. This pickup signal waveform [24] signifies the transient response of the system arrangement which theoretically contains a range of frequencies. By carrying out summations over the period during which the signal is present, liftoff distance, specimen conductivity and the thickness of the specimen can be determined [24]. Typical specifications for PEC gauges are given below [24]:

- Minimum thickness for low alloyed aluminium: 0.1 mm
- Maximum thickness: 10 mm
- Accuracy: (relative permeability 1.0)
  - strip thickness greater than 2.0 mm: 2 μm $\pm 0.5\%$
  - strip thickness less than 2.0 mm: 1 μm $\pm 0.1\%$
- minimum strip width: 270 mm
- operating temperature: 5 to 55^{o}C

Peak-to peak voltages of up to 20 V_{p-p} have successfully been used in pulsed eddy current applications to evaluate materials dimensions [25, 26]. This implies that weak magnetic fields are used to evaluate a material for thickness, cracks, inclusions and resistivity. They work with such low energies, that they are harmless unlike x-ray gauges.

It can be sumarizesd that PEC techniques are:

- Contact-free

- Totally insensitive to non-conducting materials
- harmless

1.7 Summary and conclusion

The environment in the hot mill is harsh and many physical phenomena cannot be readily applied to gauge the profile of a sheet for on line feedback/feedforward control of the rolling process. Sheet temperatures, coolant sprays and a general presence of a harsh industrial environment are a challenge to the gauges. Although radiation, optical and laser gauges show high levels of accuracy, the industrial environment in the hot rolling mills renders them unsuitable for on-line profile guaging. Eddy current techniques on the other hand can be used to eliminate the harsh industrial environment since they will not be induced in the environment. However, there are other factors involved in the rolling process that could be important to the development of a PEC application in this environment. These factors were explored in this chapter and are summarized as:

- The tested strips begin the rolling process at a temperature of about 560^{o}C. Temperature changes are therefore inevitable in the evaluated specimen.
- The rolling process implies a moving specimen as opposed to a stationary one. Changes in velocity might be vital to the gauging of the profile in pulsed eddy current application.
- The strip is not restricted and may not necessarily be horizontal at all times leading to varying pass line angles and pass line distances.
- The rolling process results in changes in the nominal thickness with a profile that may vary during the rolling schedule.
- The mill does not have the luxury of rolling one alloy type leading to inevitable differences in materials properties such as conductivity and permeability.

The study describes an investigation of PEC toward the development of a profile gauging system. The main thrust of the work is the development of a method to extract information relevant to profile gauges from the PEC system eliminating environmental, physical, dynamic and material effects.

The thesis is divided into chapters covering the following topics:

- Chapter 1 has given an overview of the rolling mill environment, the existing profile gauging in the mills and the problems that have led to the investigation described in the study.
- A literature review of research undertaken on Pulsed Eddy Currents and present practices of extracting information on specimen thickness is presented in chapter 2.
- A report on the development of a PEC system model that was used to predict system parameters and to verify results from the PEC system probes is described in chapter 3.
- A simulation environment was developed using Matlab and Simulink and this is discussed in chapter 4
- The model was verified by a set of experimental tests deemed to be relevant to hot mill profile definition. Validation of the model is presented in chapter 5
- A simulation study was done and is presented in chapter 6 to establish a basis on which decision on source amplitudes and frequencies in conjunction with probe parameters are made.
- Experiments involving specimen temperatures and thicknesses, and the results there of are presented in chapter 7. Simulations were used in situations were specimen parameters involved could not be emulated.
- Chapter 8 presents the analysis and discussions of experiments and simulations. A method of extracting thickness measurements from other influences is established in this chapter.
- Findings of the study and their implications, limitations, recommendations and a conclusion are presented and discussed in chapter 9.

Chapter 2

EDDY CURRENTS: A LITERATURE REVIEW

2.1 Introduction

It has been established in chapter 1 that eddy currents are only induced in conducting medium. The technique ignores the harsh industrial environment and is therefore a good candidate for evaluating sheet profile for aluminium hot rolling mills. Existing practices in PEC applications, especially for thickness gauging, are explored in this chapter.

Eddy currents are generated when time varying magnetic fields are applied to conducting materials satisfying Faraday's law [27]. These currents flow in such a way that secondary magnetic fields are produced to oppose the applied (primary) magnetic field satisfying Lenz's law [27]. The directions of the currents and the magnetic fields in Figure 2.1 illustrates both Faraday's and Lenz's laws.

Pulsed eddy currents (PEC) have favourable advantages over conventional eddy currents (CEC). They are a result to the sum of a continuum of odd number harmonics of the fundamental sinusoidal waveform frequency of the pulse [21, 22]. Therefore, a transient response (figure 2.2) obtained from the

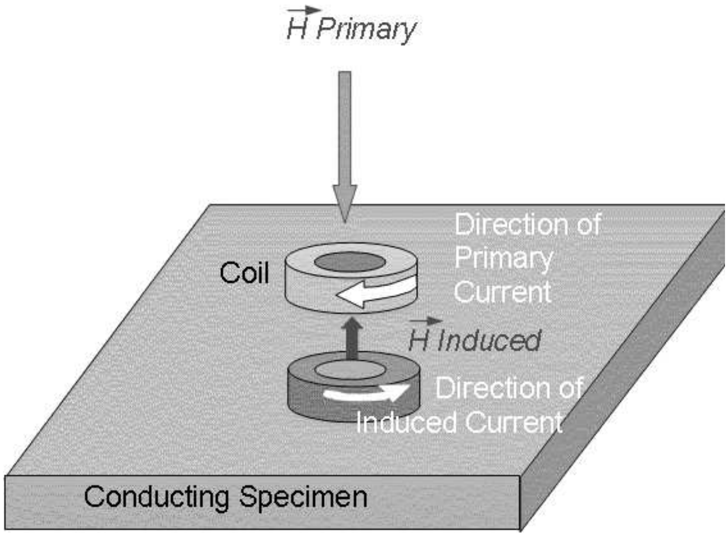

Figure 2.1: An illustration of Faraday's and Lenz's laws for eddy currents induced in a conducting specimen.

pulsed eddy current system contains many frequencies. Because of the skin effect [18, 28], the depth to which eddy currents penetrate the tested specimen depends on the frequency of applied field in CEC. However, skin effect depends on the duty cycle period of the probing pulse in PEC [18]. Therefore using PEC allows the inspection of various specimen depths with just one pulse as opposed to the multiple frequency scans required for CEC.

Changes in various specimen characteristics such as thickness, conductivity and permeability affect the eddy currents induced in the specimen [22, 29]. Various techniques have been employed to harness effects of the induced eddy currents on the magnetic field that creates them. Sensors employed by various researchers include:

- Hall effect sensors; though more sensitive than coil sensors, they have several factors that introduce nonlinear deviations to the Hall voltage [30]. These factors include temperature, magneto-resistance and contact problems among others.
- Giant Magneto- resistive (GMR) sensors; investigated by Ward and Moulder [31], compared the relative abilities of a coil sensor and the GMR sensor to harness information from multiple layers of metal. The signal from the GMR sensor was found to be eight times stronger.

- Superconductive quantum interference devices (SQUID) were used by Podney [32] in his test bed instrument that operated at 5 Kelvin. The applications are limited to laboratory conditions.
- Coil sensors have been used by Waidelich *et al* [29], Lefebvre *et al* [33] and others [19, 24, 34].

Coil sensors have been used by many researchers [29, 33, 19, 24, 34] with promising results. Thickness gauges with accuracies of 2 μm $\pm 0.5\%$, for thicknesses greater than 2.0 mm have been developed for aluminium cold rolling mills [24].

Coil probes used by researchers include:

- A single coil acting simultenuously as the drive coil and the pickup coil [19] .
- A sliding coil probe with the drive coil and the pickup coil placed side-by-side [29].
- A reflection coil probe with the drive coil and the pickup coil placed concentric to each other [25, 26].

The drive coil is the source for the time varying magnetic field while the pickup coil presents the effects of the generated eddy currents.

2.2 Position of the pickup coil

Waidelech and Lahmeyer observed that the pulse energy received from the tested specimen was the same on both sides of the specimen [29]. A receiving probe (pick-up coil) could be placed on either side of the specimen and the received signal found to be the same for both situations. They also observed that moving the pick-up coil away from the drive coil in the sliding probe arrangement resulted in the signal strength from the pickup coil decreasing

[29]. This suggests that the drive coil and the pickup coil should be placed tightly together to maximise pickup coil signal strength.

Lefebvre and Dubois [33] and other researchers [25, 26] used the pickup coil and the drive coil on the same side to successfully carry out evaluations on materials. When a pulsed magnetic field is setup by the drive coil, the voltage signal received in the pickup coil contains information on the specimen characteristics which include thickness, conductivity and permeability.

It has been found experimentally by various researchers [19, 34, 35], that the referenced subtracted signal observed at either a pickup coil or a drive coil takes on a characteristic shape similar to that shown in figure 2.2(c). This signal will rise to a peak value, decrease going through zero, reach a negative peak and then gradually approach zero.

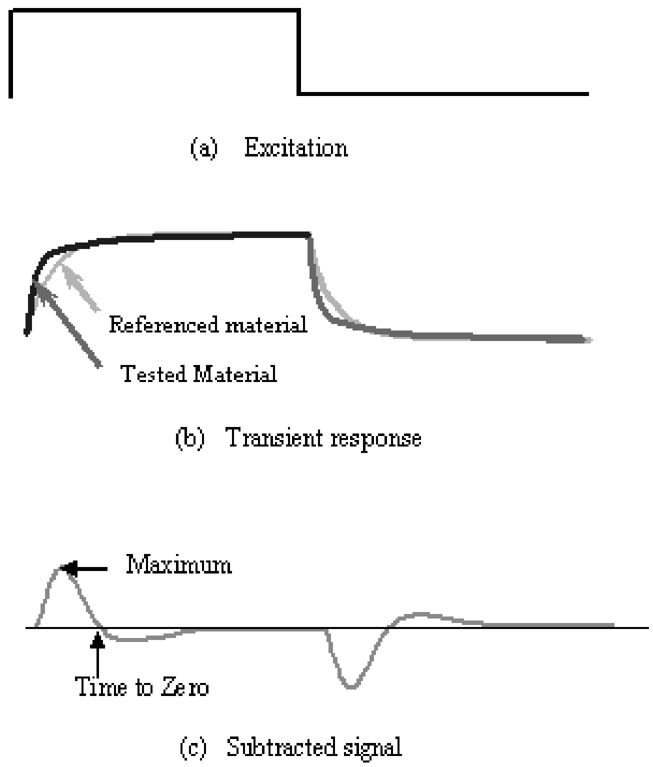

Figure 2.2: An illustration of a referenced subtracted signal observed at a drive coil.

The signal has three discernible features:

- peak amplitude,
- time to peak amplitude
- and time to zero crossing.

The three features are dependent on various parameters of the system [23, 19, 35, 36] among which are:

- the thickness of the tested specimen,
- lift-off (see section 2.4),
- conductivity of the specimen
- and permeability of the specimen.

2.3 Thickness and Pulsed Eddy Currents

Results for a physics co-op work term report written by Brian Wallace [1] (Table 2.1) show:

- Maximum amplitude increases with increased thinning (decreasing thickness).
- Time to maximum amplitude decreases with increased thinning (decreasing thickness).
- Time to zero crossing decreases with increased thinning (decreasing thickness).

These results agree with the conclusions reported by Waidelich and Lahmeyer [29] which were:

- the peak of the observed output pulse decreased with increasing thickness and that the peak voltage varied approximately inversely with the fourth power of the thickness of the metal.

Table 2.1: Amplitude and time of flight for an A-scan [1]

%Thinning	Max. Amplitude (V)	Time to Max. (μs)	Time to zero (ms)
3.75	0.143585	66	0.239
16.25	0.342407	55	0.207
38.75	0.621643	56	0.194
52.5	1.539307	45	0.160

- the time delay of the peak of the received pulse increased as the thickness of the metal increased. This delay was approximated to vary as the 1.6 power of the thickness of the metal.

2.4 The Lift-off problem

In eddy current applications, the distance between the pick up coil and the specimen is referred to as lift-off. Variations in this parameter tend to affect the time delay to the peak of the received signal in the reference subtracted signal [19]. A crossing point for varying steps of lift-off with all other parameters kept constant was first observed by Waidelich and Haung [29]. In their investigation of the crossing points observed under various scenarios, they concluded that a crossing point at a specific time, could be found for any parameter such as lift-off, thickness of the specimen, conductivity of the specimen, and permeability of the specimen. For the coils they used in their experiments, they observed that the crossing point for the changing lift-off distance was at time $t = 0.0165$ s, while that for the changing conductivity was at a time $t = 0.125$ s. They suggested that computations on the signals could be used to find the position where the maximum variation of parameter might be observed in the pulse response of the system. They also suggested that using time gates would allow for the elimination of unwanted parameter effect on the received signal. They pointed out that if the pulse read out was adjusted to occur at the crossing point, the response of the system would relatively be independent of the parameter associated with that particular crossing point. They also pointed out that on the other hand, positions in time could also be found where maximum variation of a parameter might be observed in a pulse response system. This concept was effectively used in the lift-off point of Intercept (LOI) to:

- characterise material loss with gap and lift-off variation [25]
- successfully map out corrosion [26]
- detect cracks under installed fasteners [37]
- quantify defects and their locations in multilayered specimen [38]

2.5 Analysis of the received pulsed eddy current signal

From section 2.3 and 2.4, it can be concluded that the potential application of PEC to thickness gauging has relied on the analysis of a referenced received signal features, such as:

- Amplitude
- Time delay to peak of the received pulse
- And/or time delay to zero crossing of the received signal

These features are unique to coil sensors [29, 39]. In addition to being sensitive to changes in material thickness, the features of the referenced signal have also been found to be sensitive to lift-off and the conductivity of the material [33].

Giguere *et al* [26] and Lefebvre *et al* [33], have reported on the successful use of the crossing point phenomenon in eliminating lift-off effects in PEC evaluation of conducting specimen. They were able to extract the thickness of a material independent of lift-off by time gating the signals around the time of the lift-off point of intersection. Safizadeh *et al* [39] however observed that the crossing point actually varied and they considered other aspects of the signal to separate effects due to lift-off and thickness.

In their experiments to establish the effects of lift-off and specimen thickness on the PEC received signal, Safizadeh *et al* [39] first analysed the received signal in the time domain and then in the time-frequency domain. They carried out an analysis on the signals received with variation in thickness and/or lift-off distance, in the time-frequency domain, using the Wigner-ville distribution [39, 40]. Their study showed that the time-frequency analysis of PEC signals provides specific visual patterns that could be related exclusively either to the lift-off distance or the material loss (reduction in thickness). Their analysis shows that changes in specimen thickness affects the lower frequency range of the recieved transient signal while changes in lift-off distance affect a higher frequency range agreeing with other reseachers.

Researchers at ABB have analysed the pulse induced in the coil by considering the signal at different times of the transitional period [24]. The ABB technology is based on the measurement of the voltage pulse induced in the coil when the current is suddenly interrupted. After the abrupt interruption of the constant excitation current, the magnetic field produced by the eddy current in the metal sheet is measured as a factor of the voltage it induces in the coil. They explained that at the instant of interruption, the eddy current is present only on the surface of the workpiece and has not yet penetrated deeper into the substrate. By tracing the entire penetration sequence via the voltage induced across the coil, three unique signal values at three different times can be derived. They quantify the three parameters by taking integrals over specific times of the signal. These parameters include

- the lift-off,
- the electrical resistivity of the specimen and
- the thickness of the specimen.

Lift-off affects earlier times of the signal while changes in the thickness of the specimen affect later times[24]. This agrees with the findings made by Safizadeh *et al* [39] and comfirms that information on the thickness of a material is stored in the later times of a period of the received PEC signal.

Grman [41] reported on the application of Wavelet Transformation in Eddy Current Testing. Wavelet analysis has some similarities with the traditional Fourier analysis [21] which involves representing a signal as the sum of sines and cosines of various frequencies. Fourier analysis is not good at investigating non stationary signals where the component frequencies change with time because it averages key features of a time varying signal over the entire length of the signal meaning that fine detail is lost [42]. Short Fourier transform, developed to overcome this problem by averaging short duration components, cannot capture those components that last for longer periods. However, wavelet analysis is able to take into account the scale as well as the time shift of the signal components. Using narrow wavelets for high frequency features and wider wavelets for longer lasting features, allows one to zoom in on individual small scale, high frequency component or pan out to pick large-scale, low-frequency components. The process involves the convolution of the wavelet function [43] with the signal and presents signal information in a manner that separates various aspects of the same [42, 43, 44, 45].

In his paper, Grman [41] defines wavelet transforms as a shifted version of a wavelet function of time, scale and location. The results of the wavelet transform are many coefficients which are a function of scale and position. He used the continuous wavelet transform command from Matlab wavelet toolbox. The application was geared toward multiple-frequency Eddy Current method. For each frequency, an absolute value for all wavelet coefficients was calculated. The purpose was to localise and classify defects by using wavelets with different levels of scale and location to convolute with the eddy current signal.

The Continuous Wavelet Transform (CWT) is highly redundant (there is a lot of repetition of information between transformation coefficients) and it uses large amounts of computer memory. Discrete Wavelet Transforms (DWT) [42] developed to address the problem of redundancy, have proved to be popular and the technique is widely available within common software packages like Matlab. However, even though the discretized wavelet transform is used to address the redundancy problem of continuous wavelet transforms, and can be computed on a computer, these computations may take anywhere from a couple of seconds to a couple of hours [46], depending on the signal size and the required resolution. Therefore one can conclude that wavelet transform would be cumbersome for an on line application.

2.6 Modeling Pulsed Eddy Current systems

In this study, modeling the PEC system served as a means of acquiring an understanding of the phenomena involved in the formation of the received PEC signal but also as a means of providing a simulation environment for the study. There has been a great deal of effort put into modeling and simulating eddy current response by various researchers [47, 48, 49, 50, 51, 52, 53]. This section provides a brief literature overview of some of the accomplishments achieved by previous researchers.

Bowler and Johnson [49], present an idealised equivalent circuit for the drive coil in free space. The coil considered had a rectangular cross section and its axis was perpendicular to the surface of the specimen (conductor). A bipolar square wave voltage, the amplitude of which determined the amplitude of the coil current was the source to the system. An RC filter that determined the time variation of the coil (the value of the resistance was as high as 4048 ohms) and a trans-conductance amplifier that ensured that the coil current was proportional to the filter voltage and independent of the coil resistance, conditioned the source. Bowler *et al* [49], in their paper, explore field theory, coil fields and time domain fields. They calculate the *emf* of a coil due to transient eddy-currents in a half-space conductor from closed-form integral expressions. They point out that circuit theory alone is not suited to the prediction of the coil *emf* due to the induced eddy currents if the coil is placed on a conducting half plane.

Hurley and Duffy [54], reported on the calculation of self and mutual impedances of planar magnetic structures on ferromagnetic substrates a scenario analogous to the setup of a coil placed on one side of a specimen. The spiral coil in air was represented by a lumped parameter model. The input impedance of the spiral coil in air was calculated numerically and validated experimentally. They reported that placing the coil on a magnetic substrate leads to a doubling of the coil inductance. They developed a set of formulae for calculating self and mutual impedances of planar coils on homogeneous ferromagnetic substrates. The formulae were derived from Maxwell's equation and served as useful gauge for simpler approximations.

The field produced by a current carrying coil placed on a conducting specimen generates eddy currents in the specimen. These generated currents experience both resistive and reactive losses inflicted by the conducting specimen. Many researchers have used finite element analysis to characterise the effect of the induced eddy currents on the primary field due to the reflected field of the conducting medium [50, 51, 52]. Hurley and Duffy [54], in their paper on the calculation of self and mutual impedances in planar magnetic structures established formulae that represented the substrate impedance and validated them against the finite element approach. There was good agreement between the two approaches.

The finite element approach is a numerical method [55, 56, 57]. It provides solutions to problems that would otherwise be difficult to obtain. These are normally problems that are represented by partial differential equations (PDE) or as intgeral equations. The approach either completely elimimates the PDE leading to a steady state problem, or it approximates the PDE to ordinary differential equations. These are then numerically solved using standard techniques such as Runge-Kutta [58]. Finite element method uses mesh discretization of a system into a set of subsystems. The system then becomes a collection of elements joined together at nodes. Dividing a system into smaller subsystem, allows one to focus on regions within the system where high variations in investigated parameters occur. In simulation this would allow for a reduction in simulation time.

Aulder *et al* [53] gave a review on the advances in quantitative eddy current nondestructive evaluation. They explored literature on the change in probe impedance due to the defect in the specimen. The probe response was explored in the frequency domain but could be converted to the time domain for pulsed eddy current applications by taking Fourier transforms.

2.7 Summary and conclusion

From the literature review carried out in this section, it can be concluded that obtaining a signal from the PEC system is a relatively easy and straight forward procedure. However, analysing the signal received from the system to separate effects from the various parameters involved, proves to be the major challenge.

Researchers have used various ways of harnessing the effect of eddy currents on the primary magnetic field. Hall effect sensors, Giant Magneto-resistive sensors, Superconductive quantum interference devices and coil sensors are among the techniques used to detect changes due to the induced eddy currents. Coil sensors have been used by many researchers with promising results. They are further investigated for profile gauging in aluminium hot rolling mills.

Various techniques have been used to analyse the PEC signal. Time-gating, Wigner distribution and wavelet theory have been used to separate information from the received signal. It has been established that lift-off affects earlier times of the signal half period while changes in the thickness of the specimen affect later times and conductivity affects the middle times of the of the signal.

The study described in this thesis involves the PEC system signal harnessing, analysis and processing. The purpose being to make holistic recommendations toward the development of a profile gauging system applicable in aluminium hot rolling mills. An effective way of processing a value that defines profile in a temperature changing specimen is sought for. An electrical representation of the PEC system is assumed and developed in chapter 3. Expressions characterising the alumnium sheets as resistance and inductance for the PEC system model were one of the major developments in the modelling process. Though the basis of the modelling is anchored on findings from literature, these findings are developed further to suit the investigated scenario.

Chapter 3

MODELING A PULSED EDDY CURRENT SYSTEM

The process of modelling the PEC system served two purposes; that of acquiring a good understanding of the system and also providing a suitable environment to simulate profiles that could not be readily emulated experimentally. A report on the development of a model of the envisaged PEC system that can be used to make informed predictions on a profile gauging system is presented in this chapter. The system is seen as three electrical circuits coupled to each other by principles of electromagnetism. In these circuits, the coils and the specimen are represented by lumped resistances and inductances. This approach is used in electrical engineering systems in the derivation of their equivalent circuits [59]. Mathematical expressions for the various aspects of the model are derived using fundamental physical phenomena. Understanding the nature of the generated eddy currents assisted the characterisation of the specimen as resistance and inductance presented to the eddy currents as they swirl in the bulk of the material. The dynamics involved in the whole scenario are considered and addressed. Effects of temperature changes, limitations presented by the concept of skin effect and the effects of specimen thickness are considered and included in the mathematical expressions that are developed for the specimen characterisation.

3.1 Introduction

Variables present in aluminium hot rolling mills that affect the signal received from the PEC system (section 1.4) were considered and accounted for in the developed model. These include:

- The tested sheets begin the rolling process at a temperature of about 560^oC. Temperature changes are inevitable in the evaluated specimen.
- The rolling process implies a moving specimen as opposed to a stationary one. The sheet moves up to a speed of 3 m/s. Changes in velocity might be vital to the gauging of the profile.
- The rolling process results in changes in the nominal thickness with a profile that may vary during the rolling schedule.

The sections that follow report on the development of the various mathematical expressions that were susquently used to develop the simulation environment (chapter 4) that was used for the study.

3.2 Pulsed Eddy Current System Model

On the strength of Waidelich and Lahmeyer's observations and conclusions [29], the investigations on the received signal were carried out with the test probe placed on one side of the specimen.

Figure 3.1 shows a vertical cross sectional view of a single coil probe placed with its axis perpendicular to the specimen. It illustrates the dimensions of a coil and other system parameters. These include:

- coil length l_{dg}
- inner radius r_1

- outer radius r_2
- liftoff x
- specimen with thickness y

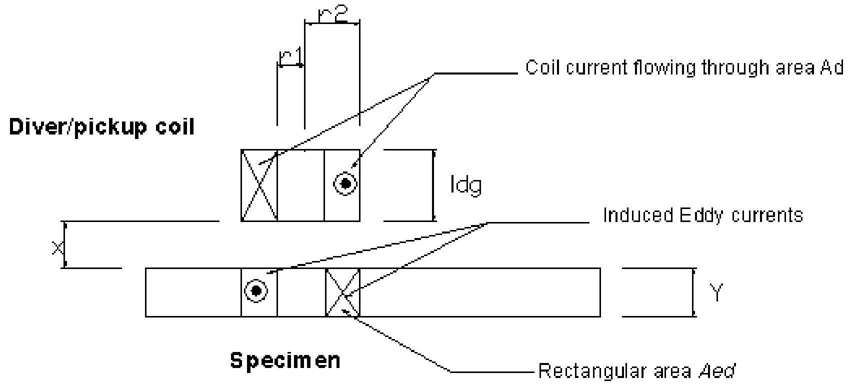

Figure 3.1: Cross sectional view of single coil probe configuration on a specimen with thickness y at liftoff x. The coil has an inner radius r_1 and an outer radius r_2.

The cross sectional view of the setup for a sliding coil probe and a reflection coil probe are given in figure 3.2. A reflection coil probe was used in this study. The electric circuit model representing the probe in close proximity with the specimen is shown in figure 3.3. The subscripts d, p and s refer to the drive coil, pickup coil and specimen parameters respectively.

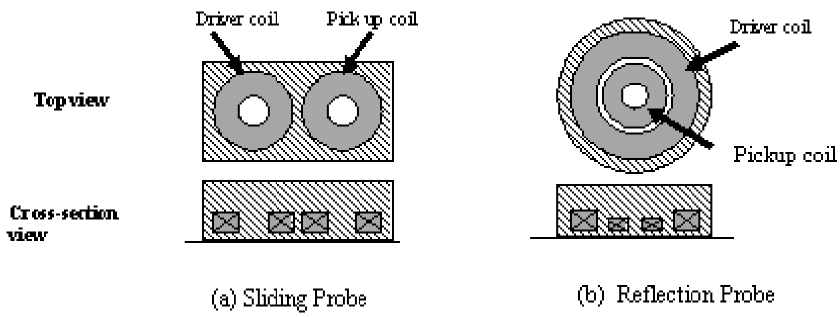

Figure 3.2: Orthographic view of a sliding probe and the reflection probe

A pulsating supply voltage, $v_d(t)$, is connected across the drive coil and the received signal is taken across a resistance, R_o, that is connected in series with the pickup coil. The drive coil and the pickup coils are characterised by the resistances R_d and R_p and the inductances L_d and L_p. The two coils interact with each other through their self and mutual inductances, L_d, L_p and M_{dp}, and also through the electric and magnetic fields in and around them.

As discussed in section 2.6, finite element approach has been used for the analysis of eddy currents induced in conducting materials by various researchers [50, 51, 52, 60, 61, 62, 63]. However, other researchers have developed formulae for calculating self and mutual impedances of planar coils on homogeneous ferromagnetic substrates [54]. Lumped parameter models were used to represent impedances. Impedances were calculated numerically and validated experimentally. The approach in this study considers a lumped representation of the specimen by a resistance and an inductance. An analytical approach is used in the development of the specimen characterisation to suit the simulation environment used for the study. Since most circuit theories seek to reduce complicated circuit networks to simple equivalences of source and impedance, the complexity of the modelled lumped parameters is carefully considered in the analytical appraoch. The aim being, to develop two equations representing the inductance L_s and the resistance R_s that the probed material presents to the eddy currents generated in it. In this approach, the specimen impedance is seen to interacts with the probe impedances, currents, emfs and associated magnetic fields, governed by electromagnetic rules. The system is modeled as a whole; the final effects harnessed and observed in the probe pickup coil signal.

The proposed system is surrounded by a non-conductive environment that represents the industrial environment.

3.3 The probe parameters

In this section, the expressions for the voltages, currents, resistances and inductances of the drive and the pickup coil are derived analytically using well known circuit and electromagnetic theories.

3.3.1 Drive coil current $i_d(t)$

To allow for signal interaction between networks in the Matlab and Simulink simulation environment developed in chapter 4, solutions for the drive coil current and the pickup coil current had to be established. In this section, an equation for the drive coil current, $i_d(t)$ (equation 3.7), is derived.

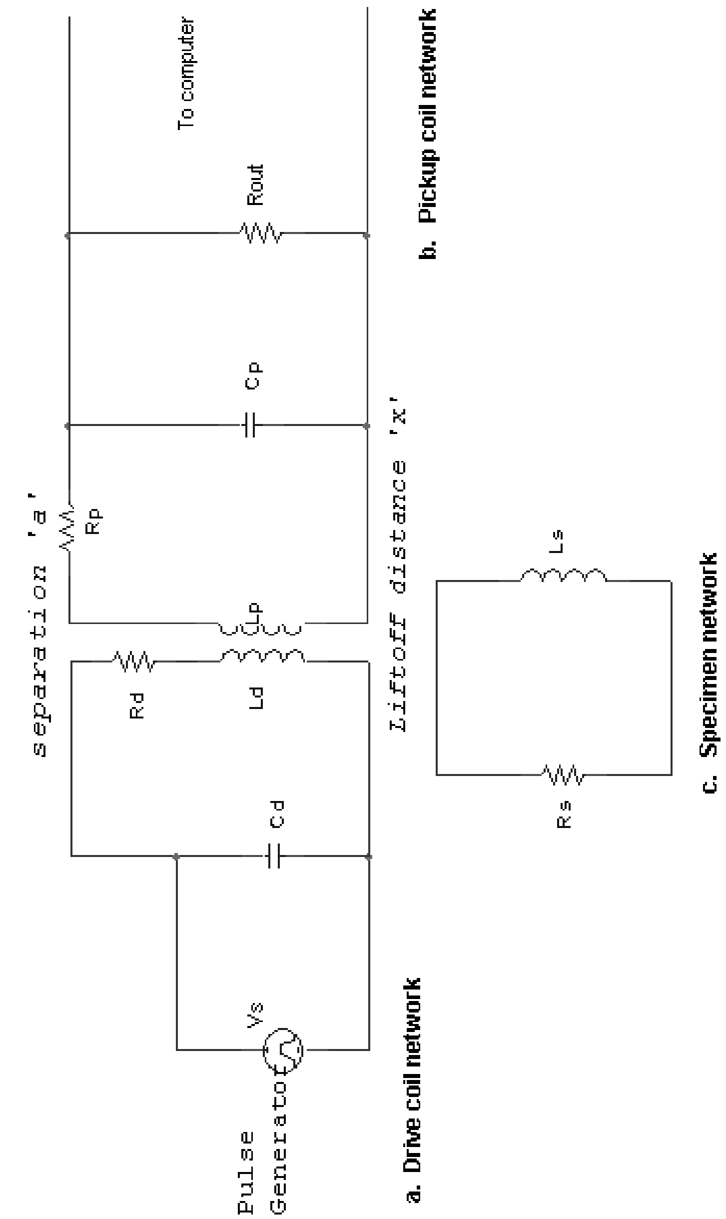

Figure 3.3: Electrical Circuit representation of a Sliding/reflection probe in close proximity with the tested specimen.

The three networks of figure 3.3: the drive coil circuit, network ($\boldsymbol{a}$), the pickup coil circuit, network ($\boldsymbol{b}$) and the specimen circuit, network ($\boldsymbol{c}$), are interconnected through electromagnetic laws. A changing flux due to a current in another coil will induce a voltage in the coil proportional to the mutual inductances of the two coils [64, 65]. The voltage induced in the drive coil circuit v_{dp} due to the current i_p in the pickup coil is:

$$v_{dp} = M_{dp}\frac{di_p}{dt} \tag{3.1}$$

where M_{dp} is the mutual inductance of the two coils represented by [66]:

$$M_{dp} = M_{pd} = K_{dp}\sqrt{L_p L_d} \tag{3.2}$$

and K_{dp}, a coefficient of coupling, is dependent on coil orientation with respect to each other.

In the same way, a voltage v_{ds} due to the current i_s (induced eddy currents) in the specimen is induced in the drive coil:

$$v_{ds} = M_{ds}\frac{di_s}{dt} \tag{3.3}$$

The voltage appearing cross the primary source, v_d(t), in the time domain, is the sum of effects due to self inductance L_s, the resistance in the circuit R_T and the mutual inductances M_{dp} and M_{ds}. This is expressed as:

$$v_d(t) = R_T i_d + Ld\frac{di_d}{dt} + M_{dp}\frac{di_p}{dt} + M_{ds}\frac{di_s}{dt} \tag{3.4}$$

Representing the sources due to mutual inductances M_{dp} and M_{ds} as $v_{dp}(t)$ and $v_{ds}(t)$, equation 3.4 becomes:

$$v_d(t) = R_T i_d + Ld\frac{di_d}{dt} + v_{dp}(t) + v_{ds}(t) \tag{3.5}$$

Re-arranging equation 3.5:

$$R_T i_d + L_d\frac{di_d}{dt} = v_d(t) - v_{dp}(t) - v_{ds}(t) \tag{3.6}$$

The expression on the right hand side of equation 3.6 represent the primary and secondary sources in circuit ($\boldsymbol{a}$) of figure 3.3. The required solution for the drive coil current in the differential equation (equation 3.6) is found by applying forward and inverse Laplace transformation [67] to the equation. The solution to the drive coil current is derived by considering primary voltage source $v_d(t)$ and the secondary voltage sources ($v_{dp}(t)$ and $v_{ds}(t)$). An inverse laplace transform yields the solution:

$$i_d(t) = (v_d(t) - v_{dp}(t) - v_{ds}(t))e^{\frac{R_T}{L_d}t} \tag{3.7}$$

3.3.2 The primary magnetic field as a function of the drive current i_d*(t)*

In this section, an expression for the primary magnetic field, $B_x(t)$ (equation 3.12), is derived as a function of the drive coil current, $i_d(t)$.

The drive coil current $i_d(t)$ produces a magnetic flux density around it that is quantified using Boit-Sarvat law [68, 69]. A conducting element of wire with a small length ds carrying a steady current I will produce a magnetic field dB at a point a distance r from the element. The produced field is perpendicular to the direction of the current flow and to the direction of a unit vector $\hat{r}$ in the direction of the point. The field is directly proportional to the current and the magnitude ds of the element but it is inversely proportional to r^2. These observations are summarized mathematically as [68]:

$$dB = \frac{\mu_o}{4\pi}\frac{Ids \times \hat{r}}{r^2} \tag{3.8}$$

To evaluate the magnetic field for the conductor, an integration over the whole length of the conductor is required.

$$dB = \frac{\mu_o I}{4\pi}\int \frac{ds \times \hat{r}}{r^2} \tag{3.9}$$

For a circular coil with radius r_1 and N_d number of turns the magnetic field created by the coil is derived from equation 3.9 by considering the current flowing through each turn as $i_d(t)$. If the field is considered at a point a distance x from the bottom of the coil, equation 3.9 is modified to include the distance x and it becomes [68, 69]:

$$B_x(t) = \frac{\mu_o N_d i_d(t) r_1}{4\pi(x^2 + r^2)^{3/2}}\oint ds \tag{3.10}$$

$$\oint ds = 2\pi r_1 \tag{3.11}$$

Equation 3.10 becomes:

$$B_x(t) = \frac{\mu_o N_d i_d(t) {r_1}^2}{2(x^2 + {r_1}^2)^{3/2}} \tag{3.12}$$

$B_x(t)$ is the primary magnetic field at a lift-off distance x referred to in chapter 2.

For the magnetic induction, $B(t)$, at the center of the drive coil $x = 0$ and $B(t)$ is expressed as:

$$B(t) = \frac{\mu_o N_d i_d(t)}{2r_1} \tag{3.13}$$

3.3.3 Electromotive force induced in the pickup coil and the pickup current

In this section, expressions for the electromotive force, $E_p(t)$, induced in the pickup coil (equation 3.18) and the pickup current, $i_p(t)$ (equation 3.20) are derived.

The primary magnetic field (equation 3.12) due to the current flowing in the drive coil (equation 3.7), induces an electromotive force (emf) both in the pickup coil and in the specimen. In this section, we consider the emf, $E_p(t)$, induced in the pickup coil.

An expression for the electromotive force, $\epsilon_p(t)$, induced in the pickup coil is derived by applying Faraday's law of induction and Lenz's law [27]. Faraday's law states that the emf induced in a circuit is directly proportional to the time rate of change of the magnetic flux, Φ_B, through the circuit and Lenz's law states that the induced current and the induced emf in the conductor are in such a direction as to set up a magnetic field that opposes the change that produced them. This is expressed mathematically as:

$$E_p(t) = \frac{-d\Phi_B}{dt} \tag{3.14}$$

The magnetic flux Φ_B is expressed in terms of the magnetic field density B as:

$$\Phi_B = \oint B.dA \tag{3.15}$$

where dA is a small area cut by the magnetic field.

$$E_p(t) = -A_p cos\Psi \frac{dB(t)}{dt} \tag{3.16}$$

A_p is the area cut by the flux density at the centre of the drive coil $B(t)$ and Ψ is the angle between the magnetic field lines of the magnetic induction $B(t)$ and the axis of the pickup coil.

Using the same approach used for the drive coil circuit, the pickup coil circuit represented in network (***b***) of figure 3.3, the induced emf $\epsilon_p(t)$, in the time domain, is the sum of effects due to self inductance L_p, the resistance in the circuit R_p and the mutual inductances M_{pd} and M_{ps}. This is expressed as:

$$E_p(t) = R_o i_p + R_p i_p + Lp\frac{di_p}{dt} + M_{pd}\frac{di_d}{dt} + M_{ps}\frac{di_s}{dt} \tag{3.17}$$

Representing the sources due to mutual inductances M_{pd} and M_{ps} as $v_{pd}(t)$ and $v_{ps}(t)$, equation 3.17 becomes:

$$E_p(t) = (R_p + R_o)i_p + Lp\frac{di_p}{dt} + v_{pd}(t) + v_{ps}(t) \tag{3.18}$$

Re-arranging equation 3.18:

$$(R_p + R_o)i_p + L_p\frac{di_p}{dt} = E_p(t) - v_{pd}(t) - v_{ps}(t) \tag{3.19}$$

The expression on the right hand side of equation 3.19 represent the secondary sources in circuit (***b***) of figure 3.3. The required solution for the pickup coil current $i_p(t)$ in equation 3.19 is found by applying Laplace transformation [67] to the equation and the inverse laplace transform yields the solution:

$$i_p(t) = (E_p(t) - v_{pd}(t) - v_{ps}(t))e^{\frac{(R_p+R_0)}{L_p}t} \tag{3.20}$$

The pickup coil current is expressed in terms of the secondary sources $\epsilon_p(t)$, $v_{pd}(t)$ and $v_{ps}(t)$

3.3.4 Resistance and Inductance of the drive coil and the pickup coil

Resistance R_d of drive coil and R_p of the pickup coil

Expressions for the drive coil resistance, R_d (equation 3.27), and the pickup coil resistance, R_p (equation 3.31), are derived in this section.

The resistance of a resistive material is related to the material's resistivity and dimensions as [70]:

$$R = \frac{\rho l}{a} \tag{3.21}$$

R, a, l and ρ represent the resistance, cross-sectional area, length and resistivity of the conductor respectively.

A wire with a cross sectional diameter d_d used to construct the drive coil would have a cross sectional area a_d given by the expression below.

$$a_d = \frac{\pi d_d^2}{4} \tag{3.22}$$

The drive coil is a solenoid and is constructed using a wire conductor with a cross sectional area a_d, a length l_d and resistivity ρ_d.

We seek to express the resistance as a function of the coil dimensions and the characteristics and dimensions of the wire from which it is constructed. The length of the wire l_d is calculated from the number of turns that can fit in the cross sectional area of the solenoid coil A_d multiplied by the average length of each turn. The drive solenoid coil has an inner radius r_1, an outer radius r_2 and a height l_{dg}. The area A_d is expressed as:

$$A_d = (r_2 - r_1) l_{dg} \tag{3.23}$$

It is observed that the number of conductors that can fit in the solenoid cross-sectional area constitutes the number of turns that make up the solenoid winding. However, the conductor has a circular cross-sectional area and there will be area that cannot be occupied by the conductors. A fill factor k_f estimated by taking the ratio of the turn value determined at the time of winding $N_{det.}$ to the calculated turn value $N_{cal.}$, is used to determine the actual number of turns.

$$K_f = \frac{N_{det.}}{N_{cal.}} \tag{3.24}$$

The fill factor is always less than one and experimental results presented in Appendix B, show that K_f lies between 0.7 and 0.9 depending on the wire diameter and that the thinner the wire that forms the winding, the higher the factor. This factor was used as a fitting factor in the simulation environment. The number of turns in the drive coil was calculated using the equation 3.25.

$$N_d = K_f \frac{A_d}{a_d} \tag{3.25}$$

The resistance of a wire conductor is given by the expression in equation 3.21. The length of the drive coil wire can be calculated in terms of the number of turns N_d and the inner and outer radii of the solenoid,r_1 and r_2, using equation 3.26.

$$l_d = N_d \pi (r_1 + r_2) \tag{3.26}$$

Using all the expressions derived above (equations 3.21 to 3.26) the resistance of the drive coil is expressed as:

$$R_d = \frac{\rho_d N_d \pi (r_1 + r_2)}{a_d} \tag{3.27}$$

Knowing the wire size and shape and the former size and shape, together with the possible range of the fitting factor k_f allows the model to fit the measured values of the test probe to the simulated values.

Similarly, the resistance of the pickup coil with an inner radius r_3, an outer radius r_4, a wire diameter d_p is derived using the same procedures as those used for the drive coil. They are summarised as:

$$a_p = \frac{\pi d_p^2}{4} \tag{3.28}$$

$$A_p = (r_4 - r_3) l_{pg} \tag{3.29}$$

$$N_p = K_f \frac{A_p}{a_p} \tag{3.30}$$

$$R_p = \frac{\rho_p N_p \pi (r_3 + r_4)}{a_p} \tag{3.31}$$

Inductance L_d of drive coil and L_p of the pickup coil

Expressions for the drive coil inductance, L_d (equation 3.33), and the pickup coil inductance, L_p (equation 3.34), are derived.

The inductance L of a solenoid coil is derived using coil dimensions and Maxwell's equations. For a solenoid coil with core cross sectional area A_c, height l and N number of turns, (see figure 3.4), the inductance of the solenoid is expressed as [70]:

$$L = \frac{\mu N^2 A_c}{l} \tag{3.32}$$

μ is the permeability of the material used for the wire.

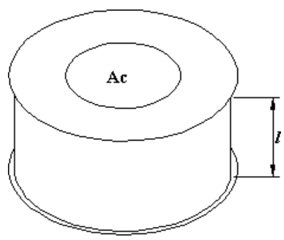

Figure 3.4: An illustration of solenoid dimensions

Therefore, L_d and L_p the inductance of the drive coil and the pickup coil are expressed as:

$$L_d = \frac{\mu_d N_d^2 A_{cd}}{l_{dg}} \tag{3.33}$$

$$L_p = \frac{\mu_p N_p^2 A_{cp}}{l_{pg}} \tag{3.34}$$

Where the subscripts d and p refer to the drive coil and pickup coil parameters respectively.

3.4 Specimen parameters

The specimen was modelled as resistance and inductance that interact with the induced eddy currents. A single resistance and inductance was used to represent the specimen. Figure 3.3 shows the cross sectional area occupied by the eddy currents. The currents occupy a ring with an inner radius and an outer radius similar to the drive coil dimensions. Aluminium is conductive and obeys Ohm's law and this law is used in the development of the expressions that characterise the specimen. The expression relating the dimensions of a conductor, to the resistance the conductor offers to an electric current (equation 3.21), also applies to the dimensions of the ring occupied by the circulating eddy currents. Therefore representing the specimen as a single resistance and inductance was deemed to be appropriate to characterise the conducting ring in the bulk aluminium specimen. However, care is taken to address changes in the ring dimensions that could be a result of various physical phenomena like skin effect and inner and outer radius paths within the specimen.

In this section, expressions for the electromotive force, $E_s(t)$ (equation3.36), induced in the specimen, the eddy current $i_s(t)$(equation 3.39) in the specimen and those of the specimen resistance, $R_s(t)$ (equation 3.59), and inductance, $L_s(t)$(equation 3.68), are derived using analytical methods.

3.4.1 Electromotive force induced in the specimen

The rolled aluminium sheet is a bulk piece of solid metal with no possible displacement currents. Aluminium is isotropic with a resistivity, ρ_s of 27 nΩm and a relative magnetic permeability μ_s of approximately one [71]. The analysis of the aluminium specimen is done at a macroscopic level, and therefore no atomic effects are considered.

The scenario in this study is an interface problem with a boundary between the industrial environment and the tested aluminium metal sheet. The environment is not conductive and it has a relative permeability μ_e of approximately one [71]. The primary magnetic field that is a result of the pulsating currents in the drive coil will therefore induce circulating eddy currents in the conductive aluminium specimen and not in the non-conductive environment.

The relative permeability of the environment and that of aluminium are both approximately one. Considering a field normal to the specimen surface, the magnetic fields in both media are therefore equal. Therefore, the magnetic field just at the entrance of the specimen is the same as that at the surface of the specimen and is expressed in equation 3.12 as $B_x(t)$.

The presence of the magnetic induction $B_x(t)$ incident perpendicular to the surface of the aluminium specimen induces an electromotive force (emf) in the specimen but not in the non-conductive environment. As discussed earlier, this emf results in circulating currents, commonly referred to as eddy currents, in the bulk aluminium body.

An expression for the electromotive force, $E_s(t)$, induced in the specimen is again derived by applying Faraday's law of induction and Lenz's law [27]. This is expressed mathematically as:

$$E_s(t) = -A_s cos\theta \frac{dB_x(t)}{dt} \tag{3.35}$$

A_s is the area cut by the flux density B_x and θ is the angle between the field B_x and the normal to the specimen surface.

Figure 3.3c represents the specimen network. The induced emf $\epsilon_s(t)$, in the time domain, is the sum of effects due to self inductance L_s, the resistance in the circuit R_s and the mutual inductances M_{sd} and M_{sp}. This is expressed as:

$$E_s(t) = R_s i_s + Ls\frac{di_s}{dt} + M_{sd}\frac{di_d}{dt} + M_{sp}\frac{di_p}{dt} \tag{3.36}$$

Representing the sources due to mutual inductances M_{sd} and M_{sp} and $v_{sd}(t)$ and $v_{sp}(t)$, equation 3.36 becomes:

$$E_s(t) = R_s i_s + Ls\frac{di_s}{dt} + v_{sd}(t) + v_{sp}(t) \tag{3.37}$$

Re-arranging equation 3.37:

$$R_s i_s + L_s \frac{di_s}{dt} = E_s(t) - v_{sd}(t) - v_{sp}(t) \tag{3.38}$$

The expression on the right hand side of equation 3.38 represent the secondary sources in circuit $\boldsymbol{c}$ of figure 3.3. The required solution for the pickup coil current $i_p(t)$ in equation 3.39 is found by applying Laplace transformation [67] to the equation and the inverse laplace transform yields the solution:

$$i_s(t) = (E_s(t) - v_{sd}(t) - v_{sp}(t))e^{\frac{R_s}{L_s}t} \tag{3.39}$$

The eddy currents are expressed in terms of the secondary sources $E_s(t)$, $v_{sd}(t)$ and $v_{sp}(t)$

3.4.2 Skin effect

The induced eddy currents expressed in equations 3.39 result in a secondary magnetic induction B_{xs} that opposes the primary magnetic field according to Lenz's law. This opposing field tends to screen the interior depth of the aluminium sheet from the applied field, and the total magnetic field decays exponentially with distance into the sheet. This phenomenon is known as the skin effect [72]. The characteristic decay length is termed the skin depth. The skin depth is defined as the depth at which the magnetic field decreases to *1/e* of its value at the surface of the specimen. The commonly used notation for the analysis of eddy current penetration $\delta(t)$, for a unit step, is expressed as [73]:

$$\delta(t) = \sqrt{\frac{4t}{\mu\sigma}} \tag{3.40}$$

For pulsed eddy currents, each applied waveform is characterised by a duty cycle (a time in a cycle when the pulse is present). Equation 3.40 shows that the penetration depth into the aluminium sheet depends on the time (duty cycle), magnetic permeability and conductivity of the sheet. The longer the duty-cycle of the pulse, the deeper the eddy currents will penetrate the specimen sheet. This agrees with Waidelich's findings [19, 29] that thicker aluminium specimens needed longer duration pulses to effect total penetration.

3.4.3 Eddy Currents and skin effect

The eddy current density decreases exponentially as the depth penetrated by the currents increases [72]. To express the current density as a function of the specimen thickness we use the definition of skin depth (section 3.4.2). At a depth $y = \delta(t)$, the current density $J(y,t)$ a function of time t and depth y will have decayed to *1/e* of the current density at the surface of the specimen. If $J(r)$ is the current density at the surface of the specimen at a radius r from the inner edge, at radius r of the eddy current ring (see Figure 3.1), the current density at depth y is expressed mathematically as:

$$J(y,t) = J(r)/e \tag{3.41}$$

For an exponential decrement of the current density as the depth of penetration increases, the current at a depth $y \leq \delta(t)$ is expressed as:

$$J(y,t) = J(r)e^{-y/\delta(t)} \tag{3.42}$$

The path on the inside edge of the ring is shorter than that on the outside edge with consequential higher current density on the inside edge of the eddy current ring. This can be approximated by inverse relationship between the current density $J(r)$ and the radius r increasing from the inner radius r_1 to the outer radius r_2 of the conducting ring and is expressed mathematically as:

$$J(r) = \frac{K}{r} \tag{3.43}$$

To get the actual current density $J(r,y,t)$, a function of eddy current ring radius, depth into specimen and time, we combine the current density $J(y,t)$ a function of depth and time (equation 3.54) and $J(r)$ a function of the eddy current ring radius (equation 3.55). $J(r,y,t)$ becomes:

$$J(r,y,t) = \frac{K}{r}e^{-y/\delta(t)} \tag{3.44}$$

The total eddy current, $i_s(t)$, induced in the specimen is derived from equation 3.44 by finding the integral of the varying eddy current density both radially and into the thickness of the specimen. For an infinitely thick specimen, the total eddy current within the eddy current ring of an inner radius $r1$ and an outer radius r_2 can be expressed as:

$$i_s(t) = \int_{r_1}^{r_2} \int_{-\infty}^{0} J(r, y, t) \, dy \, dr \tag{3.45}$$

Substituting for $J(r, y, t)$ (equation 3.45), and solving for $i_s(t)$ for a specimen with a thickness y is done in the following steps:

$$i_s(t) = \int_{r_1}^{r_2} \int_{y}^{0} \frac{K}{r} e^{-y/\delta(t)} \, dy \, dr \tag{3.46}$$

Re-arranging equation 3.46 and finding the integrals for the indicated limits

$$i_s(t) = \int_{r_1}^{r_2} \frac{K}{r} \int_{y}^{0} e^{-y/\delta(t)} \, dy \, dr \tag{3.47}$$

$$i_s(t) = \frac{K}{r} rln \frac{r_1}{r_2} \delta(t)(1 - e^{-y/\delta(t)}) \tag{3.48}$$

The total induced eddy current at an instant in time $i_s(t)$ is written in terms of the current density $J(r, y, t)$ by substituting $J(r, y, t)$ in equation 3.60 using equation 3.56 to get equation 3.61.

$$i_s(t) = J(r, y, t)\delta(t)r.ln \frac{r_1}{r_2} \left(\frac{1}{e^{-y/\delta(t)}} - 1 \right) \tag{3.49}$$

The expression for the eddy currents given in equation 3.49 takes the skin effect into consideration and is used to arrive at equations that present mathematical expressions of the specimen resistance R_s and self inductance L_s of the specimen.

3.4.4 Resistance presented by the specimen to the eddy currents

Equations for the specimen resistance R_s (equation 3.59) and specimen inductance L_s (equation 3.68) are derived in this section.

Aluminium is resistive and obeys Ohm's law. A potential difference $\triangle V$, a result of the emf $\epsilon_s(t)$ induced in the specimen by the primary magnetic field is maintained in the specimen resulting in the circulating eddy currents $i_s(t)$ (equation 3.39). For a uniform conductor of a length l, the potential difference is related to the induced emf by:

$$\triangle V = \epsilon_s(t)l \tag{3.50}$$

Ohm's law written in terms of resistivity ρ yields:

$$J(r, y, t) = \frac{\triangle V}{\rho_s l_{ed}} \tag{3.51}$$

where ρ_s is the resistivity of the aluminium specimen, l_{ed} is the eddy current path length in the specimen. Equation 3.63 is re-arranged to give:

$$\triangle V = \rho_s l_{ed} J(r, y, t) \tag{3.52}$$

The potential difference $\triangle V$ is related to the total eddy current $i_s(t)$ and the resistance presented by the specimen R_s by:

$$\triangle V = i_s(t) R_s \tag{3.53}$$

Equating equations 3.52 and 3.53 and substituting for $i_s(t)$ (equation 3.49) yields:

$$\rho_s l_{ed} J(r, y, t) = J(r, y, t)\delta(t) r.ln\frac{r_1}{r_2}\left(\frac{1}{e^{-y/\delta(t)}} - 1\right) R_s \tag{3.54}$$

Geometric mean radius of the eddy current conducting ring r_o

The path of the inner radius of the ring is shorter than that of the outer radius and therefore the resistance on the inner radius is lower. Hurley and Duffy [54] showed that an integration of the current density between the inner radius $r1$ and outer radius r_2 of a planar section when the width to height ratio $w : h$ moving away from 1 with w greater than h, an equal current division occurs at the radius given by the geometric mean (GM)r_o of the inner and outer radius and it is given by the expression:

$$r_o = \sqrt{r_1 r_2} \tag{3.55}$$

The eddy current path l_{ed} through which the eddy currents follow, signifies the length of the conductor in equation 3.66 and it is quantified as a function of the geometric mean radius as:

$$l_{ed} = 2\pi r_o \tag{3.56}$$

The formula for the specimen resistance R_s is obtained after reducing equation 3.66 and substituting the radius with the geometric mean radius r_o.

$$R_s = \frac{\rho_s l_{ed}}{\delta(t)\left(\frac{1}{e^{-y/\delta(t)}} - 1\right) r_o.ln\frac{r_1}{r_2}} \tag{3.57}$$

Temperature changes in the specimen

The resistivity of a conductor ρ varies approximately linearly with temperature over a limited temperature range [74, 75]. Let ρ_{sT1} be the resistivity of the specimen at temperature T_1 and ρ_{s20} the resistivity of the specimen at 20^oC, then:

$$\rho_{sT1} = \rho_{s20}(1 + \alpha T_1 + \beta T_1^2 + \gamma T_1^3....) \tag{3.58}$$

Substituting for resistivity at a temperature T_1 into equation 3.57, the resistance presented by the specimen to the eddy currents at temperature T_1 is expressed as:

$$R_{sT1} = \frac{\rho_{sT1} l_{ed}}{\delta(t)\left(e^{y/\delta(t)} - 1\right) r_o.ln\frac{r_1}{r_2}} \tag{3.59}$$

3.4.5 Inductance presented by the specimen to the eddy currents

The equation 3.59 is completely equivalent to the expression for the resistance of a conductor with length and cross-sectional area. Let a_s be the cross-sectional area occupied by the eddy currents then:

$$R_{sT1} = \frac{\rho_{sT1} l_{ed}}{\delta(t)\left(e^{y/\delta(t)} - 1\right) r_o.ln\frac{r_1}{r_2}} \equiv \frac{\rho l_{ed}}{a_s} \tag{3.60}$$

This implies that the area a_s cut by the eddy current flow can be expressed as:

$$a_s = \delta(t)\left(e^{y/\delta(t)} - 1\right) r_o.ln\frac{r_1}{r_2} \tag{3.61}$$

This area that cuts the eddy current flow is assumed to be approximately rectangular for the conditions when the thickness is less than or equal to the skin depth (see figure 3.1), the sides of the rectangle will take on the dimensions $\delta(t)\left(e^{y/\delta(t)} - 1\right)$ as the depth y changes and $r_o.ln\frac{r_1}{r_2}$ as the radii r_1 and r_2 vary.

The self inductance expressed as a function of the total flux $\Phi_s(t)$ and the eddy current change that it opposes $i_s(t)$ is [68, 69]:

$$L_s = \frac{\Phi_s(t)}{i_s(t)} \tag{3.62}$$

The total flux expressed in terms of the flux density B_x and the area A_s it cuts is:

$$A_s(t) = \pi r_1^2 \tag{3.63}$$

$$\Phi_s(t) = B_x \pi r_1^2 \tag{3.64}$$

Also the magnetic flux density B_x is related to the current by the expression:

$$\oint B_x(t)ds = \mu_s i_s(t) \tag{3.65}$$

Using the dimensions of the area cut by the eddy currents a_s,

$$\oint ds = 2\left(\delta(t)(e^{y/\delta(t)} - 1) + r_o \ln\frac{r_2}{r_1}\right) \tag{3.66}$$

The magnetic field B_x around the eddy current ring derived using equations 3.65 and 3.66 can be expressed in terms of the radial and depth parameters of the eddy current conducting ring.

$$B_x(t) = \frac{\mu_s i_s(t)}{2\left(\delta(t)(e^{y/\delta(t)} - 1) + r_o \ln\frac{r_2}{r_1}\right)} \tag{3.67}$$

Substituting for $B_x(t)$ in equation 3.64 and for Φ_s in equation 3.62 yields expression for the specimen inductance L_s:

$$L_s = \frac{\mu_s \pi r_1^2}{2\left(\delta(t)(e^{y/\delta(t)} - 1) + r_o \ln\frac{r_2}{r_1}\right)} \tag{3.68}$$

3.4.6 Moving Specimen and Stationary Probe

The rolling process implies a moving specimen as opposed to a stationary one (chapter 1). To investigate the effects of a moving specimen on the received pickup coil signal, an analysis of these effects is carried out in this section.

The majority of eddy current applications involve moving media. Eddy currents can be created by relative motion between the magnetic field lines and the medium. This condition leads to an additional term in equation 3.47 [68]. Eddy currents can therefore be produced by two mechanisms of induction:

- Eddy currents induced by time-varying excitation and represented by the term $\frac{\partial H}{\partial t}$ or $\frac{\partial B}{\partial t}$
- Eddy currents induced by motion and represented by the term $curl(v \times H)$ or $curl(v \times B)$

Moon [76] uses a magnetic Reynolds number R_m to evaluate the type of eddy currents that dominate.

$$R_m = \sigma \mu L v \tag{3.69}$$

where L is the characteristic length of the body in contact with the magnetic field lines, σ and μ are the conductivity and the permeability of the body and v is the relative velocity between the body and the field. If R_m is small the eddy currents induced by time-varying excitation prevails while for large values of R_m, the effects of motion dominate. When R_m is of the order unity neither of the two effects can be ignored.

With R_m as the determining factor for the predominant eddy current type present in the specimen, considering the characteristic length L of the specimen in contact with the primary field and the maximum velocity of the tested specimen (section 1.1), R_m is of the order 10^{-2}. This value is much smaller than unity and the eddy currents induced by time-varying excitation prevail over those induced by motion.

To verify this, experiments were carried out using a longer specimen. The specimen was 1000 mm long. To begin with, voltage readings were recorded across the pickup coil circuit output resistance with the coil kept stationary. Then observations were made on the received signal with the coil moving at speeds between 0 mm and 150 mm per second (see Appendix A). Results agreed with the prediction that there should be no observable effects on the received signal due to specimen movement. Therefor, a quasi-static approximation was adopted for the model.

3.5 Summary and Conclusion

A model for the pulsed eddy current system envisaged for this application has been developed and presented. The system is seen as electrical circuits coupled to each other by principles of electromagnetism. Mathematical expressions for the various aspects of the model have been derived. The dynamics involved in the whole scenario have been addressed. An investigation on sheet movement resulted in the assumption of a quasi-static approximation for the system. Effects of temperature changes have been explored and included in the developed expressions. Limitations presented by the concept of skin effect have been considered using analytical methods. Skin effect affects the final expression for the resistance and inductance of the specimen as the thickness of the material changes. The expressions are a function of skin depth $\delta(t)$, which in turn is a funcion of time t. The derived formulae are consolidated in chapter 4, carefully considering their interrelationships and arriving at a complete model that was used in a simulation study presented in chapter 6. The model is validated in chapter 5 and a discussion on differences in experiment and simulated results are compared with an analysis of the errors that are presented by the model in the same chapter. The equations developed to represent the specimen give PEC signals that match perfectly with results from experiments, for the time periods considered in the signal analysis process.

Chapter 4

MATLAB AND SIMULINK SIMULATION ENVIRONMENT

4.1 Introduction

The mathematical expressions developed for the pulsed eddy current system in chapter 3 were converted into an interactive simulation environment using Matlab and Simulink [77, 78, 79]. Most of the expression were dynamic first order differential equations. Background on solving such expressions stems from Laplace transforms [67]. Subsystems were represented by transfer functions. The transfer functions are defined as the ratio of the Laplace transform of the output to the Laplace transform of the input, provided the initial conditions are zero[67, 80]. These were interlinked with differentiation, gain, product, summing, source and sink blocks, offered by the Simulink environment; and used to weave the system model in order to achieve its dynamic electromagnetic nature. The ultimate outcome of this exercise was a simulation environment that was used as a tool for further investigative exercises.

4.2 Simulink model

Simulink works with transfer functions to give a solution to a dynamic system. The environment has a source library that offers possible signal sources that can be used to test the model [77, 78, 79]. The pulsed eddy current system model uses the pulse generator as the source to the system. It also provides a linear library that includes blocks that emulate linear mathematical expressions. System transfer functions, state-space representations, simple gain, summers, derivatives, integrators, products are among possible blocks that can be interconnected to represent systems in a Simulink environment [77, 78, 79]. Simulink block diagrams use lines to represent pathways for signals between blocks in a model. As the model increases in complexity, it can be simplified by grouping blocks into subsystems. This facility allows for the reduction in the number of blocks displayed, the keeping of functionally related blocks together and the establishment of hierarchy. Block interconnection can also be achieved by the use of a tag system [77, 78, 79]. This reduces the use of interconnecting pathways within blocks and subsystems.

Simulink and Matlab were used together to create the simulation environment. Variable parameters together with mathematical expressions that represent their relationships were entered in the Matlab command window as an m-file. Variable parameters, defined as those parameters that can be manipulated by choice of component dimensions or component materials, formed the basis of all other calculated parameters that were vital to the simulation, analysis and visualization of model results. A block diagram and a Matlab m-file are the outcome of the development and are presented in Appendix C.

Considering the electrical circuit used to model the PEC system and shown in figure 3.3, the current $i_d(t)$ from the primary source $v_d(t)$ is generated from the simulink environment when the said voltage is connected as an input to the transfer function of network a of figure 3.3. Equation 4.1 is a first order differential equation representing the electrical behaviour of this network. Its Laplace transform is given in equation 4.2.

$$v_d(t) = R_T i_d + Ld\frac{di_d}{dt} + v_{dp}(t) + v_{ds}(t) \tag{4.1}$$

The drive coil current $i_d(t)$ is the output of network a and the voltages $v_d(t)$,

$v_{dp}(t)$ and $v_{ds}(t)$ represent the input.

$$V_d(s) = R_T I_d(s) + sL_d I_d(s) + V_{dp}(s) + V_{ds}(s) \tag{4.2}$$

Manipulating this algebraic expression gives the transfer function as:

$$\frac{I_d(s)}{V_d(s) - V_{dp}(s) - V_{ds}(s)} = \frac{1/L_d}{s + R_T/L_d} \tag{4.3}$$

Equations 4.3 is the transfer function of a system represented in figure 4.1.

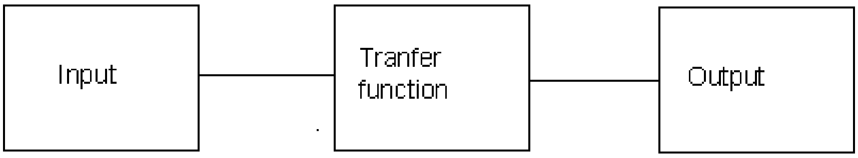

Figure 4.1: System block diagram

Equation 4.3 is represented by the blocks in the diagram of figure 4.1 as indicated below:

- The sum of the pimary and secondary voltage soures $V_d(s) - V_{dp}(s) - V_{ds}(s)$ is the input
- $\frac{1/L_d}{s+R_T/L_d}$ is the transfer function
- $I_d(s)$ is the output

Similarly, the expressions for the induced electromotive force in the pickup coil network b of figure 3.3 and that in the specimen network c of the same figure, included here as equations 4.7 and 4.8,

$$E_p(t) = R_p i_d + Lp\frac{di_p}{dt} + v_{pd}(t) + v_{ps}(t) \tag{4.4}$$

$$E_s(t) = R_s i_s + Ls\frac{di_s}{dt} + v_{sp}(t) + v_{sd}(t) \tag{4.5}$$

would result in expressions for their respective transfer functions given in equations 4.6 and 4.7.

$$\frac{I_p(s)}{E_p(s) - V_{pd}(s) - V_{ps}(s)} = \frac{1/L_p}{s + R_p/L_p} \tag{4.6}$$

$$\frac{I_s(s)}{E_s(s) - V_{sp}(s) - V_{sd}(s)} = \frac{1/L_s}{s + R_s/L_s} \tag{4.7}$$

The induced electromotive forces E_p and E_s are functions of the derivatives of magnetic field $B(t)$ (equation 4.9) and $B_x(t)$ (equation 4.8) respectively. They are represented with the use of derivative blocks available in the Simulink environment. The magnetic fields $B(t)$ and $B_x(t)$ are functions of the drive current $i_d(t)$.

$$B_x(t) = \frac{\mu_o N_d i_d(t) {r_1}^2}{2(x^2 + {r_1}^2)^{3/2}} \tag{4.8}$$

$$B(t) = \frac{\mu_o N_d i_d(t)}{2r_1} \tag{4.9}$$

Also the secondary sources due to the mutual inductances of the three networks in figure 3.3, $v_{dp}(t)$, $v_{ds}(t)$ are functions of either one of the three currents $i_p(t)$, $i_s(t)$ and $i_d(t)$. These are represented by differentaition blocks in the simulink environment with the indicated curents as the inputs to these blocks. Equations 4.10 and 4.11 are example equations of these secondary sources.

$$v_{dp} = M_{dp}\frac{di_p}{dt} \tag{4.10}$$

$$v_{ds} = M_{ds}\frac{di_s}{dt} \tag{4.11}$$

Transfer function blocks available in Simulink were used to achieve the solutions for the currents (figure 4.1). Appropriately interlinking the solutions from these block with gain blocks used together with product, addition and difference blocks resulted in an interlinked model for the PEC system. During the simulation process, all calculations for the various model parameters developed in chapter 3 are carried out by Matlab and are then made available to Simulink through the software workspace resource.

Some of the mathematical expressions modelled by Simulink graphical environment are presented in appendix C in figures C.1 to C.6. These are given as an example of the decreasing hierarchy typical to the Simulink environment and used in the development of the simulation environment.

4.2.1 Simulink solvers

Simulink simulates a dynamic system by computing its states at successive time steps over a specified time span, using information provided by the model. The process of computing the successive states of a system from its model is what is referred to as solving the model[78, 79]. Simulink provides a set of programs, known as solvers. Each have a particular approach to solving the model. These solvers are either fixed-step continuous solvers or variable-step continuous solvers. Both types of solvers compute the time of the next step by adding a step size to the time of the current time. The step sizes for the fixed-step continuous solver are fixed, and the accuracy of the solver depends on choosing small enough step sizes that accommodate all significant changes in the system. Those of the variable-step size continuous solver vary. They are reduced to increase, accuracy when a model's states change rapidly and increased to avoid taking unnecessary steps when the model's states change slowly

In order to decide on a solver for the modelled system experimentation with the various solvers offered by Simulink is advised by the program developers. After experimenting with the various solvers offered by Simulink, the investigated pulsed eddy current system required a variable-step size continuous solver, a solver based on an explicit Runge-Kutta [58] formula. It is a one step solver in that when computing a function $y(t_n)$, only the solution at the immediately preceding time $y(t_{n-1})$, is needed.

4.2.2 Runge-Kutta method

The Runge -Kutta method [58] is the numerical method used by the Simulink model to solve differential equations. It yields approximate numerical values of the solution. A method like the Runge-Kutta may be applied if a differential equation cannot be solved by an exact method, but in this case, it is applied because an electronic computer is used to solve differential equations in the developed Simulink model. In each step h of this method, four auxiliary quantities are computed and using them, a new value is computed [58].

The truncation error [79] is of the order h^5 and the method is therefore, a fourth-order method.

4.2.3 Finite element method and Simulink solvers

In section 2.6 and 3.2, it was noted that many researchers have used finite element analysis to characterise the effect of the induced eddy currents on the primary field due to the reflected field of the conducting medium [50, 51, 52]. It was also noted that finite element approach is a numerical method [55, 56, 57] that provides solutions to problems that would otherwise be difficult to solve. It is further noted that these problems are normally represented by partial differential equations (PDE) or as intgeral equations and that the approach either completely elimimates the PDE leading to a steady state problem, or it approximates the PDE to ordinary differential equations (ODE) that are then numerically solved using standard techniques such as Runge-Kutta [58].

The model that was developed in chapter 3 was mostly represented by first order ordinary differential equation (ODEs) that expressed the electrical behaviour of the model network. The finite element approach approximates PDEs to ODEs and then numerically solves using standard techniques. Matlab and Simulink solvers are based on Runge-Kutta method and was therefore a good approach to characterise the the PEC system effects.

4.3 Variable parameters

4.3.1 Solenoid parameters (Drive coil or pickup coil)

As is mentioned by some researchers [33], the choice of coil dimensions is important in an application. Transient locus (time constant) is dependent on the coil dimensions and therefore the choice of these parameters is vital to the system's performance. Parameters that could be varied for a solenoid included:

- Diameter of the wire conductor used for the windings (d_d or d_p)
- Resistivity of the wire material (ρ_d or ρ_p)
- Fill factor (k_f), (see appendix A)
- Permeability of the solenoid core material (μ_d or μ_p)
- Inner radius of the solenoid (r_1 or r_3)
- Outer radius of the solenoid (r_2 or r_4)
- Length of the solenoid (l_{dg} or l_{pg})

4.3.2 Specimen parameters

The specimen parameters that could be varied included:

- Thickness (y)
- Permeability (μ_s)
- Resistivity (ρ_s)
- Temperature (T)
- Wobble angle (θ)
- Temperature coefficient (α and β)
- Skin depth($\delta(t)$)

4.3.3 Other variables

The distance of separation between the probe and the specimen, referred to as the lift-off (x), is another variable that was considered in the model.

4.4 Calculated parameters

Some parameters used in the model were calculated from the variable parameters. Matlab was used to effect the calculations and most of the results from these calculations were used in the analysis carried out in chapter 8. By using Matlab programming syntax, mathematical expressions derived in the previous chapter were processed to give solutions for the calculated variables. These calculated parameters are manipulated by the choice of the parameters referred to as variable. Chapter 3 was committed to deriving mathematical expressions that model such parameters.

4.5 Summary and Conclusion

The development of a Matlab/Simulink simulation environment has been described in this chapter. Various mathematical expressions developed in chapter 3 have been consolidated to a complete PEC simulation environment. The developed environment emulates the PEC system as a whole. Equations that express the character of system components were ordinary differential equations. Matlab and Simulink solvers, based on the Runge-Kutta technique were therefore a good choice for the simulation environment. The model is validated against experimental data in chapter 5 and a simulation study is carried out on pulsed eddy currents and their possible use in profile thickness gauging in aluminium hot rolling mills in chapter 6.

Chapter 5

VALIDATING THE PEC SYSTEM MODEL

5.1 Introduction

A report on the validation of the simulation environment developed in the previous chapters is given in this chapter. Validations were carried out against data received from experiments. Various investigative experiments were carried out to facilitate the comparison between simulated data and data obtained from experiments in order to make the validation of the developed model possible. The PEC system model was validated as a whole by observing the signal received from the pickup coil using simulations that emulated the experimental environment. Results observed at the pickup coil both experimentally and by simulation are an indication of the validity of the model as a whole.

The process started with the comparison between measured and calculated values of the various parameters that make up the test probe used in the study. These parameters include:

- coil resistances
- coil inductances

- Number of coil turns

A good fit of these probe parameters allowed for an initial run of experiments to be carried out in order to establish the validity of the modelled probe. These were experiments and simulations carried out on the test probe in the absence of any specimen. These experiments and simulations assisted in setting the factors k_f and the coupling factors k_{pd}, k_{ps} and k_{ds} that are discussed in the modelling process documented in chapter 3. These factors are fitting factors necessary to take into account the circular cross section of the wire used to wind the coil fitting into the rectangular cross sectional area of the coil dimensions.

After ascertaining that the probe signals harnessed from the model simulation and those harnessed from the experiments fitted satisfactorily, other experiments and simulations could then be carried out to validate the model for the various features reported in literature by other researchers. Also comparisons between results from experiments and those from simulations were carried out on the effects of specimen temperature and thickness on the test probe signals. These served as a basis to justify the model for the simulation studies carried out in chapter 6. Experiments included Pulsed eddy current tests on:

- an aluminium sheet with constant thickness (3 mm) at constant temperature (room temperature of about 25^{o}C) and the probe placed at varying lift off distances (1 mm to 6 mm) in steps of 1 mm.
- an aluminium sheet with a constant thickness (1 mm, 2 mm or 3 mm) with the probe placed at a constant lift-off distance (1.2 mm) from the specimen. The specimen temperature dropping from 300^{o}C to 25^{o}C in steps of 50^{o}C.

5.2 Equipment used for measurements, experiments and simulations

5.2.1 Measurements

A reflection test probe was used for this study. Resistances of this probe were measured using Kiethley 2400 source meter [81]. This is a four-wire system with the following specifications:

- Source voltage 5 μV - 210 V
- Measured voltage 1 μV - 211 V
- Source Current 50 pA - 1.05 A
- Measure current 10 pA - 1.05 A
- Measured resistance 100 $\mu\Omega$ -211 MΩ
- Maximum source power 22 W
- Accuracy for 20 Ω range, 0.10% + 0.003 Ω, within 1 year of claibration
- Calibration date 2006

5.2.2 Simulations

Simulations were carried out using a personal computer. Calculations were done using the Matlab environment. These values now available to the Matlab workspace were used by the developed Simulink model in the simulation process. After a simulation, the output from the Simulink model was made available to the Matlab workspace and the collected data exported to other environments or used within the Matlab environment to validate the model output against experimental results.

5.2.3 Experiments

The setup for experiments used in this study is shown as a block diagram in figure 5.1. A Sampo 1617 function generator, with an internal resistance of 50 Ω, was connected through a signal conditioning circuit to the eddy current reflection probe. The probe was placed on the tested specimen and the voltage across the pickup circuit output resistance R_{out} was collected using a PC30FA, 11 channel data collection card, with an input range of -5 to +5 volts and an input impedance of 500 MΩ. The data was stored on the personal computer for further processing.

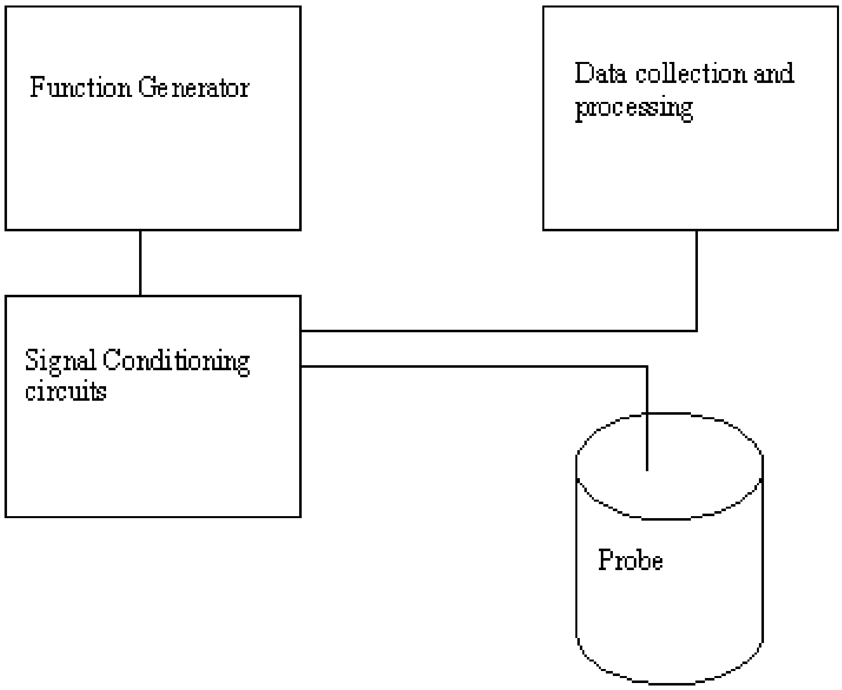

Figure 5.1: Block diagram of the Pulsed eddy current setup used in this study.

5.3 Results and observations

5.3.1 Measured and calculated parameters of the test probe

Table 5.1 shows the measured and calculated values of the parameters of the reflection probe used for the experiments.

Table 5.1: Measured values and calculated values for the reflection probe used in this study

	Drive coil		Pickup coil	
	Measured	Calculated	Measured	Calculated
Wire diameter (mm)	0.18	-	0.18	-
Inner radius (mm)	6.35	-	4.25	-
Outer radius (mm)	8.75	-	6.35	-
Resistance (Ω)	17.6	17.597	10.9	10.899
Inductance (mH)	-	1.56	-	0.53
Coil length (mm)	9	-	9	-
Lift-off (mm)	1	-	1	-
Wire length (m)	25	25	15	15.4
Number of turns	530	537	464	474
Time constant (ms)	-	1.15	-	0.06

It is observed that measured parameter values and those predicted by the model are in close agreement. The difference between measured and calculated:

- coil resistances is less than 0.005 Ω
- Number of coil turns is up to 10 turns

5.3.2 Validating the test probe

An initial run on the PEC system was made in the absence of a specimen in order to set the model fitting factors, developed for the probe, in chapter 3. The k_f factors for the drive coil and the pickup coil, k_{fd} and k_{fp} were set at 0.785 and 0.791 respectively. The coupling factor k_{pd} was set at 0.69. Data from simulations and from experiments for the pickup coil signal, was compared. Results from experiments and simulations together with the difference between the two plots are presented on the same graph shown in figure 5.2. The plot of the excitation was not included due to the fact that the amplitude of the pickup coil signal was much lower than that of the excitation signal. To make observations on the pickup coil signal it was necessary to focus on it alone. The following observations were made:

- The maximum difference between the two signals happens at 0.006 ms after the start of the duty cycle period and is 0.292 V. The value of the signal from the experiments, at this time is 1.418 V. The difference is therefore 20% of the signal received from the experiments at this time (0.006 ms).
- From 0.07 ms after the start of the duty cycle, the difference between the two signals is 0.000 $\pm$0.004 V which is 0.5% of the value received from the experiments at 0.07 ms.
- Significant differences between the two signals happen in the early times of the received signalduty cycle period.
- The simulated signal and the signal from experiments therefore correlate in the later times of the received signal period starting at 0.07 ms from the start of the duty cycle.

These results make the model developed for the test probe acceptable for the later times of the received signal. This is the section of the period investigated by this study in order to isolate changes in the thicknesses of the specimen from the information delivered by the received signal (see chapter 2). The test probe model is therefore acceptable for further study.

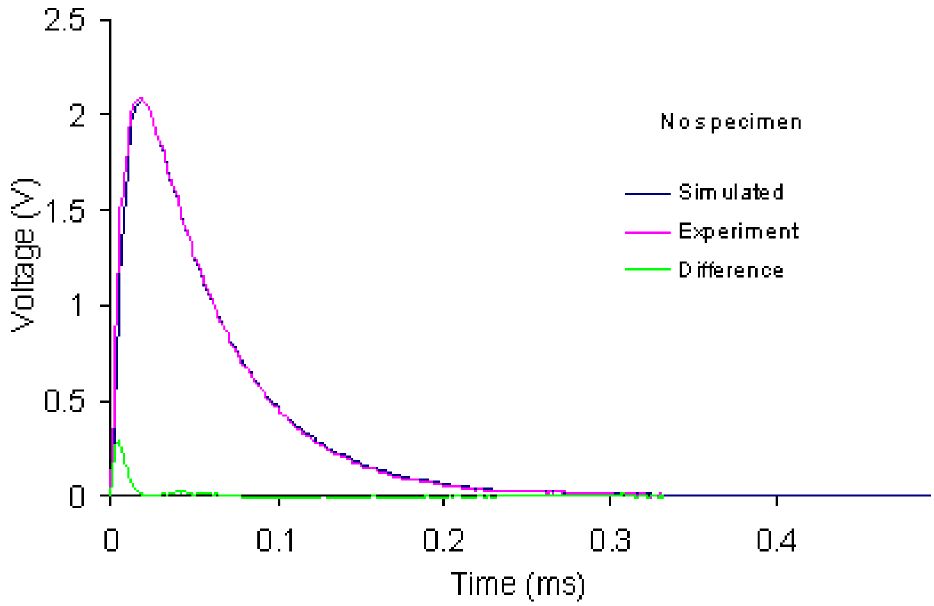

Figure 5.2: Experiment and simulated pickup coil signal with no specimen present.

5.3.3 Varying liftoff distances

Simulations for different lift-off distances on a 3 mm thick aluminium specimen at room temperature (25^{o}C), were carried out to validate the modelled system against trends observed by other researchers as well as results from experiments carried out for the study. Figures 5.3 and 5.4 show the results from experiments and the simulations.

The trends from simulated data are similar to those observed by other researchers.

- As observed by other researchers, the amplitude of the received signal increases as the lift-off distance increases tending toward that received without the presence of a specimen.
- Also, a crossing point is observed for varying lift-off distances both for the simulated and the experiment signals. The experiment LOI is at 0.156 ms and the simulated one at 0.149 ms.

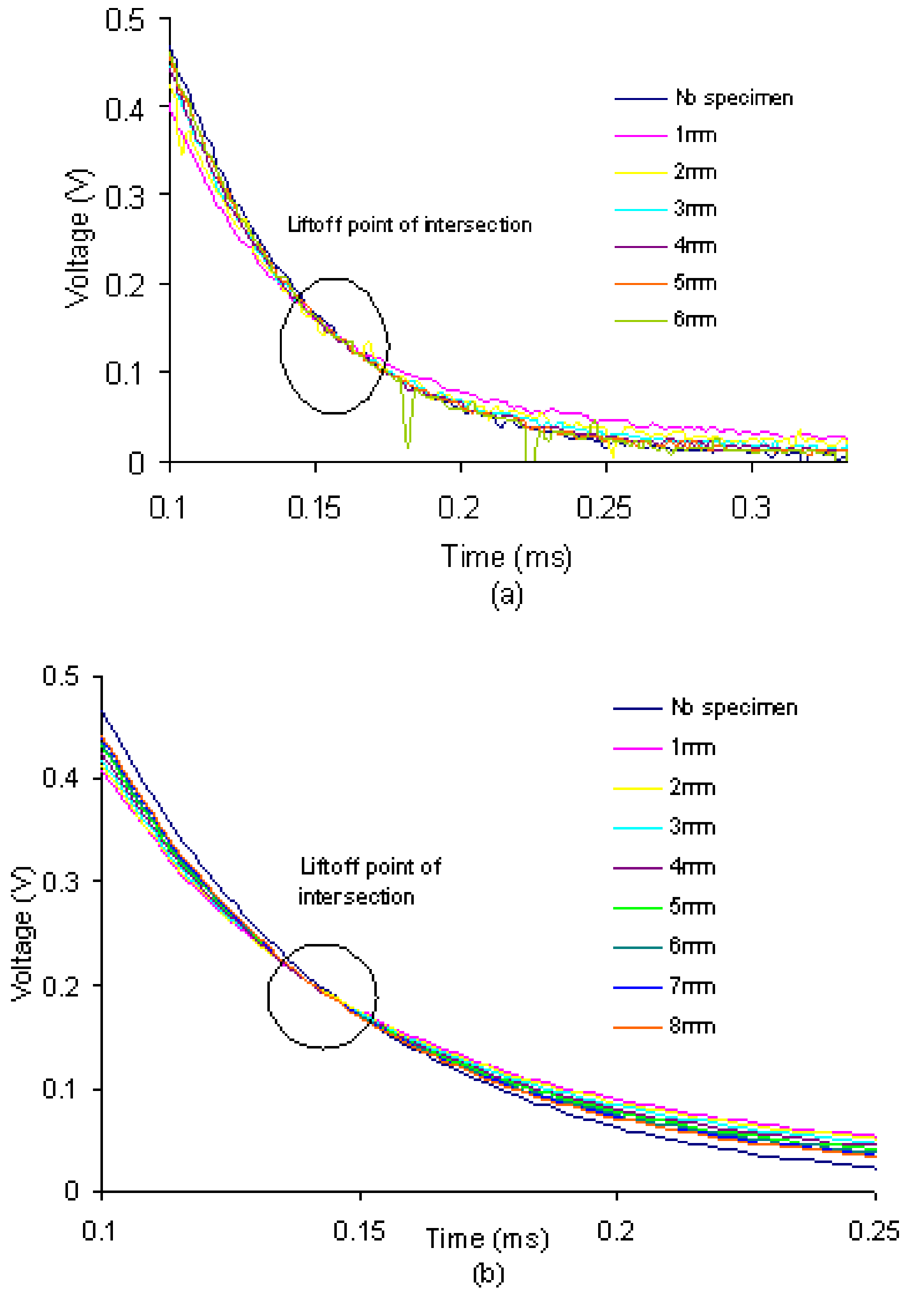

Figure 5.3: LOI observed on pickup coil signal received from (a)experiments and (b) simulations, with the probe placed on a 3 mm thick aluminium specimen at varying liftoff distances.

It is also observed that for the data received from experiments, the signals for lift-off distances of 5 mm, 6 mm and for when there is no specimen, overlap. This may indicate that as the lift-off increases, the effect of the specimen on the coil tends to become negligible.

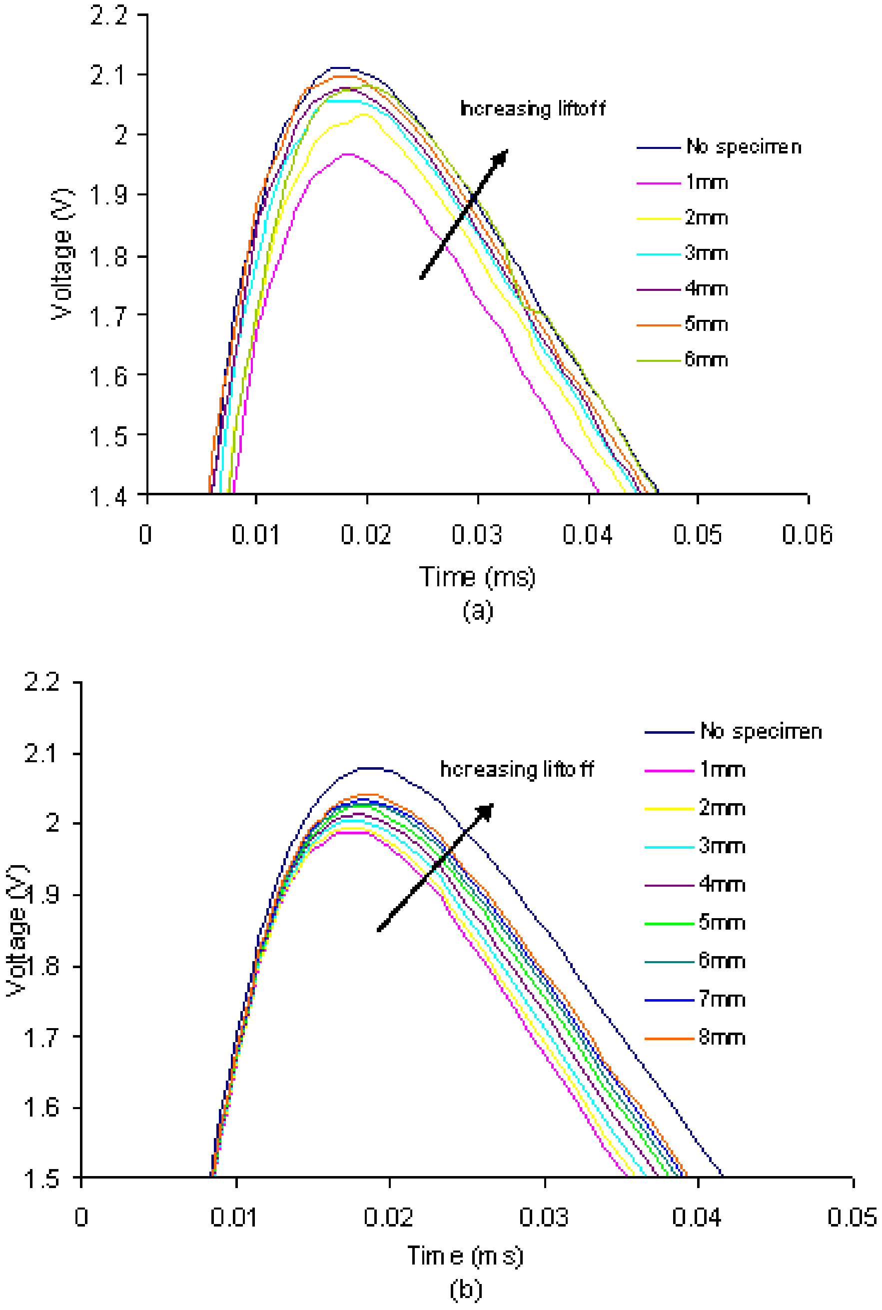

Figure 5.4: Amplitude variation in received pickup coil signal due to changes in lift-off; (a) experiment and (b) simulation results.

5.3.4 Varying specimen thicknesses and specimen temperature

Results from experiments are compared with those that are simulated for varying specimen temperatures at a constant specimen thickness. The specimen thicknesses considered included 1 mm, 2 mm and 3 mm thick aluminium plate. The probe was placed at a constant lift-off distance of 1.2 mm. The specimen was cooled from 300^0C to 250C (room temperature). The pulsed eddy current signals were observed for temperatures between 30^0C and 200^0C and results were recorded in steps of 50^0C. Samples of these results are presented in figures 5.5 to 5.7. The following observations were made:

- For all sampled results, from 0.09 ms, the difference between the simulated signal and the signal received from experiments varies from 0.000 V to 0.000 $\pm$0.003 V.
- For all sampled results, significant differences in the two signals happen in the early times of the received signal period.
- Therefore, during the later time of the received signal period, there is a good correlation between the simulated signal and the signal from experiments. This is the section of the period that is of interest for this study.

The simulated results and the results from experiments again confirm that the representation of the specimen with varying temperature is acceptable.

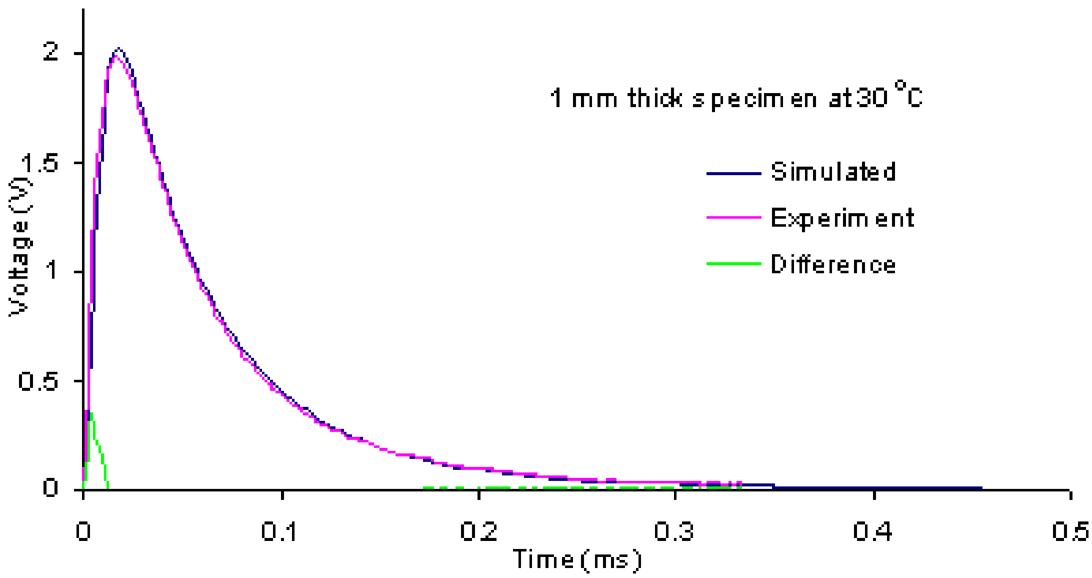
1 mm thick specimen at 30 °C
Simulated
Experiment
Difference
Voltage (V)
Time (ms)
0
0.5
1
1.5
2
0.1
0.2
0.3
0.4
0.5

(a)

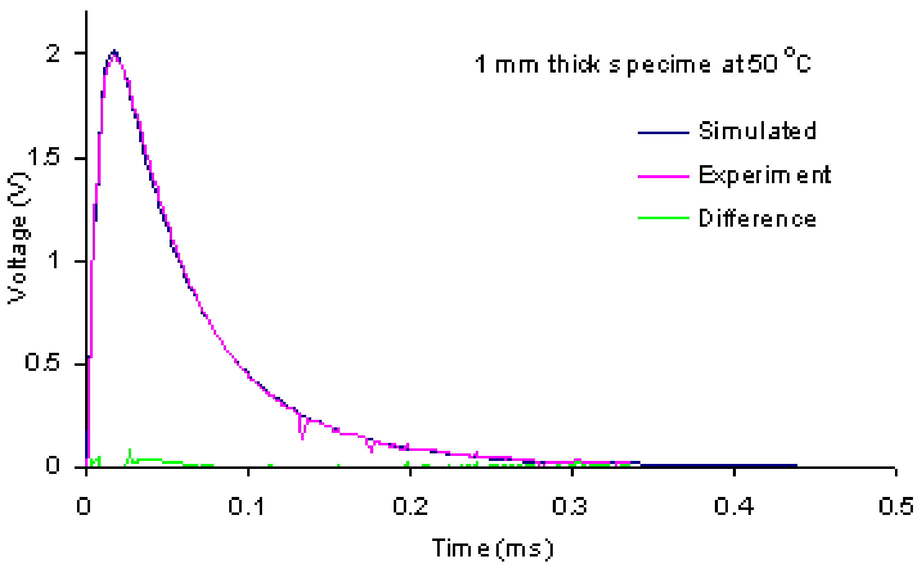
1 mm thick specime at 50 °C
Simulated
Experiment
Difference
Voltage (V)
Time (ms)
0
0.5
1
1.5
2
0.1
0.2
0.3
0.4
0.5

(b)

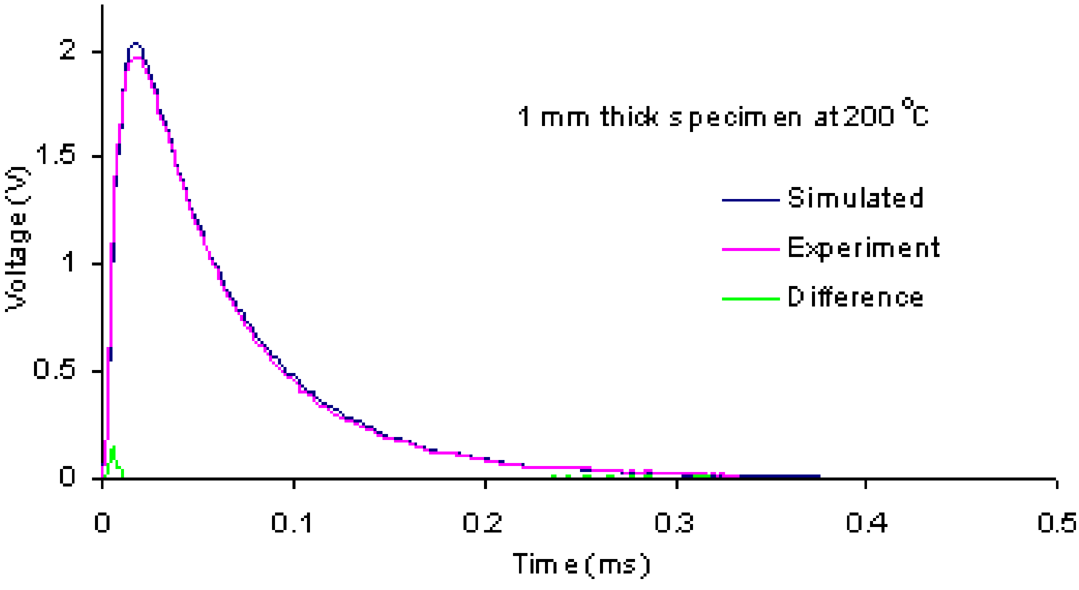

(c)

Figure 5.5: Simulated results compared with results from experiments for a 1 mm thick specimen at different temperatures.

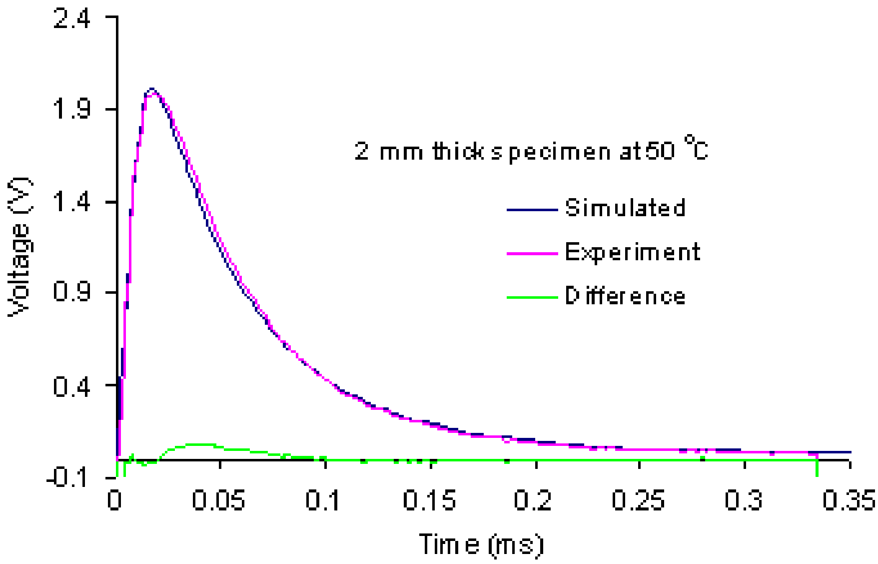

2.4
1.9
1.4
0.9
0.4
-0.1
Voltage (V)
2 mm thick specimen at 50 °C
Simulated
Experiment
Difference
0
0.05
0.1
0.15
0.2
0.25
0.3
0.35
Time (ms)

(a)

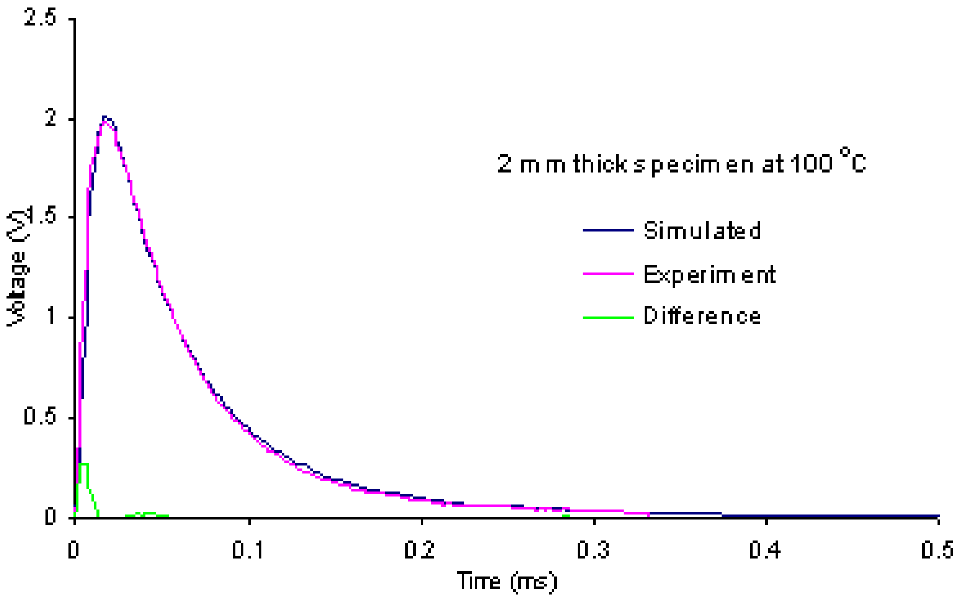

2.5
2
1.5
1
0.5
0
Voltage (V)
2 mm thick specimen at 100 °C
Simulated
Experiment
Difference
0
0.1
0.2
0.3
0.4
0.5
Time (ms)

(b)

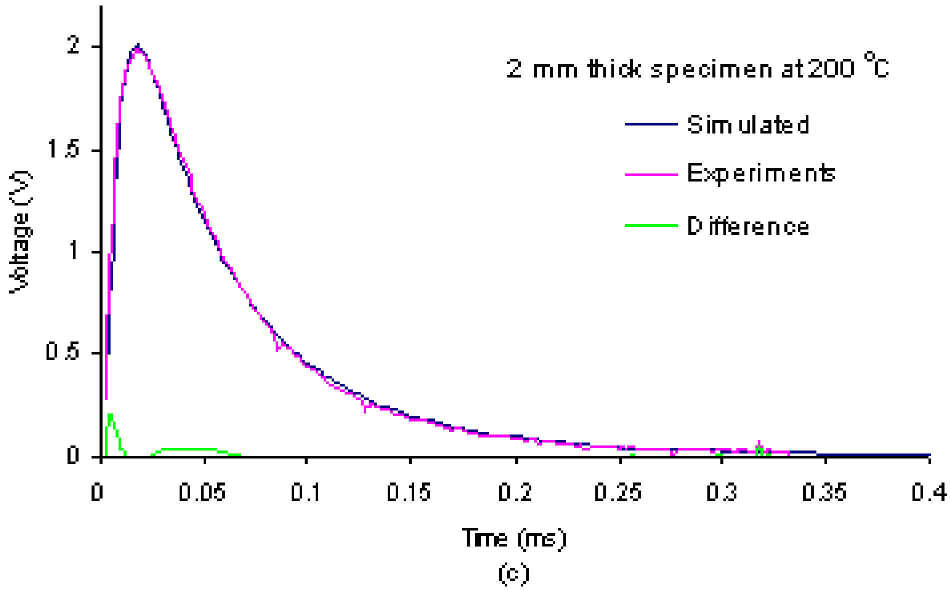

Figure 5.6: Simulated results compared with results from experiments for a 2 mm thick specimen at different temperatures.

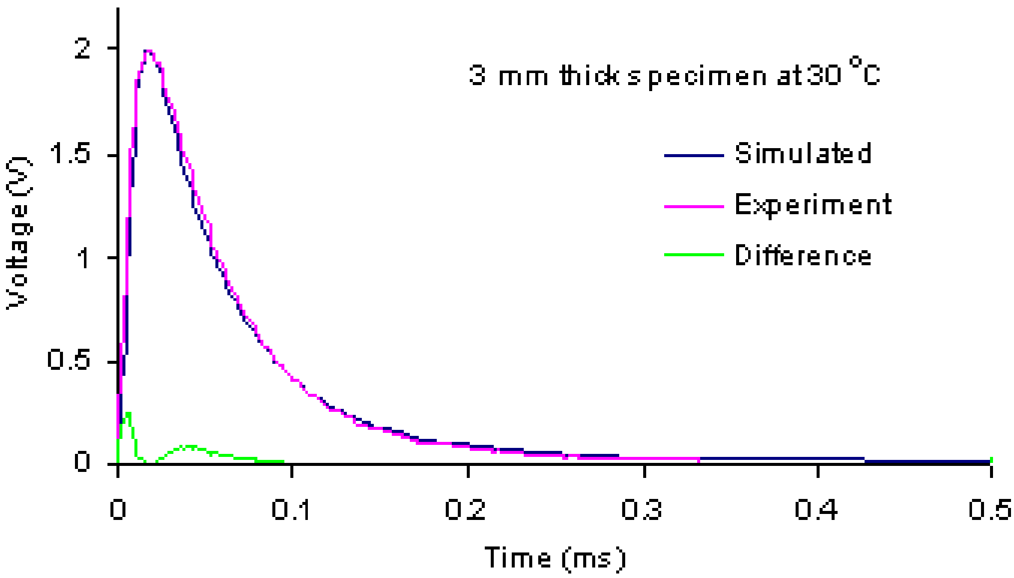
3 mm thick specimen at 30 °C
Simulated
Experiment
Difference
Voltage (V)
2
1.5
1
0.5
0
0
0.1
0.2
0.3
0.4
0.5
Time (ms)

(a)

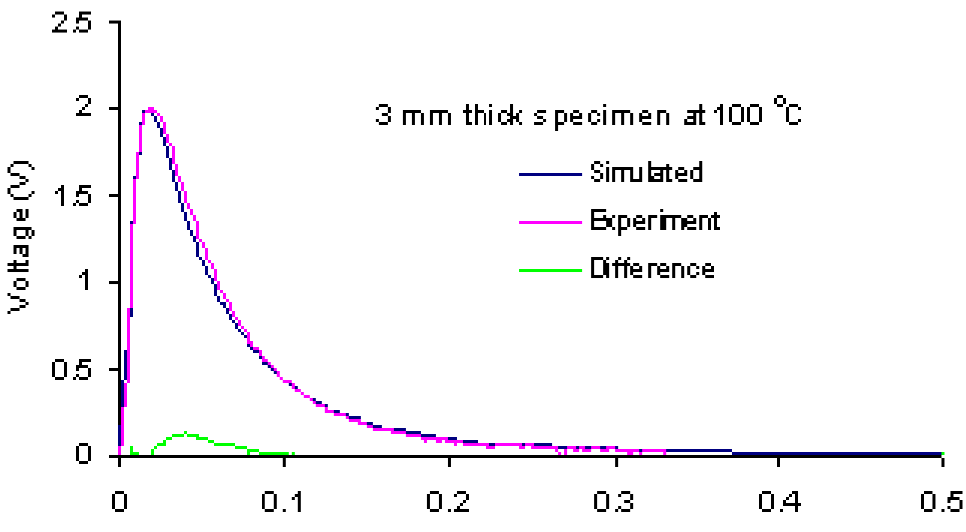
3 mm thick specimen at 100 °C
Simulated
Experiment
Difference
Voltage (V)
2.5
2
1.5
1
0.5
0
0
0.1
0.2
0.3
0.4
0.5
Time (ms)

(b)

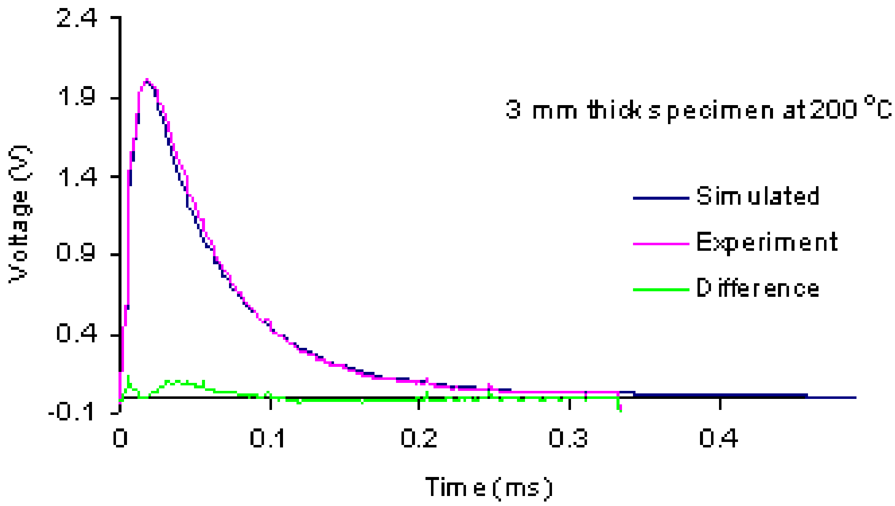

(c)

Figure 5.7: Simulated results compared with results from experiments for a 3 mm thick specimen at different temperatures.

There is a perfect match between simulated data and data from experiments, for period after 0.09 ms from the start of a new period, for some sampled result.

5.4 Discussions

The first experiments carried out had to establish the validity of the modelled test probe. Developing the profile gauging system depended on the choice of the probe characteristics. Parameters like the inner radius, outer radius length of the coil affect the resistances and inductances of the used probe as illustrated in equations 3.30, 3.34, 3.36, 3.37 repeated here as equations 5.1 to 5.4. This representation of the resistances and inductances of the test probe assisted in the choice of probe dimensions and the source frequency in order to maximise sensitivity of the system and work within the desirable steady state conditions.

$$R_d = \frac{\rho_d N_d \pi (r_1 + r_2)}{a_d} \tag{5.1}$$

$$R_p = \frac{\rho_p N_p \pi (r_3 + r_4)}{a_p} \tag{5.2}$$

$$L_d = \frac{\mu_d N_d^2 A_{cd}}{l_{dg}} \tag{5.3}$$

$$L_p = \frac{\mu_p N_p^2 A_{cp}}{l_{pg}} \tag{5.4}$$

As discussed in chapter 3, the magnitude of the magnetic field around the drive coil is proportional to the current flowing through the coil (see equation 3.11). In order to maximise the current drawn from the function generator and therefore the field available to the probing process, the resistance in the drive coil circuit was kept at a minimum; no extra series resistance was added in the drive coil circuit (see figure 3.3). The output resistance R_{out} limits the voltage to the data collection card in the personal computer to within the specified input range of -5 to +5 volts.

Investigations on the lift-off point of intersection showed that trends from simulated data were similar to those observed from experiments and agreed with those reported by other researchers(section 2.4).

- The amplitude of the received signal increased as the liftoff distance increased tending toward that received without the presence of a specimen.
- However as lift-off increased beyond 5 mm, the data from experiments showed an overlap with the signal received without the presence of the specimen. This suggested that the effect of the specimen on the test probe became negligible as the lift-off distance increased.
- A crossing point was observed for varying lift-off distances both for the simulated and the signal from experiments. The experiment LOI was at 0.156 ms and the simulated one at 0.149 ms.

Changes in temperature and thickness of a specimen affected the probe signals and manifested as a change in probe impedances. Results show a close fit between the simulated and the experiment data, for the section of interest of the duty cycle period. This confirms that the equations developed to characterise the specimen inductance and resistance (equations 5.5 and 5.6) are an acceptable representation of the specimen for that section of the period.

$$R_{sT1} = \frac{\rho_{sT1} l_{ed}}{\delta(t)\left(e^{y/\delta(t)} - 1\right) r_o . ln \frac{r_1}{r_2}} \tag{5.5}$$

$$L_s = \frac{\mu_s \pi r_1^2}{2\left(\delta(t)(e^{y/\delta(t)} - 1) + r_o \ln \frac{r_2}{r_1}\right)} \tag{5.6}$$

Results show that there is a perfect match between simulated data and data from experiments from 0.09 ms from the start of a duty cycle period. This implies that one can safely use the latter part of the signal period in further signal processing exercises.

5.5 Summary and conclusion

A report on the validation of the model developed for the study of the PEC system has been given in this chapter. Various results from experiments were compared with data received from model simulations. Some of the trends observed from experiments and model simulations were compared with those observed by other researchers. Effects of temperature were simulated and the model gave results that agree with those from experiments. It was observed that differences between the simulated signal and the signal from experiments happens in the early times of the signal. In the later times of the received signal period the difference between the simulated and the experiment results (especially after 0.09 ms) is 0.000 $\pm$0.004 V for both the signal received in the presence of a specimen and that received in its absence.

The model on the whole is a good representation of the proposed PEC system for the period of interest. The equations developed to characterise and represent the aluminium sheet in the model, are proved to be acceptable by the results shown in this chapter. In chapter 6 a report on the simulation study carried out using the developed environment to establish system performance and sensitivity is given.

Chapter 6

A SIMULATION STUDY

6.1 Introduction

The objective of this study is to investigate pulsed eddy currents for the development of a low cost profile gauge that detects differences in profile sheet thicknesses less than 4 μm. The development of a profile gauge for the finishing mill at Hullet aluminium is considered for this investigation. The sheet is rolled from a thickness of between 20 mm and 30 mm to 2 mm. For the purposes of this analysis, the three point definition of profile in hot rolling mills is considered (section 1.3). An acceptable wedge of less than 0.5% suggested for quality and a suggested deliberate crown of between 0.2% and 0.8% imply that the developed profile gauge should satisfy resolutions of up to 4 μm at the lowest required nominal thickness of 2 mm.

The studied scenarios were set out to explore the possible use of eddy currents for the industrial situation discussed in section 1.1. Quality control requirements dictate that a simple means must be found to identify a small number of parameters which can be used for profile description. Profile definition was explored in section 1.3. The work is intended to extend Pulsed Eddy Current evaluation to an application that requires an array of probes set and used in such a way that the gauged profile can be harnessed under environmental conditions that have not been investigated for PEC application (specimen changing temperature).

In this chapter, a simulation study is documented. Its purpose was to investigate coil probes that use the reflection configuration. Coil sizes, wire sizes, source voltage and frequency were varied and results from these variations presented and compared as a means of determining the best probe size for the investigations. Other factors that would influence the results of the PEC system like signal conditioning by amplification were also investigated. Probe dimensions that gave the best results were further used to investigate the system's sensitivity to very small changes in specimen thickness. The effects of specimen temperature variations on the PEC system signal were also investigated using simulation studies. The simulation environment for a reflection probe that was validated in chapter 5 was used for the simulation study. This was an empirical study taking advantage of the theoretically developed model to assess various characteristics of the envisaged PEC system.

6.1.1 Sensitivity

The study started with the exploration of source amplitudes and frequencies, coil length and core dimensions together with wire sizes. Sensitivity was assessed empirically by considering extent of the changes in the received PEC signal (outputs) that were caused by changes in source frequencies, probe dimensions and specimen conditions (inputs). The higher the ratio between a small change in the output and that in the input, the better the sensitivity. Varying probe dimensions changes probe impedances and hence the probe signals. The simulation study carried out in this chapter is to establish probe dimensions that give a good sensitivity to changes in the tested specimen. The higher the ratio between a small change in the output and that in the input, the better the sensitivity. Source amplitude and frequency, coil length and core dimensions together with wire sizes are varied in various simulation exercises to establish trends in the pickup coil signal.

6.1.2 Amplitude and frequency of the source voltage

The pulsed eddy current system uses pulsed magnetic fields to probe the investigated specimen. The amplitude and frequency of the pulsed magnetic fields are created from a pulsating voltage source. It is important to specify the amplitude and frequency of the source voltage in order to achieve total penetration of the specimen so that the PEC system can probe the specimen effectively. Deep penetration of the specimen by the magnetic field occurs at low frequencies [29]. However, external interferences especially those from nearby a.c power circuits cause problems at low frequencies in ranges below 100 Hz and internal noises especially those due to random, temperature-induced motion of electrons and other charge carriers in resistors and semiconductors cause problems at higher frequencies above 10^6 Hz respectively [82]. The model developed for this study was used to assess various situations. Simulations done at various source frequencies and voltages for the probe validated in chapter 5 were carried out and results from these simulations are presented in this section.

6.2 Simulations, results and observations

Results from simulations under different but related system conditions, were plotted on the same graphs and possible probe dimensions chosen on the basis of the noted differences in the plotted pickup coil signals. The choices made on the probe dimensions and the source voltages and frequencies for the best sensitivity and suitable steady state conditions were then used to investigate other issues. Also very small changes in the specimen thickness were studied using the chosen probe dimensions in order to establish whether the output signals corresponding to the input parameters were separated enough, for the period of interest.

6.2.1 A simulation study on the effects of coil length on the received PEC signal

Simulations in the absence of a specimen

For this study, simulations were intended to assist in the assessment of steady state conditions in the received PEC signal. These were carried out at various source frequencies for probes with different coil lengths, in the absence of a specimen. Four frequencies were chosen for the simulation study; 100 Hz, 500 Hz, 1 kHz and 1.5 kHz. All simulations were carried out using the same source voltage amplitude (20 V peak-to-peak). Simulations were carried out for the coil length (l_{dg} = 9 mm) considered in the validation (see chapter 5) and also for two other coils with different length (l_{dg}); 4.5 mm and 13.5 mm, one being shorter than the validated coil length (9 mm) while the other longer, by 4.5 mm. The radial (core) dimensions and the wire diameters were kept similar for all coils. Results from these simulations are presented in figure 6.1. For these plots, the scale on the y-axis starts at -0.1 V instead of 0.0 V to highlight the change in the signal from the positive going to the negative going pulse. It can be seen in figures 6.1 and 6.2 that for the 1.5 kHz waveform the signal changes sense at the time 0.33 ms. The voltage values at the end of each positive duty cycle period for the considered frequencies are recorded in table 6.1. Voltage values are recorded at 0.33 ms, 0.5 ms, 1 ms and 5 ms for source frequencies 1.5 kHz, 1 kHz, 500 Hz and 100 Hz respectively.

Graphs (a), (b) and (c) in figure 6.1 show plots of the received pickup coil signal at the specified frequencies for each coil length, while graph (d) gives the comparison for the different probe lengths.

Simulations in the presence of a specimen

Simulations were carried out at various source frequencies (100 Hz, 500 Hz, 1 kHz and 1.5 kHz) for probes with the same dimensions as those used in the absence of a specimen. Four different specimen thicknesses were considered for this simulation study; 3 mm, 5 mm, 7 mm and 9 mm.

Results from the simulations are categorised as follows:

- Simulations for the different probe lengths (4.5 mm, 9 mm and 13.5 mm) placed on specimen with a constant thickness (3 mm) and with varying source frequency (100 Hz, 500 Hz, 1 kHz and 1.5 kHz); figure 6.2.
- Simulations for the different probe lengths (4.5 mm, 9 mm and 13.5 mm) carried out at a constant source frequency (1 kHz) and placed on diferent

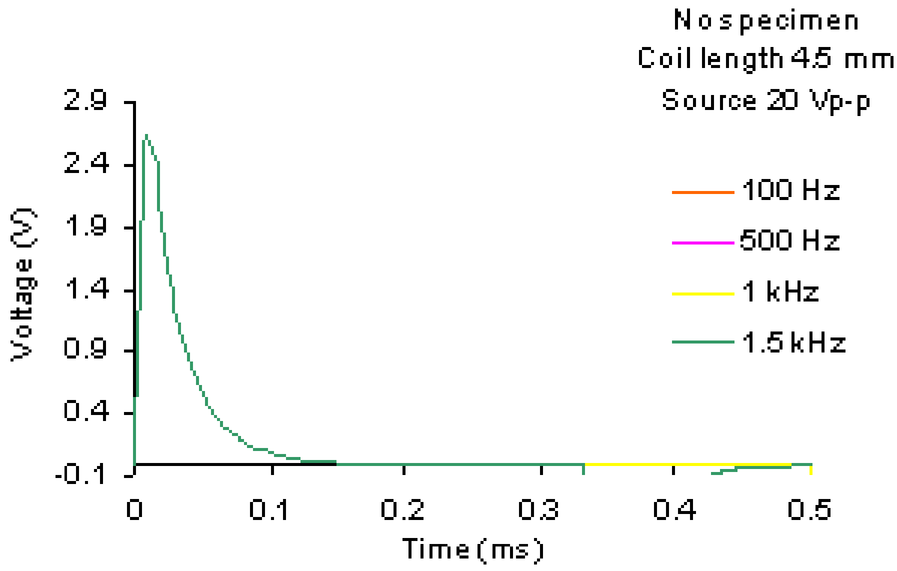

(a)

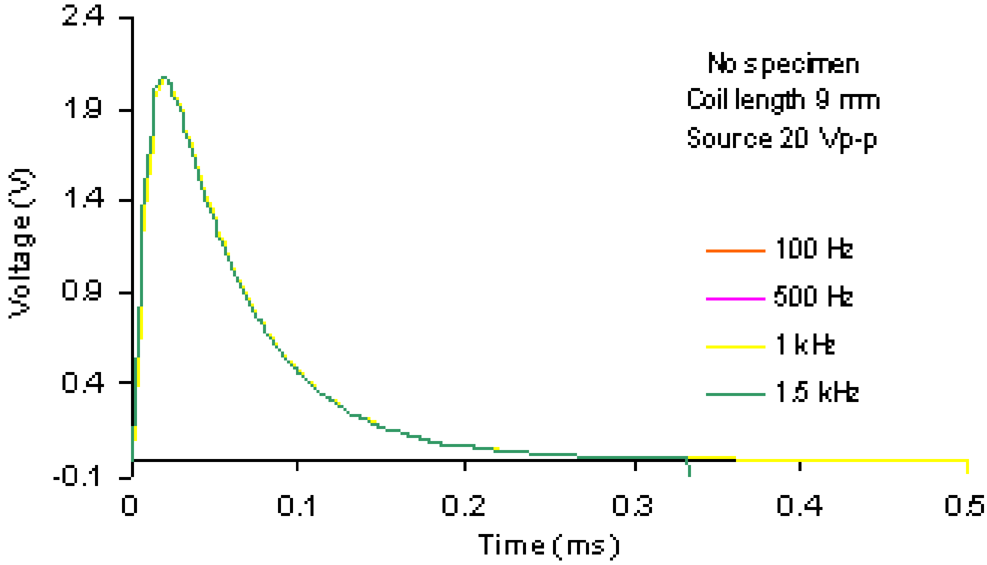

(b)

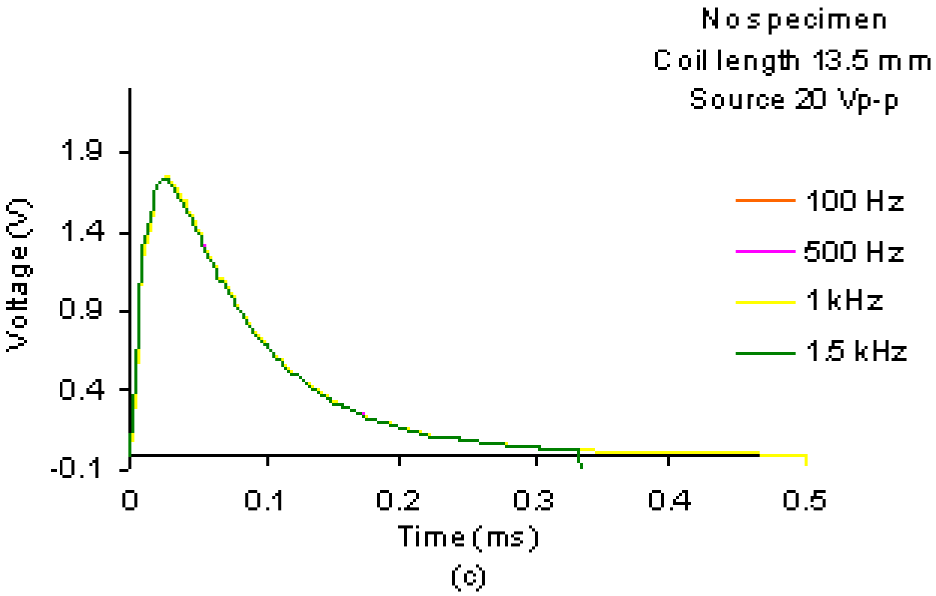

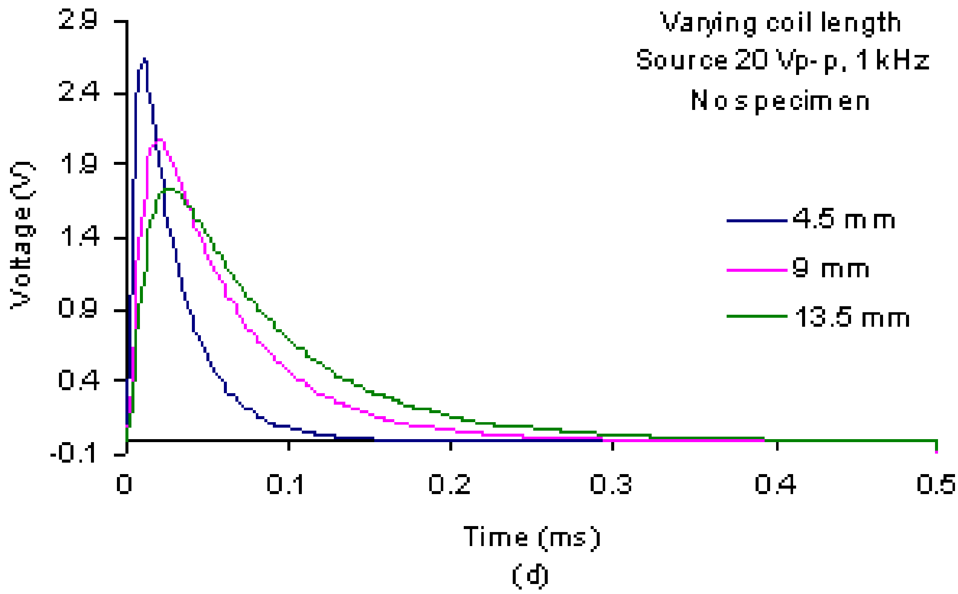

Figure 6.1: Simulated results for varied coil lengths in the absence of a specimen.

specimen thicknesses (3 mm, 5 mm, 7 mm and 9 mm); figure 6.3.

Effects on the signal due to frequency changes for the three coil lengths (4.5 mm, 9 mm, 13.5 mm) are shown in graphs (a), (b) and (c)of figure 6.2. A comparison between the different coil length is shown in graph (d) of the same figure. Effects on the signal due to changes in specimen thickness for the three coil lengths (4.5 mm, 9 mm, 13.5 mm) at a constant frequency (1 kHz) are shown in graphs (a), (b) and (c) of figure 6.3. A comparison between the different coil length is shown in graph (d) of the same figure. For all the plots, the output pickup coil voltages at the end of the relevant due cycle period are recorded in tables 6.2 and 6.3.

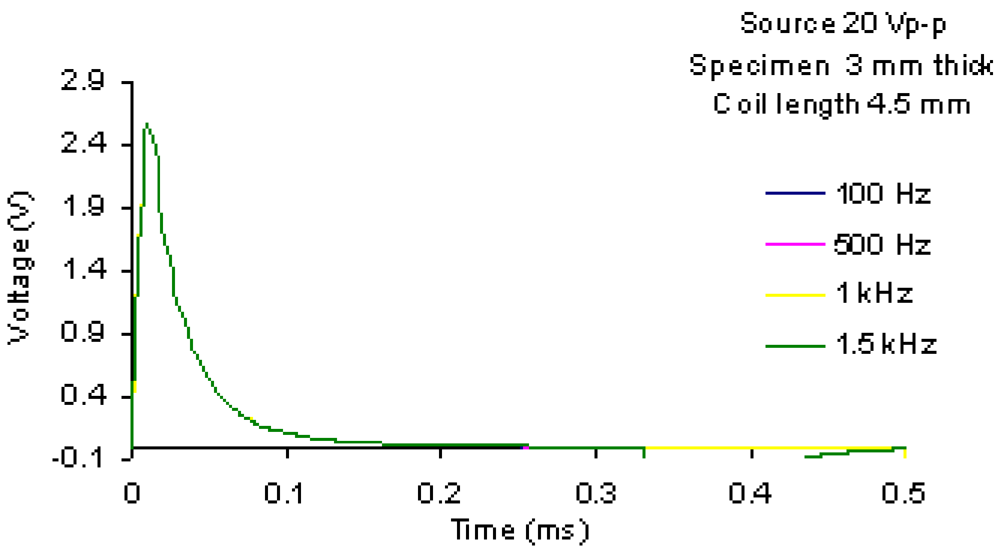

(a)

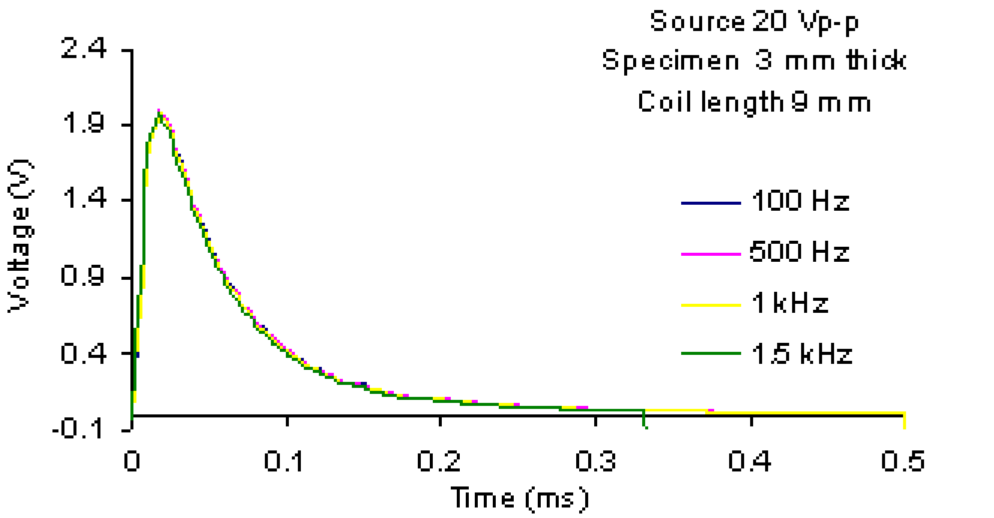

(b)

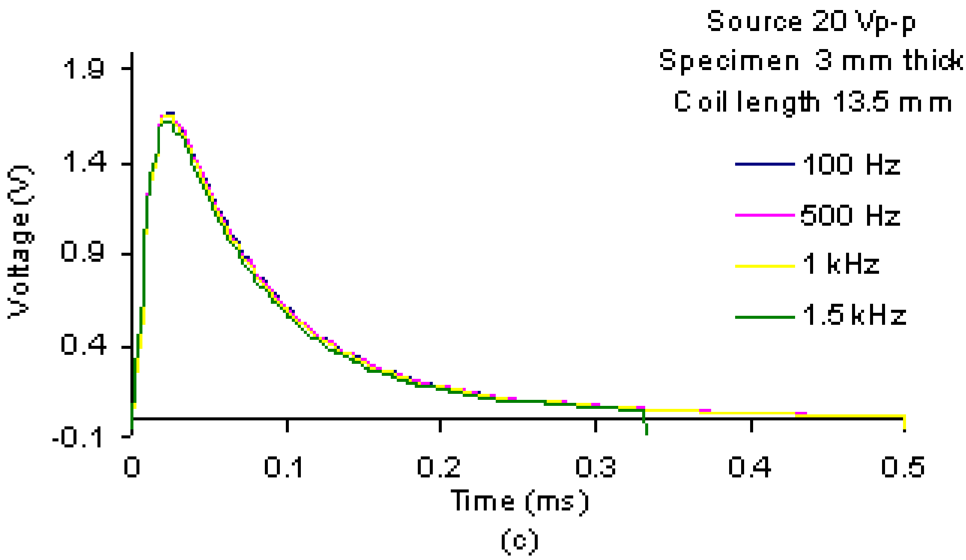

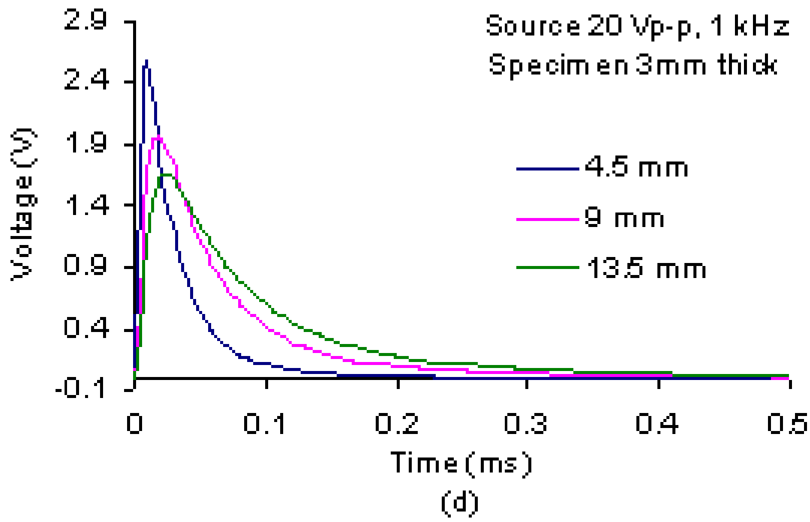

Figure 6.2: Simulated results for varied source frequencies in the presence of a 3 mm specimen.

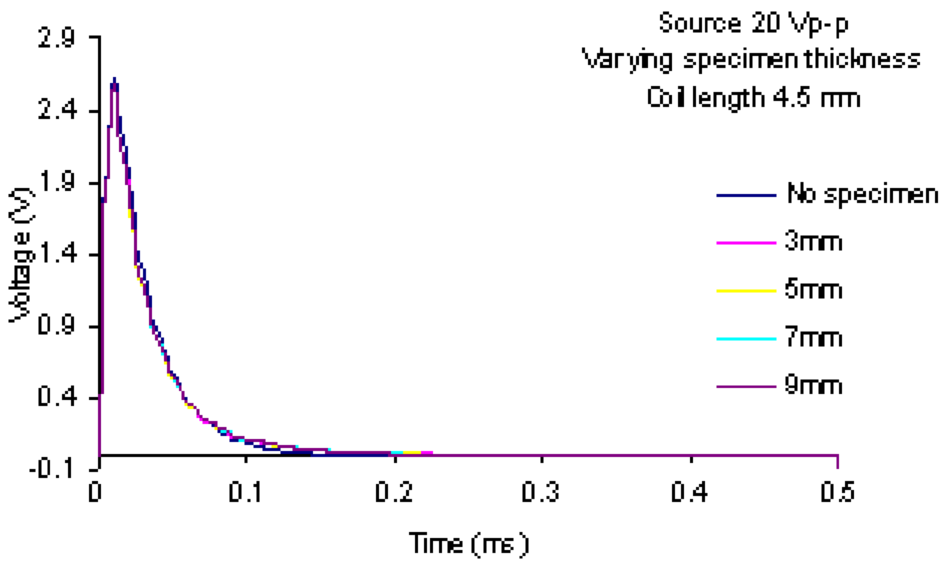
Source 20 Vp-p
Varying specimen thickness
Coil length 4.5 mm
No specimen
3mm
5mm
7mm
9mm
Voltage (V)
Time (ms)
2.9
2.4
1.9
1.4
0.9
0.4
-0.1
0
0.1
0.2
0.3
0.4
0.5

(a)

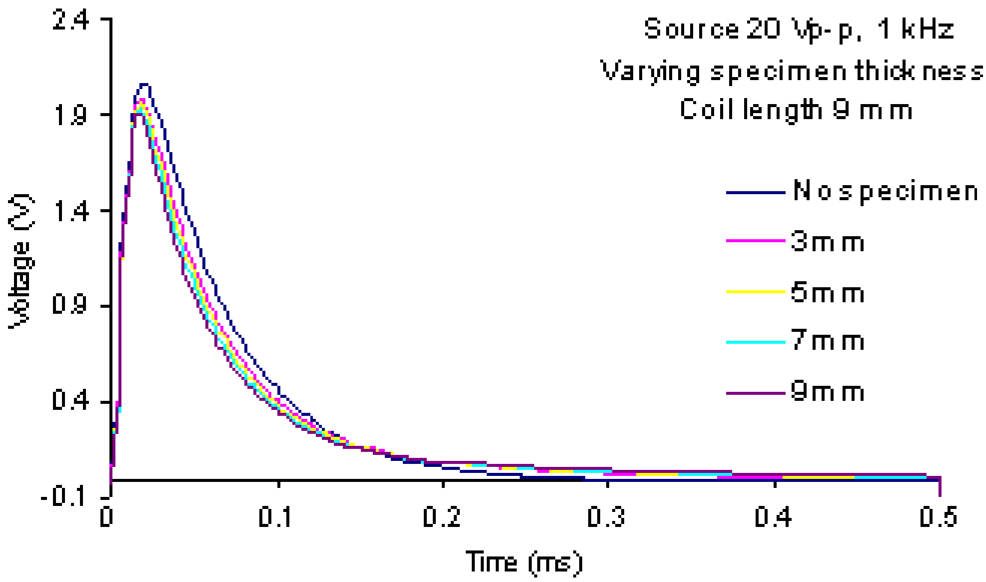
Source 20 Vp-p, 1 kHz
Varying specimen thickness
Coil length 9 mm
No specimen
3mm
5mm
7mm
9mm
Voltage (V)
Time (ms)
2.4
1.9
1.4
0.9
0.4
-0.1
0
0.1
0.2
0.3
0.4
0.5

(b)

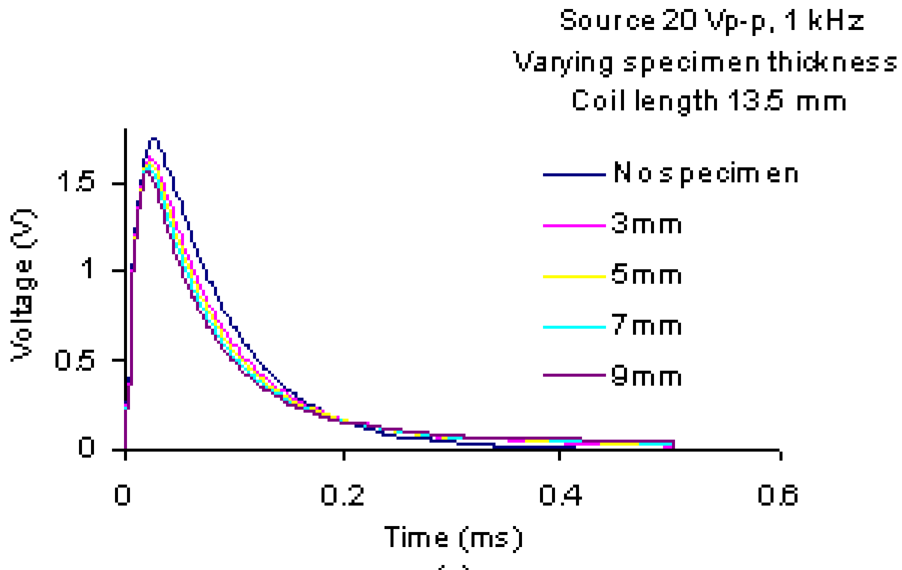

(c)

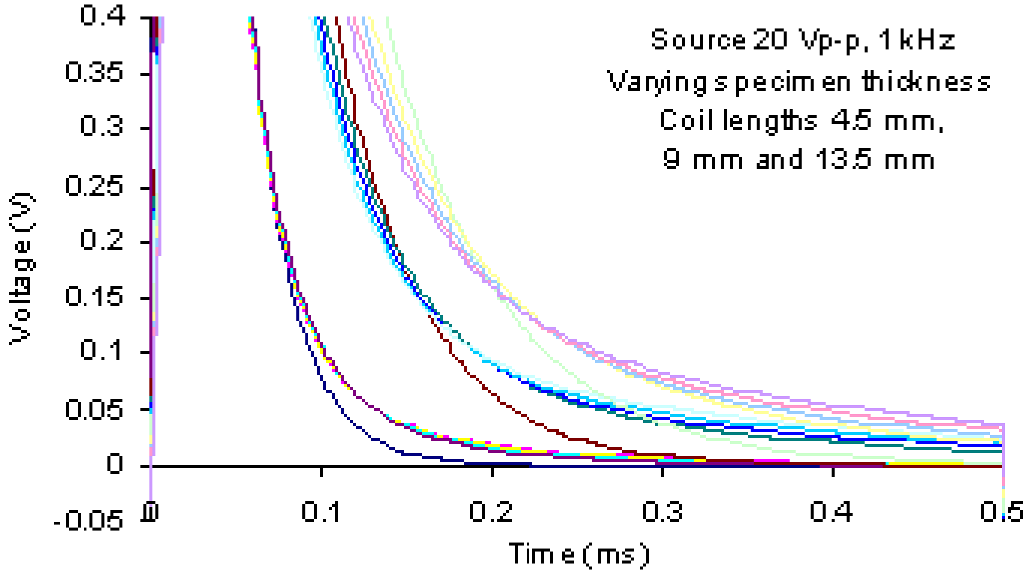

(d)

Figure 6.3: Simulated results for varied coil lengths in the presence of specimen with different thicknesses.

Observations

For the coil in the absence of a specimen, observations are summarised in table 6.1. The value of the voltages (in volts), for each coil length, at the end of a duty cycle for the used source frequency 100 Hz, 500 Hz, 1 kHz and 1.5 kHz were recorded at 5 ms, 1 ms, 0.5 ms and 0.33 ms respectively.

Table 6.1: The pickup signal voltage value, at the end of a positive duty cycle, for the investigated frequency and the considered coil length in the absence of a specimen

Frequency	100 Hz	500 Hz	1 kHz	1.5 kHz
Duty cycle period	(5 ms)	(1 ms)	(0.5 ms)	(0.33 ms)
Coil length (mm)	(V)	(V)	(V)	(V)
4.5	$2.50 \text{x} 10^{-133}$	$7.66 \text{ x } 10^{-19}$	$9.87 \text{ x } 10^{-9}$	$8.45 \text{ x } 10^{-6}$
9.0	$1.84 \text{ x } 10^{-65}$	$6.4 \text{ x } 10^{-9}$	$0.15 \text{ x } 10^{-3}$	$4.72 \text{ x } 10^{-3}$
13.5	$9.93 \text{ x } 10^{-46}$	$1.3 \text{ x } 10^{-6}$	$1.97 \text{ x } 10^{-3}$	$23 \text{ x } 10^{-3}$

- For all frequencies investigated, the pickup coil signal reaches steady state. However, their time to steady state varies.
- The output signal voltage value of 0.02 V, a value within 1% of the maximum signal value, was taken as a measure of a signal exhibiting desirable steady state conditions. Data captured in table 6.1 shows that the voltage at the end of the duty cycle, is a maximum (0.023 V) for the 13.5 m coil at a source frequency of 1.5 kHz.
- The 4.5 mm coil has the lowest voltage for all frequencies indicating that it exhibits desirable steady state conditions at an earlier time than the 9 mm coil and 13.5 mm coils.
- The 13.5 mm coil has the highest voltage for all frequencies indicating that it takes longer to reach desirable steady state conditions.

For the different coil length in the presence of a 3 mm thick specimen, observations are summarised in table 6.2. The value of the voltage (in volts) at the end of a duty cycle for the used source frequency (100 Hz, 500 Hz, 1 kHz and 1.5 kHz) was recorded for each coil length.

Table 6.2: The pickup signal voltage value, at the end of a positive duty cycle, for the investigated frequencies and the considered coil length in the presence of a 3 mm thick specimen

Frequency	100 Hz	500 Hz	1 kHz	1.5 kHz
Duty cycle period	(5 ms)	(1 ms)	(0.5 ms)	(0.33 ms)
Coil length (mm)	(V)	(V)	(V)	(V)
4.5	2.2 x 10^{-25}	3.53 x 10^{-6}	7.58 x 10^{-3}	4.44 x 10^{-3}
9.0	1.37 x 10^{-13}	8.25 x 10^{-4}	11.98 x 10^{-3}	28.2 x 10^{-3}
13.5	4.7 x 10^{-13}	1.5 x 10^{-3}	20.5 x 10^{-3}	51.2 x 10^{-3}

- At the end of the 0.5 ms duty cycle, the output signal voltage values are 20.53 mV, 11.98 mV and 0.7 mV for the 13.5 mm, 9 mm and 4.5 mm long coils respectively. This implies that the time to steady state is longest for the longest coil.
- The value of 51.2 mV at the end of the duty cycle of the 1.5 kHz source frequency, for the 13.5 mm coil, indicates that signal has not reached desirable steady state conditions.

For the different coil lengths in the presence of different specimen thicknesses (5 mm, 6 mm, 7 mm and 9 mm) at a source voltage of 20 V peak-to-peak) and a source frequency of 1 kHz, observations are surmarised in table 6.3

Table 6.3: Varying specimen thickness at a source frequency of 1 kHz for the considered coil lengths

Specimen thickness	(3 mm)	(5 mm)	(7 mm)	(9 mm)
Coil length (mm)	(V)	(V)	(V)	(V)
4.5	0.7 x 10^{-3}	0.521 x 10^{-3}	0.243 x 10^{-3}	0.113 x 10^{-3}
9.0	11.98 x 10^{-3}	16.58 x 10^{-3}	20.37 x 10^{-3}	24.15 x 10^{-3}
13.5	20.53 x 10^{-3}	26.60 x 10^{-3}	31.76 x 10^{-3}	36.98 x 10^{-3}

Analysing the out signal voltage values presented in 6.3, it can be concluded that:

- It takes longer for the longest coil (13.5 ms) to reach within 1% of the steady state conditions.

- The differences in the output signal voltage at the end of the 1 kHz duty cycle, due to specimen thicknesses, are highest for the longest coil. For the 3 mm and 5 mm thick specimens, the differences in the output voltage value at the end of the 1 kHz duty cycle, for the 4.5 mm, 9 mm and the 13.5 mm coils, are 0.179 mV, 4.6 mV and 6.07 mV respectively. This coresponds to sensitivities of 0.089 Vm^{-1}, 2.3 Vm^{-1} and 3.03 Vm^{-1} for the 4.5 mm, the 9.0 mm and the 13.5 mm coils respectively. Therefore, longer coils give better sensitivity than shorter coils.

- However, steady state conditions are not achieved for the longest coil and a compromise in coil length is necessary for an effective probe.

- The 9 mm coil makes a good compromise between desired steady state conditions and sensitivity.

6.2.2 A simulation study on effects of core dimensions on the received PEC signal

Figure 6.4, shows the effects of varying the core diameter while keeping the coil length common at 9 mm and the source frequency at 1 kHz. The observations on the pickup voltage value at the end of the 0.5 ms duty cycle derived from the 1 kHz source frequency are recorded in table 6.4.

Table 6.4: Variation in core diameter for a 9 mm coil length in the presence of the indicated specimen thicknesses

Specimen thickness	(3 mm)	(5 mm)	(7 mm)	(9 mm)
Core diameter(mm)	(V)	(V)	(V)	(V)
4.25	2.47 x 10^{-2}	3.49 x 10^{-2}	4.33 x 10^{-2}	5.16 x 10^{-2}
6.25	6.08 x 10^{-2}	6.89 x 10^{-2}	7.68 x 10^{-2}	8.55 x 10^{-2}

- Analysing table 6.4, the values of the voltages of the output signal at the end of the 1 kHz duty cycle are higher for the 6.25 mm core diameter indicating that increasing core radius, while keeping all other coil dimensions constant, increases the time to steady state of the system.

- For the 3 mm and 5 mm thick specimens, the differences in the output voltage value at the end of the 1 kHz duty cycle for the 4.25 mm and the 6.25 mm diameter cores are 10.2 mV, and 8.2 mV respectively. This coresponds to sensitivities of 5.1 Vm^{-1} and 4.1 Vm^{-1} for the 4.25 mm and the 6.25 mm core diameters respectively. Therefore, the differences due to specimen thicknesses are more evident in the received signal for the probe with the smaller core radius rendering smaller radius cores more sensitive.

6.2.3 Effects of Wire size on the recieved PEC signal

To establish the effect of wire size on the received pickup coil signal, two wire diameter sizes, 0.18 mm and 0.12 mm were considered in the simulations. The coil length was chosen to be 9 mm (it showed good compromise for steady state conditions and sensitivity). The core radius 4.25 mm was kept since it gave the best sensitvity. All other probe dimensions were kept the same (see table 5.1). Figure 6.5, shows the results of the simulations. The observations on the pickup voltage value at the end of the 0.5 ms duty cycle derived from the 1 kHz source frequency are recorded in table 6.5, for the 0.12 mm and the 0.18 mm diameter wires.

Table 6.5: Variation in wire diameter for a 9 mm coil length in the presence of the indicated specimen thicknesses

Specimen thickness	(3 mm)	(5 mm)	(7 mm)	(9 mm)
Wire diameter(mm)	(V)	(V)	(V)	(V)
0.12	2.12 x 10^{-2}	2.40 x 10^{-2}	2.80 x 10^{-2}	3.09 x 10^{-2}
0.18	1.12 x 10^{-2}	1.66 x 10^{-2}	2.04 x 10^{-2}	2.40 x 10^{-2}

- Analysing table 6.5, the values of the voltages of the output signal at the end of the 1 kHz duty cycle are higher for the 0.12 mm wire diameter, indicating that for all other dimensions kept constant, decreasing wire radius increases the time to steady state of the system.

- For the 3 mm and 5 mm thick specimens, the differences in the output voltage value at the end of the 1 kHz duty cycle for the 0.12 mm and the

0.18 mm wire diameters were 2.8 mV, and 100 mV respectively. This corresponds to sensitivities of 1.4 Vm^{-1} and 50 Vm^{-1} for the 0.12 mm and the 0.18 mm wire diameters respectively. Therefore, the differences due to specimen thicknesses become more evident as the wire diameter is increased, implying that thicker wires give better sensitivity.

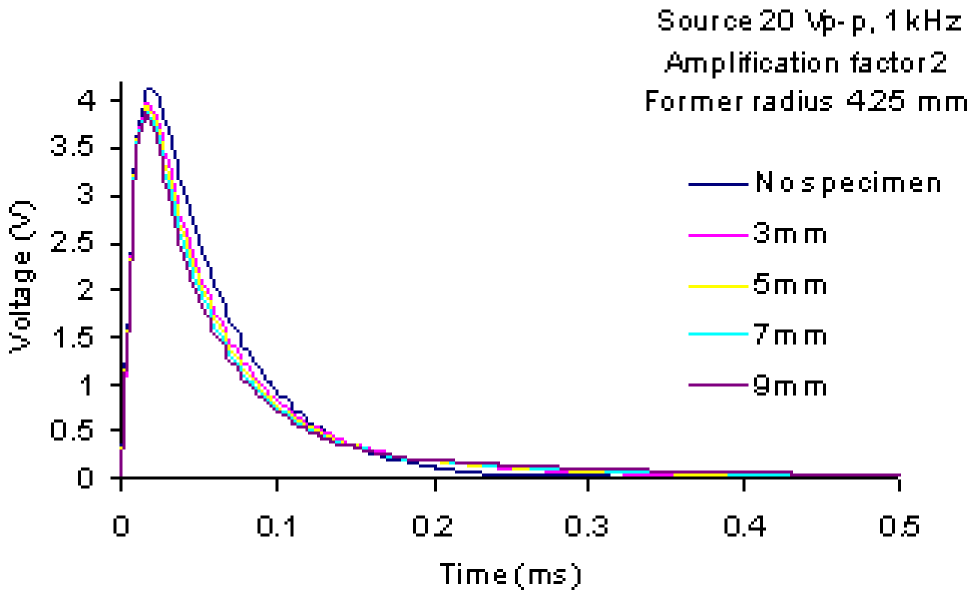

(a)

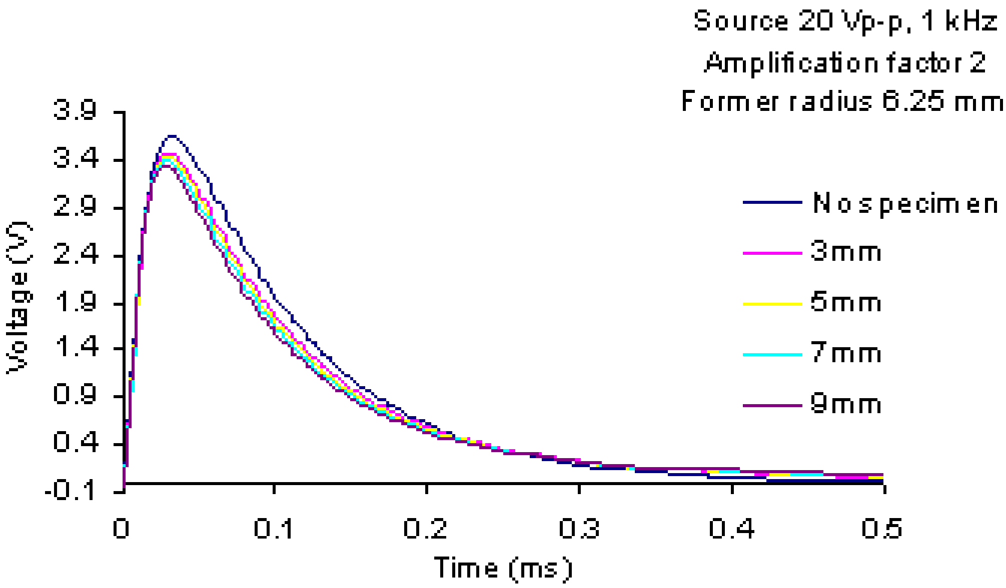

(b)

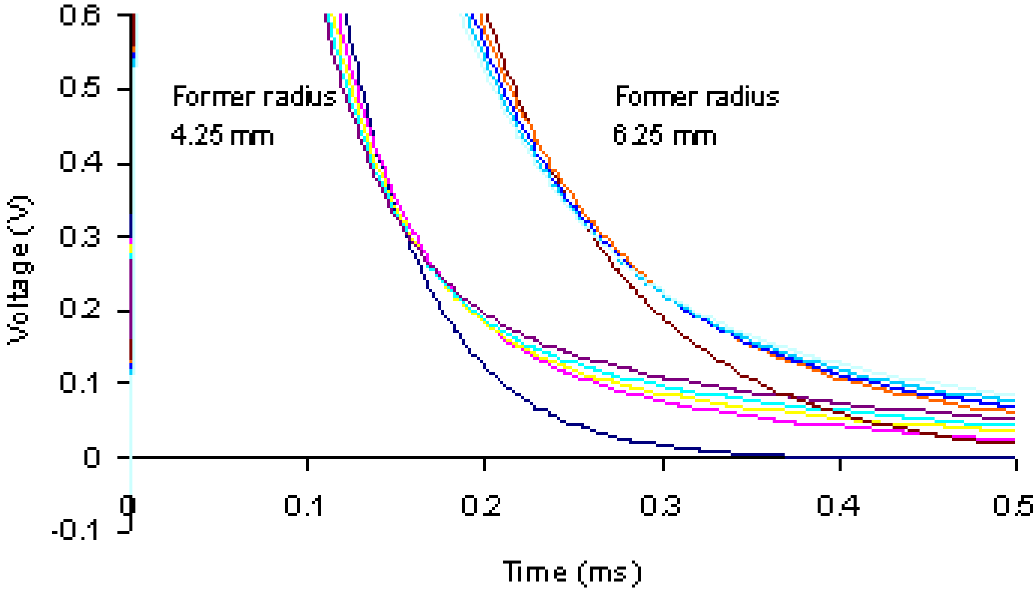

(c)

Figure 6.4: Simulated results for varied core diameter while keeping the coil length common at 9 mm

A comparison between the amplitudes of the signals received from the 9mm long coil with the wire diameters 0.12 mm and 0.18 mm are shown in figure 6.6. It is observed that in the absence of a specimen, the amplitude of the output voltage for the coil wound with the 0.18 mm wire is 2.070 V at 0.02 ms and that from the coil wound with the 0.12 mm wire is 0.895 V at 0.032 ms. Implying that the 0.12 mm wire diameter subjects the signal to a higher resistance. The thinner wire requires more length to fill the same dimensions as the thicker wire and it has a smaller cross-sectional area. Taking note of equation 3.21, page 37, the conditions implies that the thinner wire offers more resistance to the system and hence the much lower amplitude observed in the pickup coil signal.

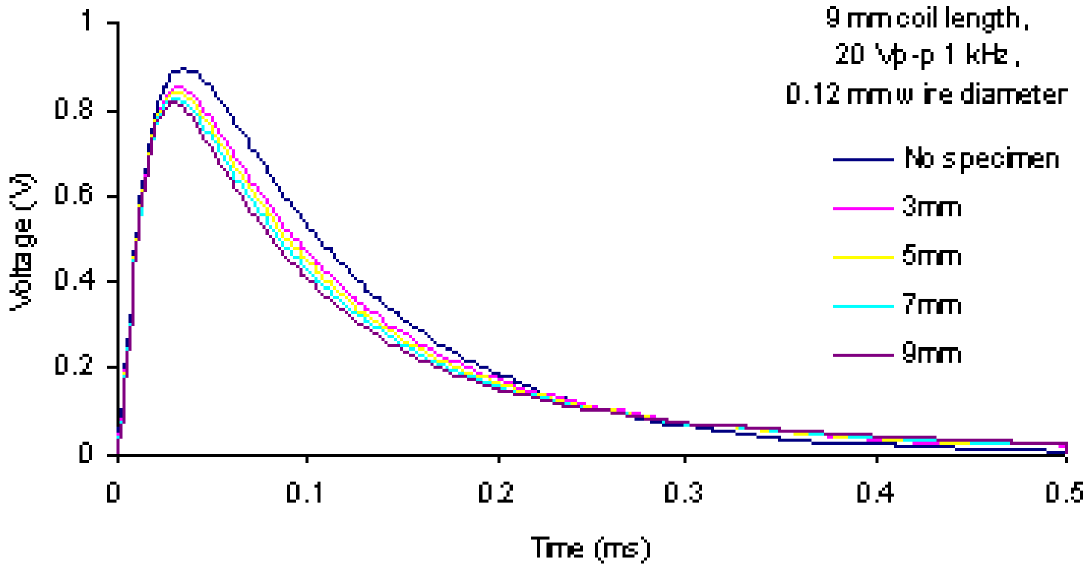
9 mm coil length,
20 Vp-p 1 kHz,
0.12 mm w ire diameter
No specimen
3mm
5mm
7mm
9mm
Voltage (V)
Time (ms)

(a)

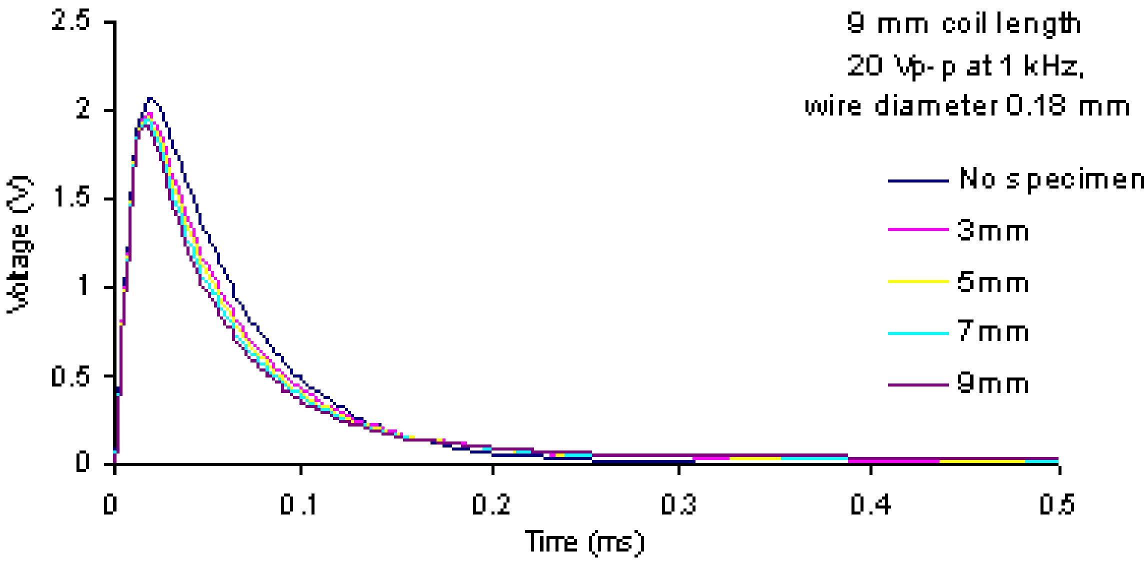
9 mm coil length
20 Vp-p at 1 kHz,
wire diameter 0.18 mm
No specimen
3mm
5mm
7mm
9mm
Voltage (V)
Time (ms)

(b)

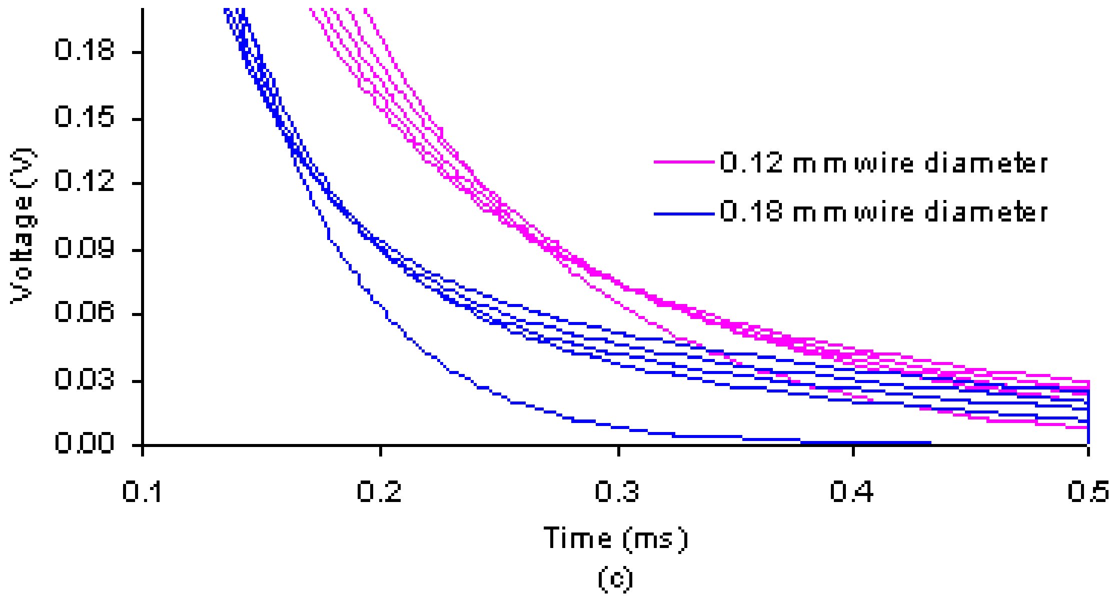

Figure 6.5: Simulated results for different wire sizes with coil length kept at 9 mm.

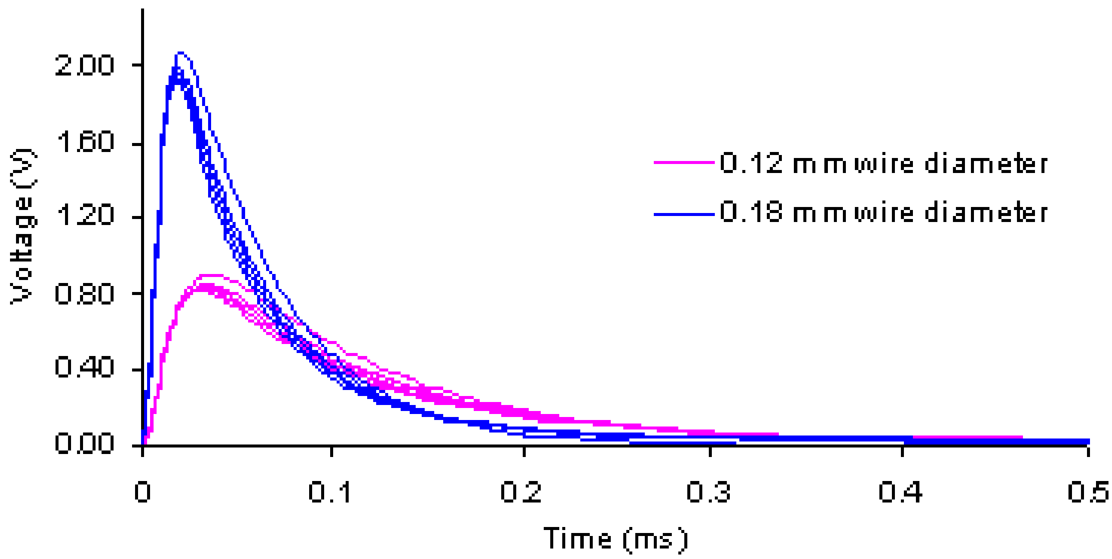

Figure 6.6: Comparing the amplitude of the simulated results for the 0.12 mm and 0.18 mm wire diameters, with all other coil dimensions kept constant.

6.2.4 Very small changes in the specimen thickness

It was important to make observations on changes in the output signal for very small changes in the input parameter, in order to establish whether the output signals corresponding to various input parameters were separated enough, for the period of interest. This would then allow further investigations, by simulation, on the effects of small changes in the thickness of the specimen. In this section a study is carried out to establish the smallest change in the thickness of the specimen that needs to occur before a noticeable change is observed in the output. Simulations were carried out using steps of 1 mm, 0.1 mm, 0.01 mm and 0.001 mm about a nominal thickness of 2 mm. The 2 mm nominal thickness was chosen because it is the smallest thickness required for the rolled aluminum sheet on the finishing mill (see section 1.2). Results are presented in figures 6.7 and 6.8. The bump observed after 0.498 ms in figure 6.8 though hardly noticeable in figure 6.7, is introduced by the excitation signal. Also small changes in specimen thickness at a nominal thickness of 2 mm for different specimen temperatures. Results are presented in figure 6.9.

Results show that:

- There is appreciable seperataion in the output signals for the smallest change chosen (0.001 mm).
- Considering the plots given in figure 6.9, for the thicknesses and the temperatures that are considered, for a small changes of 1 μm in the specimen thickness, a voltage change of 3 μV is observed. This indicates a sensitivity of 3 Vm^{-1} for all considered temperatures.

6.2.5 Source amplitude

The effect on the pickup coil signal due to the source amplitude was investigated by using the 0.18 mm diameter wire, 4.25 mm core diameter, 9 mm long probe at two source voltages; 20 V and 40 V peak-to-peak. The simulations were carried out at a source frequency of 100 Hz. Results from the simulations are presented in figure 6.10.

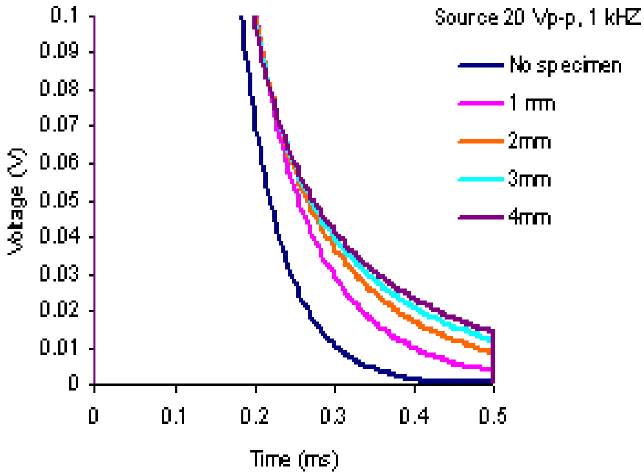

(a)

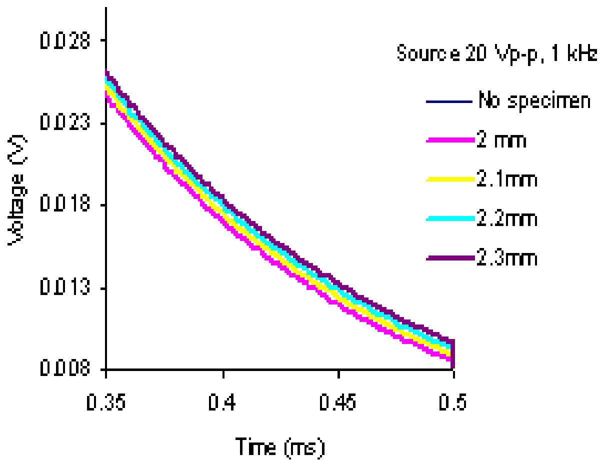

(b)

Figure 6.7: Simulated results for PEC system output signal for changes in specimen thickness of 1 mm and of 0.1 mm at a nominal thickness of 2 mm.

It is observed that differences due to specimen thicknesses are more evident in the signal received for the 40 V peak-to-peak source voltage. Sensitivity is

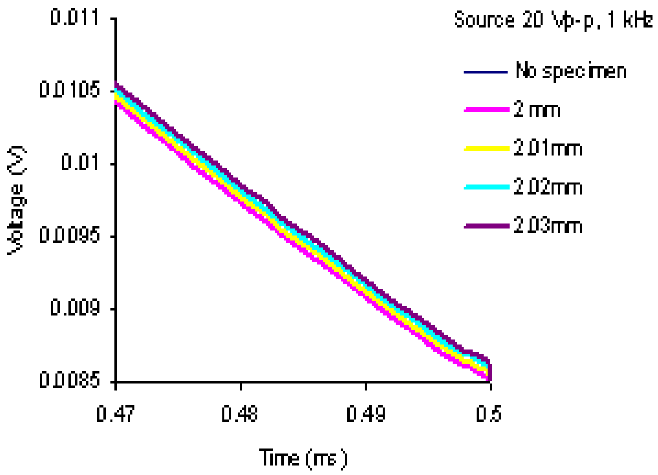

(a)

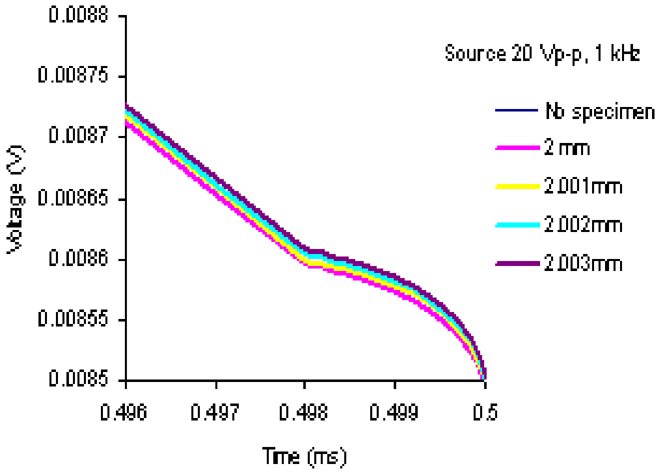

(b)

Figure 6.8: Simulated results for PEC system output for changes in specimen thickness of 0.01 and 0.001 mm at nominal thickness of 2 mm.

improved with increased source voltage.

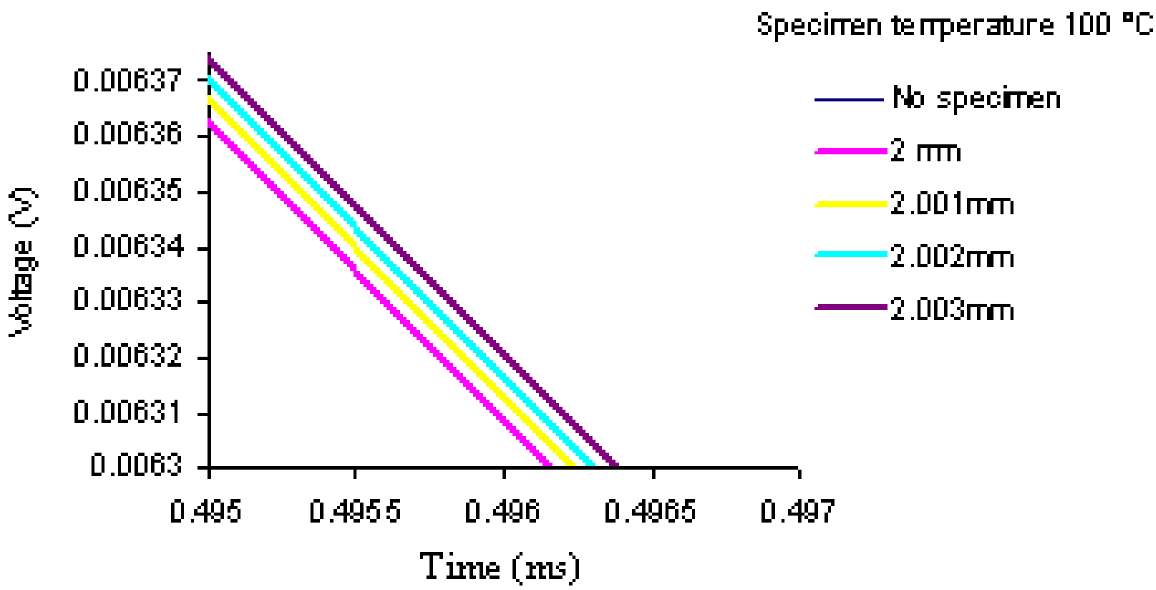
Specimen temperature 100 °C
No specimen
2 mm
2.001mm
2.002mm
2.003mm
Voltage (V)
0.00637
0.00636
0.00635
0.00634
0.00633
0.00632
0.00631
0.0063
0.495
0.4955
0.496
0.4965
0.497
Time (ms)

(a)

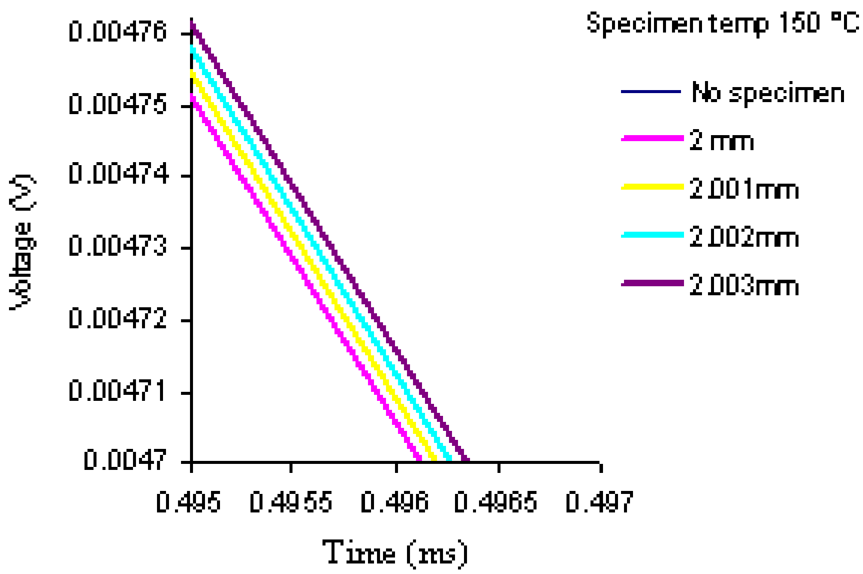
Specimen temp 150 °C
No specimen
2 mm
2.001mm
2.002mm
2.003mm
Voltage (V)
0.00476
0.00475
0.00474
0.00473
0.00472
0.00471
0.0047
0.495
0.4955
0.496
0.4965
0.497
Time (ms)

(b)

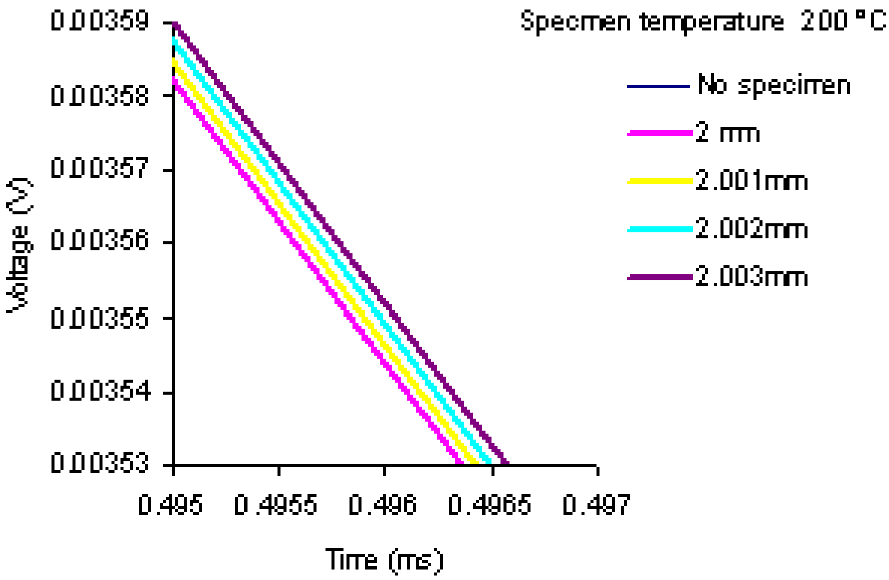

(c)

Figure 6.9: Very small changes in specimen thickness, at three different temperatures for the indicated thicknesses.

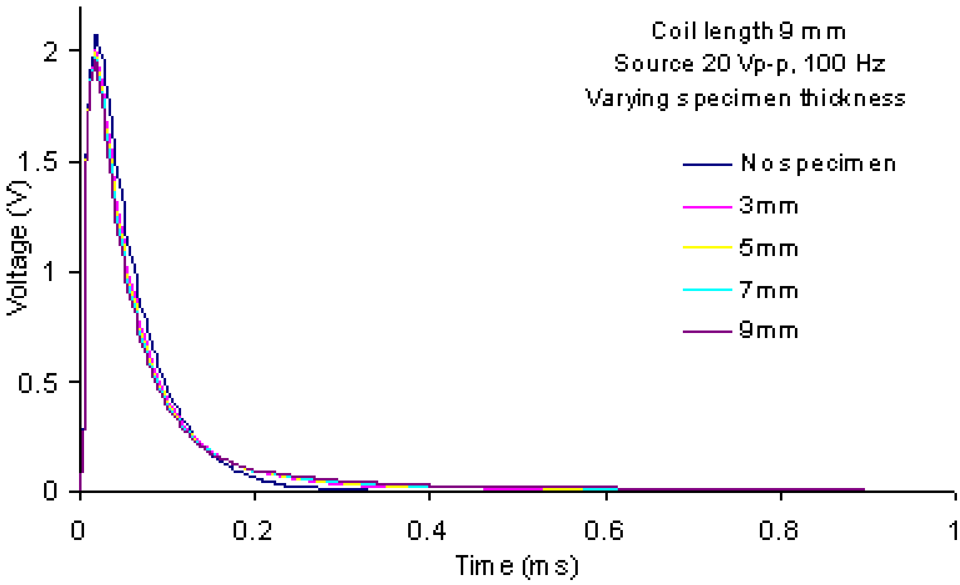

Coil length 9 mm
Source 20 Vp-p, 100 Hz
Varying specimen thickness
No specimen
3mm
5mm
7mm
9mm
Voltage (V)
Time (ms)

(a)

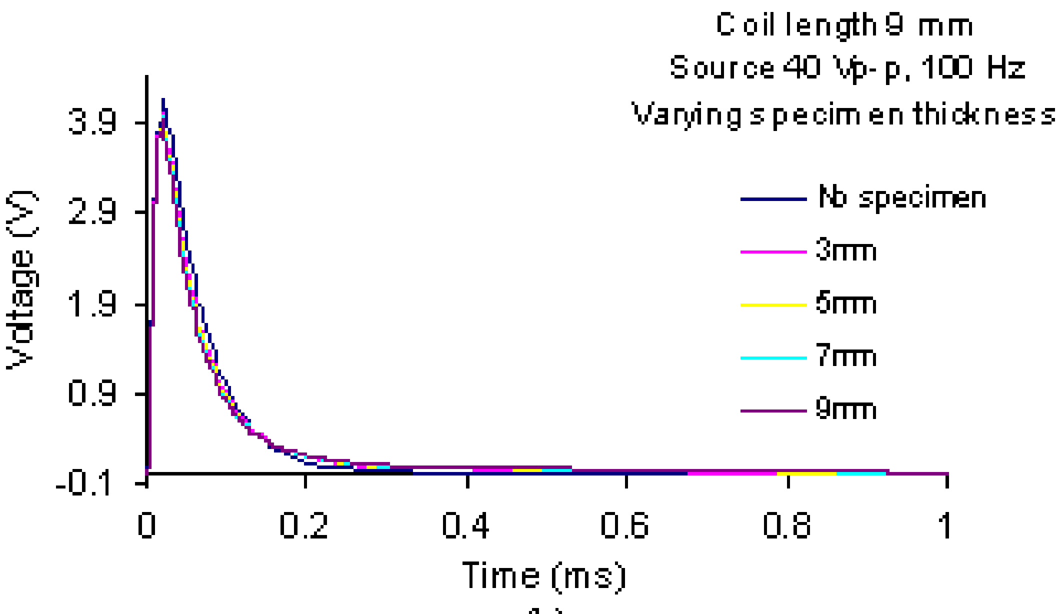

Coil length 9 mm
Source 40 Vp-p, 100 Hz
Varying specimen thickness
No specimen
3mm
5mm
7mm
9mm
Voltage (V)
Time (ms)

(b)

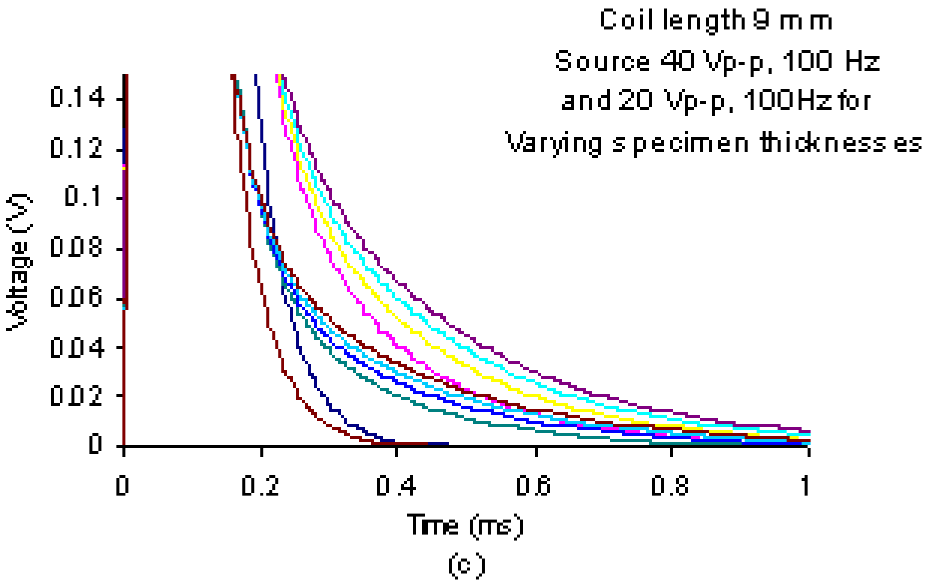

Figure 6.10: Simulated results for different source amplitude for a coil 9 mm long.

6.2.6 Study on signal conditioning of the pickup coil signal

A study was done to establish the effects of modifying/conditioning the received pickup coil signal by an amplification factor. To achieve this, the received signal was multiplied by an amplification factor. Results were compared with those received when the source voltage was increased to 40 V peak-to-peak. For a source voltage of 20 Volt peak-to-peak, the signal was multiplied by a factor of 2 and for a source voltage of 10 Volt peak-to-peak by a factor of 4. Results are presented in figure 6.11.

It is observed that the modified signals and the signal with a source voltage of 40 Volt peak-to-peak have peak voltages and loci similar to those of the 40 Volt peak-to peak system for all thicknesses. This implies that a lower voltage source can be used to achieve the same results as those achieved by a higher voltage source with the aid of an amplification factor. It is always desirable to produce an instrument that requires minimal source amplitude voltages. Although it is earlier observed that sensitivity is improved with increased source voltage amplitude, the simulation study reported in this section indicates that effects of using software/amplification achieves the same result.

The 9 mm long probe wound using a 0.18 mm diameter wire, in used for further simulation studies.

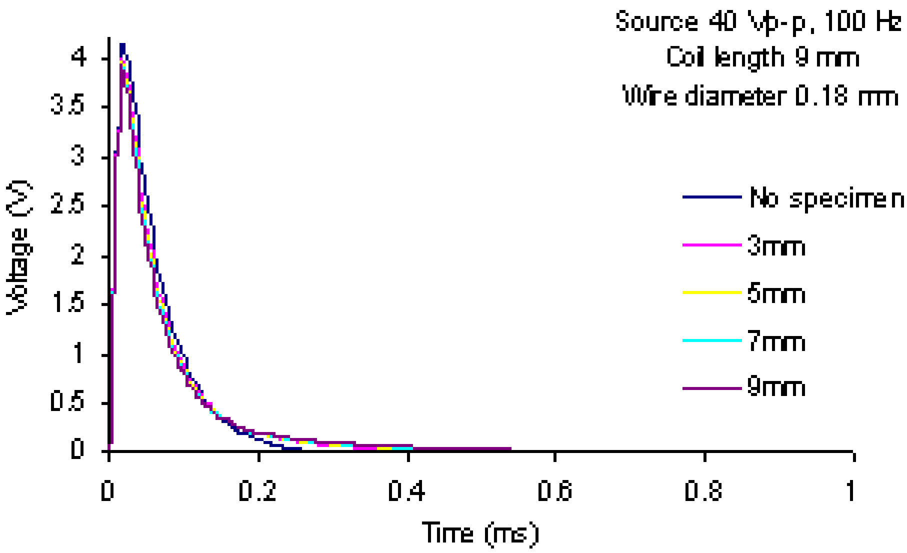
Source 40 Vp-p, 100 Hz
Coil length 9 mm
Wire diameter 0.18 mm
No specimen
3mm
5mm
7mm
9mm
Voltage (V)
4
3.5
3
2.5
2
1.5
1
0.5
0
0
0.2
0.4
0.6
0.8
1
Time (ms)

(a)

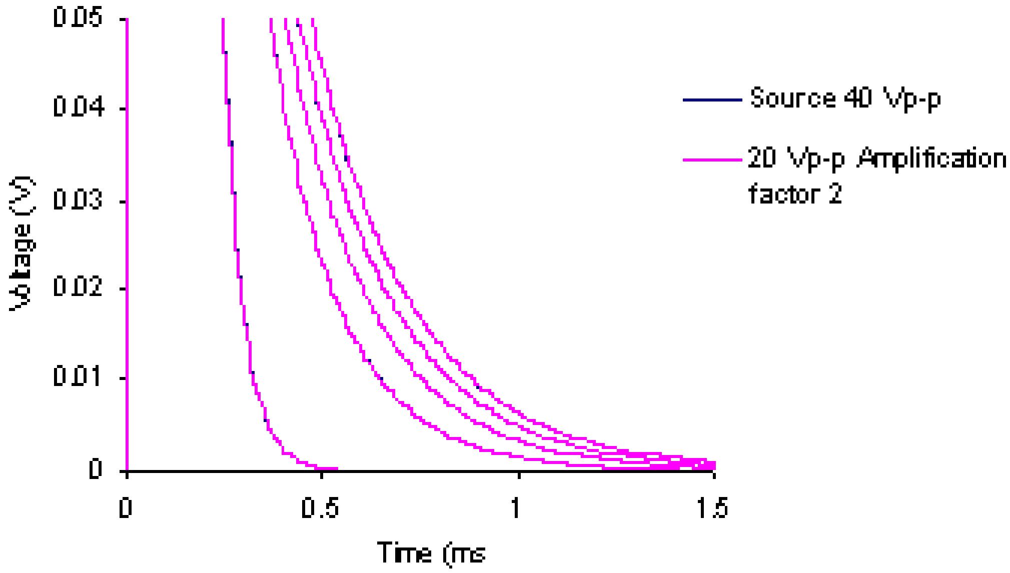
Source 40 Vp-p
20 Vp-p Amplification factor 2
Voltage (V)
0.05
0.04
0.03
0.02
0.01
0
0
0.5
1
1.5
Time (ms

(b))

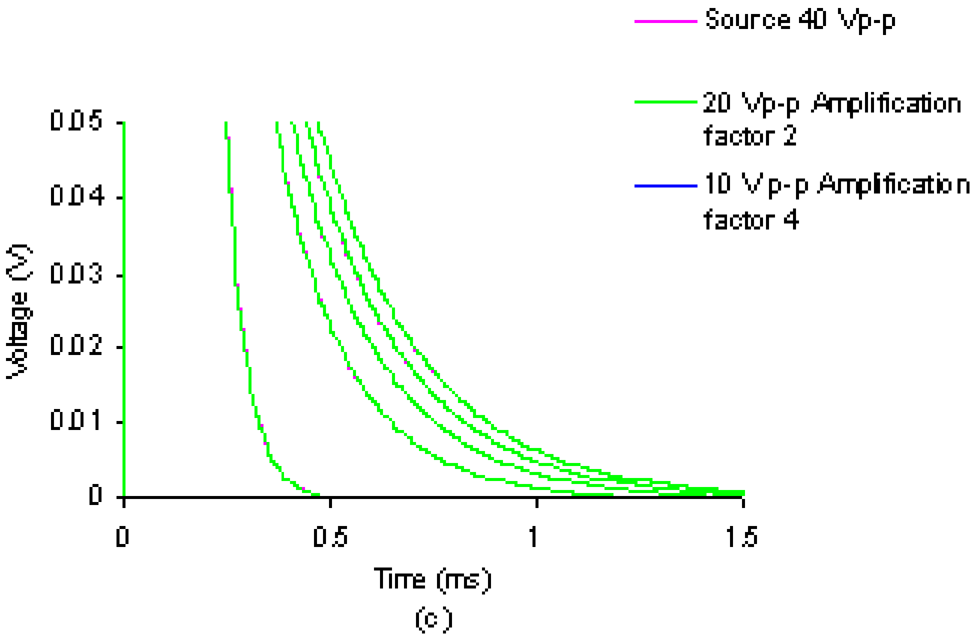

Figure 6.11: Simulated results for different source amplitude for a coil 9 mm long at the indicated amplification factor.

6.3 Discussions

The amplitude and frequency of the pulsed magnetic fields used by the PEC probe are created from a pulsating voltage source. Deep penetration of the specimen by the magnetic field occurs at low frequencies [29] and low frequency pulses would be ideal for deep specimen penetration. However, external interferences especially those from nearby a.c power circuits cause problems at low frequencies in ranges below 100 Hz and internal noises especially those due to random, temperature-induced motion of electrons and other charge carriers in resistors and semiconductors cause problems at higher frequencies above 10^6 Hz respectively [82]. In order to balance these two effects, a source frequency of 1 kHz met the requirements for further investigations.

The resistances and inductances of the probe determine the time to steady state of the signal received from the pickup coil. This is expressed as the time constant of a circuit and for a circuit with resistance and inductance the constant is expressed as the ratio between the inductance and the resistance of the circuit. The probe resistances and inductances are functions of coil dimensions and wire size (See equations 3.27, 3.31, 3.33 and 3.34) repeated here as equations 6.1 to 6.4.

$$R_d = \frac{\rho_d N_d \pi (r_1 + r_2)}{a_d} \tag{6.1}$$

$$R_p = \frac{\rho_p N_p \pi (r_3 + r_4)}{a_p} \tag{6.2}$$

$$L_d = \frac{\mu_d N_d^2 A_{cd}}{l_{dg}} \tag{6.3}$$

$$L_p = \frac{\mu_p N_p^2 A_{cp}}{l_{pg}} \tag{6.4}$$

The voltage variation in the PEC system's output is also a function of the impedances in the system (see section 3.3.3 and 4.4). Changes in coil dimensions and wire sizes therefore affect voltages and currents in the system and the choice of these dimensions is important to the systems performance. Simulations were designed and carried out to give results that would assist in choosing effective probe dimensions. The 9 mm long probe wound from a 0.18 mm wire diameter, on a 4.25 mm core diameter, gave the best sensitivity and was used to carry out further studies on system.

Eddy currents penetration of the specimen is directly dependent on the time duration of the source pulse (section 3.4.2, equation 3.40). This time duration is dependent on the frequency of the square wave used as the source to the system. The higher the frequency, the shorter the pulse duration and therefore the lower the depth penetrated by the eddy currents. Equations 3.59 and 3.68 repeated here as equations 6.5 and 6.6 characterize the specimen as resistance and inductance. These parameters are a function of the skin depth $\delta(t)$ and are therefore affected by the source frequency (equation 3.40).

$$R_{sT1} = \frac{\rho_{sT1} l_{ed}}{\delta(t)\left(e^{y/\delta(t)} - 1\right) r_o . ln\frac{r_1}{r_2}} \tag{6.5}$$

$$L_s = \frac{\mu_s \pi r_1^2}{2\left(\delta(t)(e^{y/\delta(t)} - 1) + r_o \ln\frac{r_2}{r_1}\right)} \tag{6.6}$$

Considering equation 3.40 repeated here as eqution 6.7, the 1 khz source frequency arrived at ensures eddy current penetration of up to 9.27 mm at 25 ^{0}C and 10.6 mm at 100 ^{0}C

$$\delta(t) = \sqrt{\frac{4t}{\mu\sigma}} \tag{6.7}$$

This ensures that for the finishing mill required to gauge 2 mm nominal sheet profile, the specimen is always penetrated by the eddy currents.

6.4 Summary and conclusion

A simulation study presented in this chapter was set up to explore the performance of the proposed eddy current system. Source amplitudes and frequencies were varied and investigated in conjunction with probe sizes to establish system sensitivity and the establishment of steady state in the received PEC signal. Amplification factors were explored to give an assessment on the importance of conditioning the signal by amplification. A simulation study was also carried out on the system's sensitivity for very small changes in specimen thickness. Effects of specimen temperatures on the the system signals and trends in changes both in specimen temperature and specimen thicknesses were studied. The results were presented and comparisons made.

The simulation study suggests that:

- The choice of probe dimensions is important to the system's performance.
- The choice of source frequencies should be limited to a value that allows for the establishment of steady state conditions for the chosen probe dimensions.
- Low source amplitudes can be compensated by signal amplification.
- For very small changes in specimen thicknesses, sensitivities of at least 3 Vm^{-1} for all considered temperatures were achieved from the simulated system.

The study led to choices of the probe size, source voltage and source frequency for further investigations. The 9 mm long probe wound from a 0.18 mm diameter wire, on a 4.25 mm core diameter, gave the best sensitivity and was used to carry out further studies on system. A 20 V peak-to-peak, 1 kHz source was chosen for further investigations. Results show that desirable steady state conditions were achieved at the 1 kHz source frequency and sensivities of up 3 Vm^{-1} for all considered temperatures; for the chosen coil.

Experiments carried out in chapter 7 are complemented by further simulation studies where specimen conditions could not be emulated. An analysis of the results is carried out in chapter 8. In the case where specimen specifications could not be emulated, the specimen characterisation developed in chapter 3 and validated in chapter 5 played an important role in investigation.

Chapter 7

EXPERIMENTS AND RESULTS ON SPECIMEN TEMPERATURES AND THICKNESSES

7.1 Introduction

Experiments and simulations were carried out on specimens having varying temperatures and thicknesses, at a constant lift-off distance of 1.2 mm, to investigate effects of changing specimen temperatures and thicknesses on the received PEC signal. This was done in order to establish ways of isolating effects due to specimen temperature changes from those due to changes in the thickness of the specimen. The 9 mm long coil wound with a 0.18 mm wire diatmeter, on a 4.25 mm core diameter, and a 20 Volt peak-to-peak square wave voltage source at a frequency of 1 kHz, recommended from the simulation study, were used. Results obtained from experiments and simulations carried out under varying conditions of specimen temperature and specimen thickness are reported and discussed in this chapter.

7.2 Experiments

7.2.1 Effects of temperature on the PEC signal

The Pulsed Eddy Current (PEC) system described earlier (see chapter 5) was used to conduct the experiments. Three aluminium plates with different thicknesses (1 mm, 2 mm and 3 mm) were used. The plates were heated to a temperature above 300 ^{0}C. With a thermocouple placed in a hole drilled in the plate, PEC system signals were recorded at specified specimen temperatures between 300 ^{0}C and 50 ^{0}C, in steps of 50 ^{0}C as the specimen cooled down under ambient conditions. Observations made on the PEC signal as the specimen temperature and thickness were varied are presented in figures 7.1 to figure 7.3.

Results show that:

- The locus received in the presence of a specimen always crossed that received without the specimen at a time referred to, in this study, as the time of crossing (TOC) and discussed further in section 7.2.2.
- The locus of the signal received without a specimen always reached desirable steady state conditions earlier than that received in the presence of a specimen.
- For specimen temperatures of up to 100 ^{0}C, there is a point of crossing for each specimen thickness considered in the study and is referred to as the Temperature Point of Crossing (TPC) in this study.
- The TPC increased with increasing specimen thickness: 0.132 ms for a thickness of 1 mm, 0.154 ms for a thickness of 2 mm and 0.166 ms for a thickness of 3 mm.
- The signal voltage at the TPC decreased with increasing specimen thickness: 0.258 V, 0.16 V and 0.128 V for the 1 mm, 2 mm and 3 mm specimen thicknesses respectively.

7.2.2 The time of crossing (TOC)

Tables 7.1 gives a summary of the time of crossing (TOC) for different specimen thicknesses. TOC is defined as the time at which the PEC signal received in the presence of the specimen crosses that received in the absence of a specimen.

And figure 7.2 gives a summary of the peak voltage of the loci received for

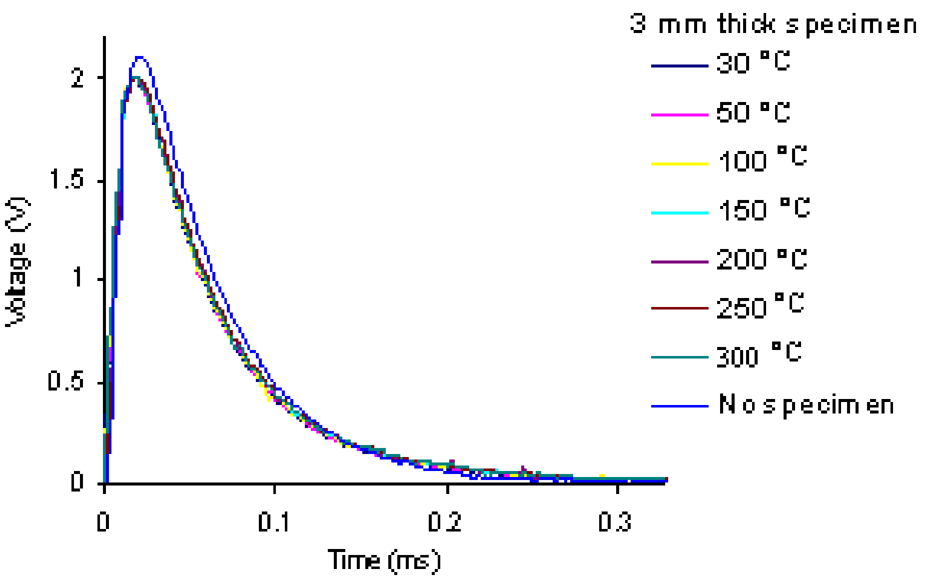

(a)

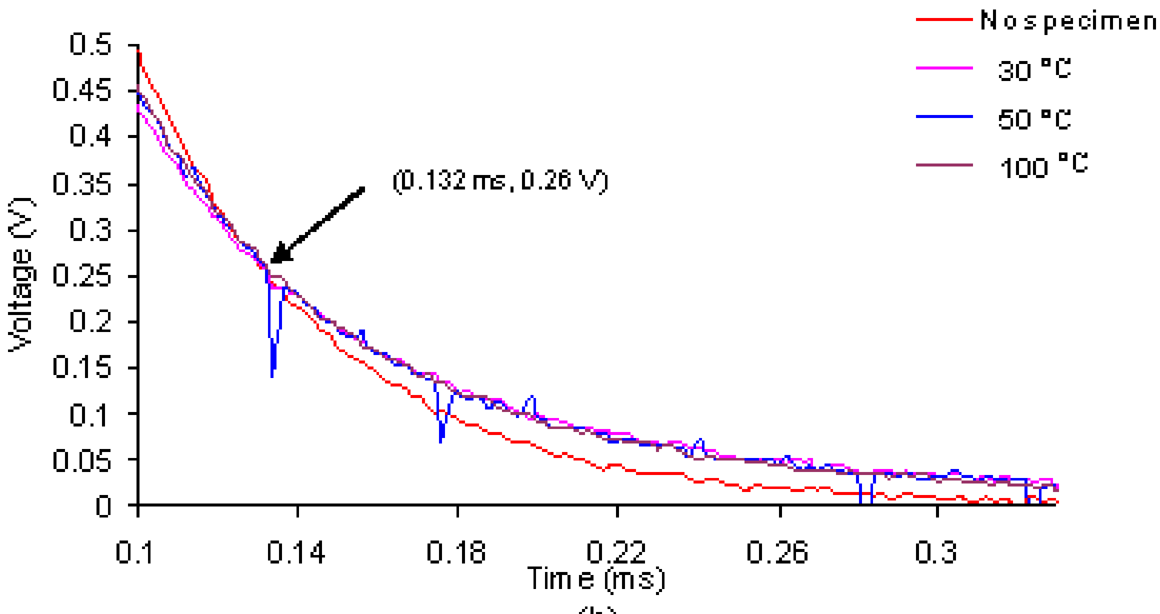

(b)

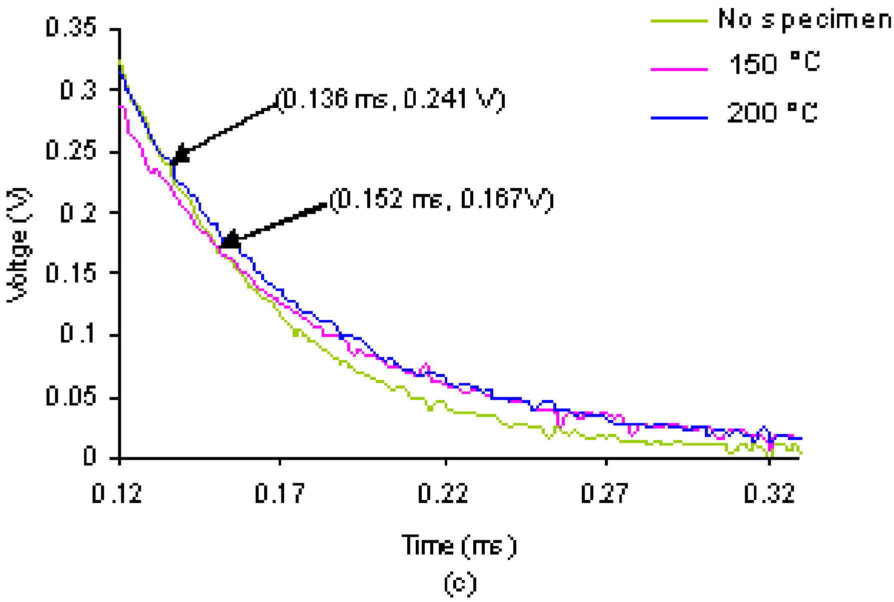

Figure 7.1: Varying temperature in a 1 mm thick specimen.

Table 7.1: Time of crossing in milliseconds in presence of specimens at indicated specimen thicknesses and temperatures

Thickness/Temperature	30 ^{0}C	50 ^{0}C	100 ^{0}C	150 ^{0}C	200 ^{0}C
1 mm	0.132 ms	0.132 ms	0.132 ms	0.15 ms	0.136 ms
2 mm	0.154 ms	0.154 ms	0.154 ms	0.144 ms	0.14 ms
3 mm	0.166 ms	0.166 ms	0.166 ms	0.142 ms	0.138 ms

specimens differing in thickness and/or temperature.

It is observed from these tables that:

- The time of crossing (TOC) increases with increasing specimen thickness.
- For low temperatures up to 100 ^{0}C the TOC is the same for a given thickness irrespective of the difference in temperature.
- For temperatures higher than 100 ^{0}C the trend in the TOC is different and decreases as the specimen temperature increases.
- The peak voltage of the signal received in the presence of a specimen is always lower than that received in the absence of the same.

- The peak voltage of the pickup coil signal is lower for thinner specimen as compared to that of thicker ones if the specimens are at the same temperature.
- Higher temperatures tend to reduce the peak voltage of the pickup coil signal received from specimens of the same thickness.

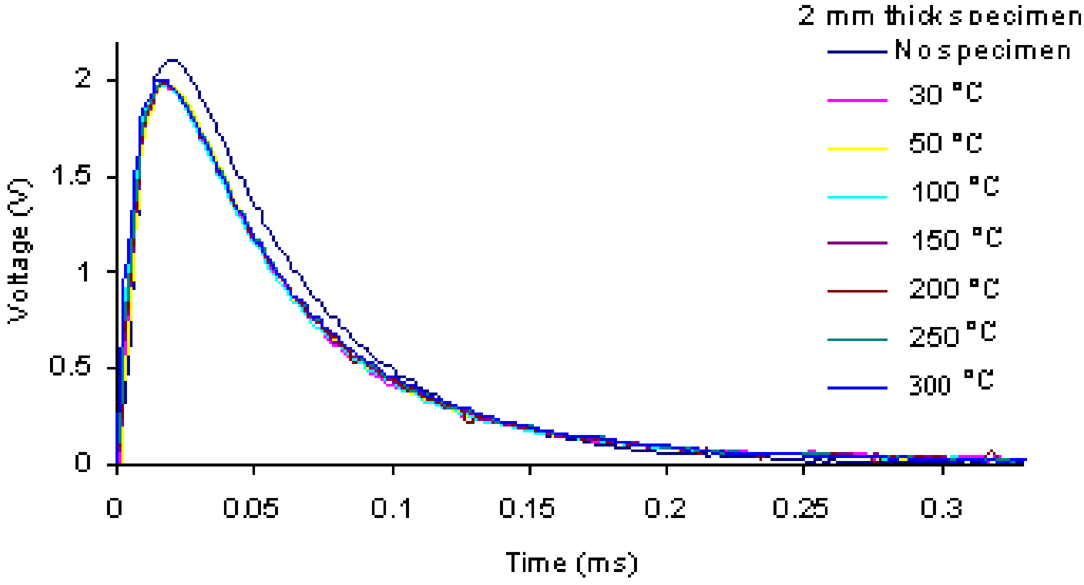

(a)

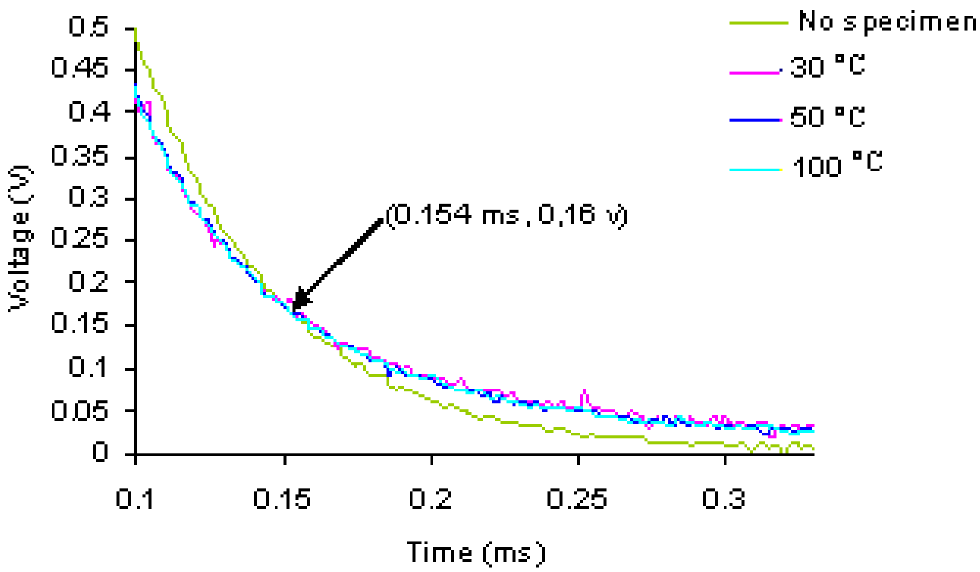

(b)

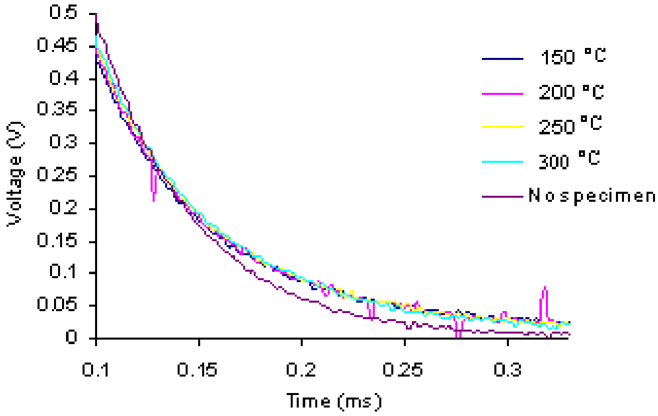

(c)

Figure 7.2: Varying temperature in a 2 mm thick specimen.

Table 7.2: The peak voltage point of the loci received in the presence of specimen with indicated specimen thicknesses at the indicated temperatures

Thickness/Temperature	50 ^{0}C	100 ^{0}C	150 ^{0}C	200 ^{0}C
1 mm	1.999 V	1.991 V	1.911 V	2.001 V
2 mm	2.018 V	1.984 V	1.984 V	1.991 V
3 mm	2.004 V	2.009 V	2.009 V	2.006 V
No specimen	2.126 V	-	-	-

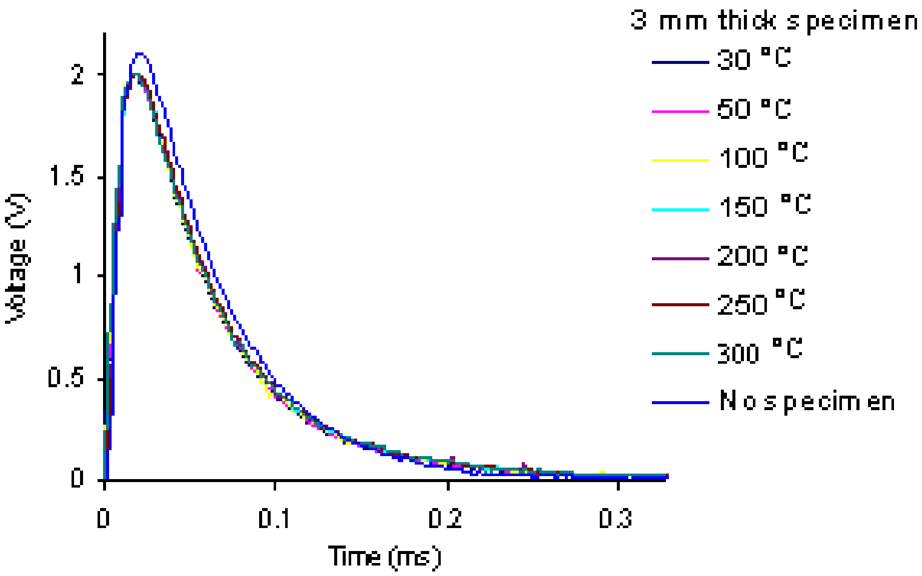
3 mm thick specimen
30 °C
50 °C
100 °C
150 °C
200 °C
250 °C
300 °C
No specimen
Voltage (V)
Time (ms)
(a)

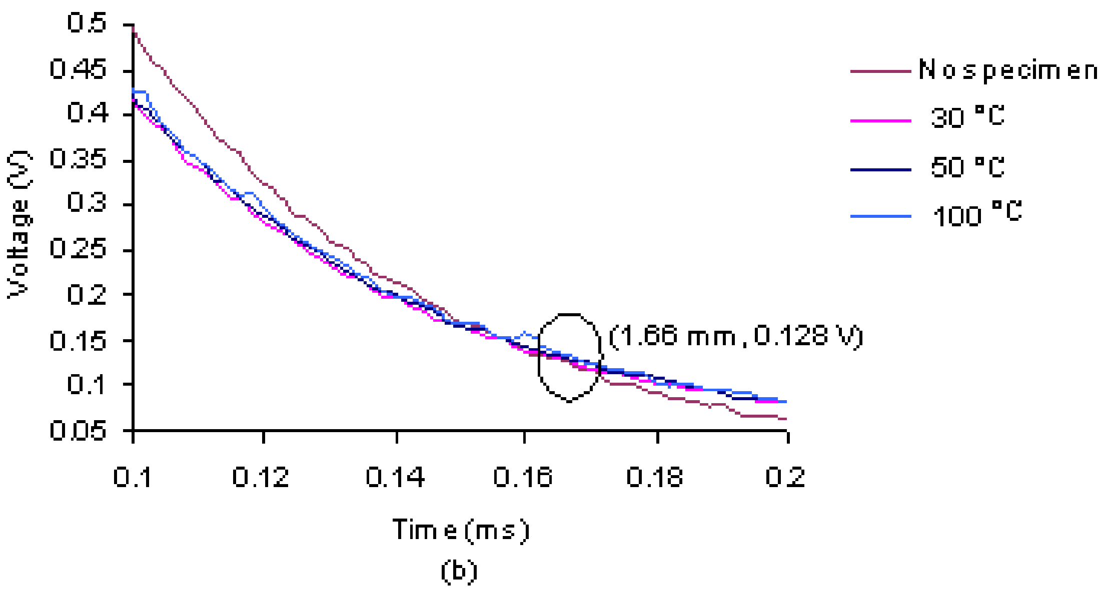
No specimen
30 °C
50 °C
100 °C
(1.66 mm, 0.128 V)
Voltage (V)
Time (ms)
(b)

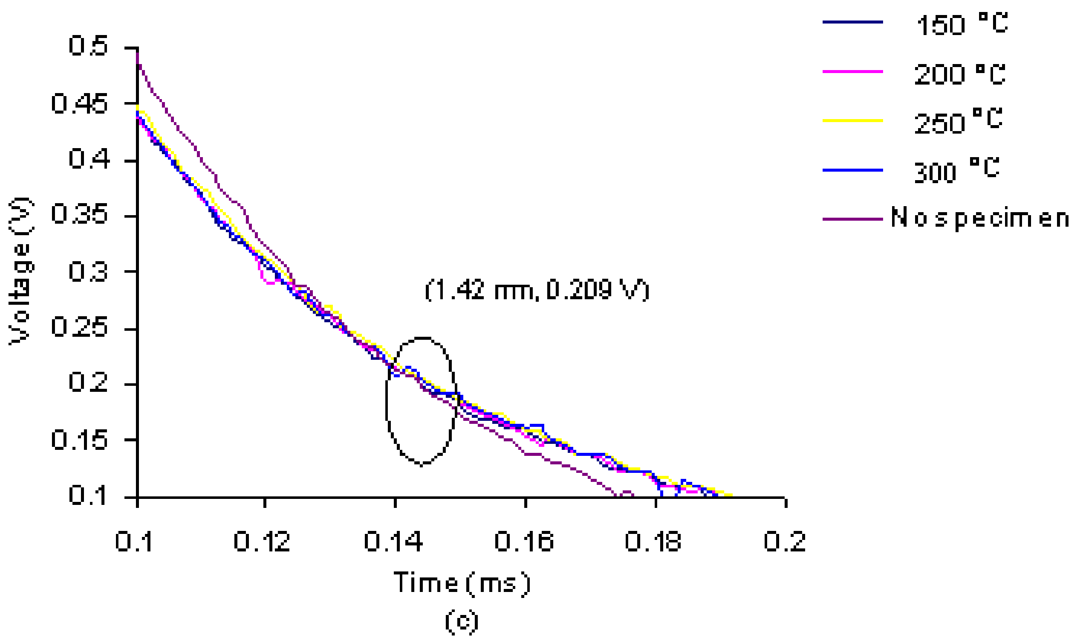

Figure 7.3: Varying temperature in a 3 mm thick specimen.

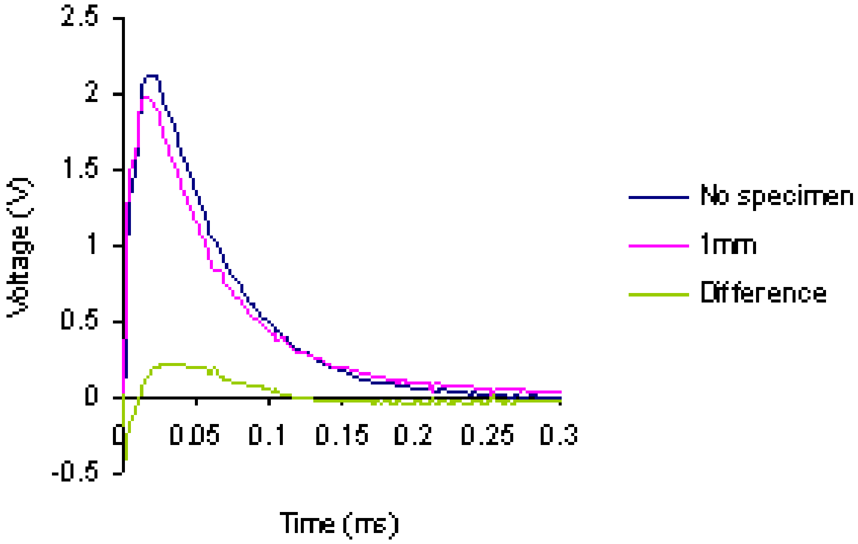
2.5
2
1.5
1
0.5
0
-0.5
Voltage (V)
0
0.05
0.1
0.15
0.2
0.25
0.3
Time (ms)
No specimen
1mm
Difference

(a)

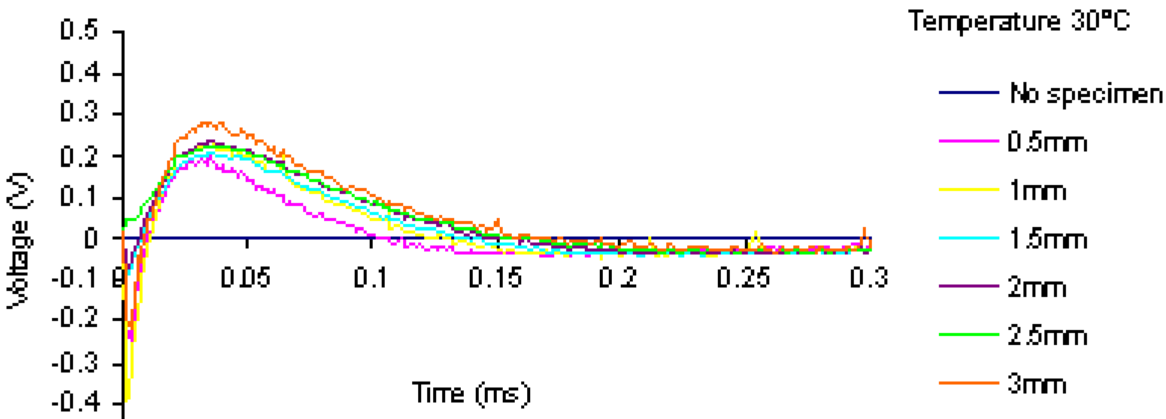
0.5
0.4
0.3
0.2
0.1
0
-0.1
-0.2
-0.3
-0.4
-0.5
Voltage (V)
0
0.05
0.1
0.15
0.2
0.25
0.3
Time (ms)
Temperature 30°C
No specimen
0.5mm
1mm
1.5mm
2mm
2.5mm
3mm

(b)

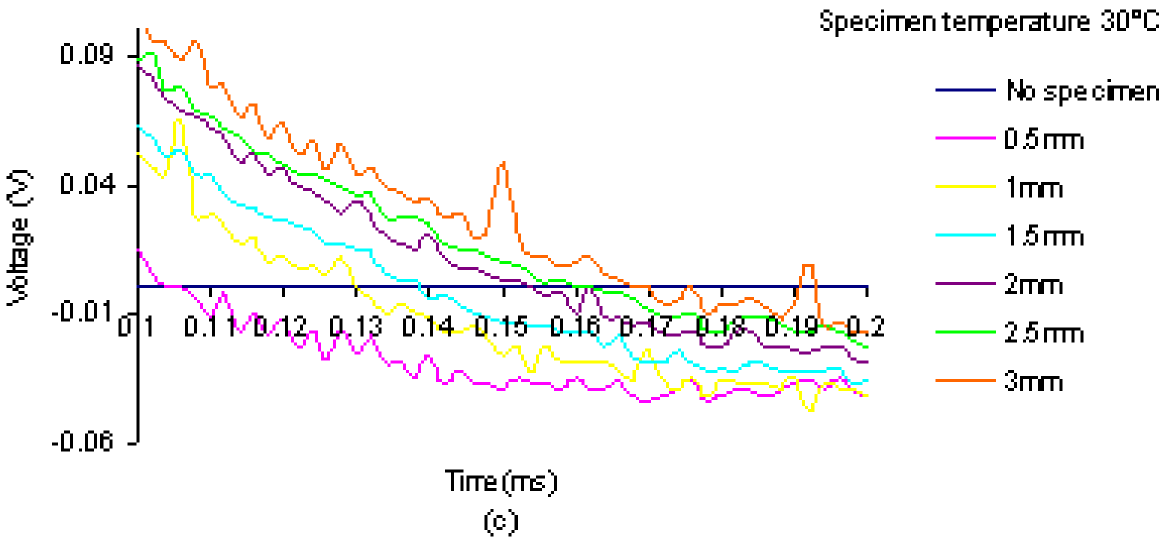

Figure 7.4: TOC coincides with the zero crossing of the difference signal.

7.2.3 Relationship between time of crossing (TOC) and specimen thickness and temperature

Since results show that at low temperatures of up to 100 ^{0}C, the time of crossing is observed to be the same for a given thickness even if the temperature varies, this trend is further investigated in this section. It is an observation that could be used to separate temperature effects from the desired effects due to specimen thickness.

The experiments carried out at an ambient temperature of 30 ^{0}C were used in investigating this observations. Results from experiments for different specimen thicknesses at 30 ^{0}C are presented in figure 7.4 and summarised in table 7.3.

Table 7.3 summarizes the results shown in figure 7.4.

Table 7.3: Presents the TOC for specimen thicknesses at 30^{0}C

Thickness (mm)	0.5	1.0	1.5	2.0	2.5	3
Time of crossing (ms)	0.104	0.132	0.138	0.154	0.162	0.166

In order to analyse the data presented for the time of crossing at 30 ^{0}C, data was collected for the same conditions but at differrent times. Data sampled at times labeled t_1 to t_5 is recorded in table 7.4.

Table 7.4: The relationship between the time of crossing (ms) for various thicknesses at a common temperature

Thickness (mm)	t_1(ms)	t_2(ms)	t_3(ms)	t_4(ms)	t_5(ms)	t_{ave}(ms)
0.5	0.116	0.098	0.098	0.102	0.102	0.1032
1	0.128	0.118	0.118	0.122	0.122	0.1216
1.5	0.142	0.13	0.136	0.134	0.138	0.136
2	0.15	0.136	0.142	0.14	0.14	0.1416
2.5	0.158	0.152	0.156	0.158	0.162	0.1572
3	0.17	0.168	0.17	0.172	0.17	0.17

For the chosen samples, various formulae were tested using Microsoft Excel and Matlab linear regression facilities to determine the formula that described the data. Table 7.5 and 7.6 shows calculated statistical data for the fitted 4 th polynomial data [83, 84, 85, 86] .

- The local average is the average time of crossing for the considered specimen thickness.
- The fitted value is the value generated by the 4 th polynomial equation for the considered specimen thickness.
- Error = $\sum$(observed value-fitted value)^2
- Pure Error = $\sum$(observed value-local average)^2
- Lack-of-fit (LOF)= 5x(local average-fitted value)^2
- For this data, 5 is the degree of freedom
- MSE =(Error)/5
- Standard Deviation = $\sqrt{(MSE)}$

Table 7.5: Calculated statistical data for the fitted 4 th polynomial that describes the relationship between the TOC and varying specimen thickness at a common specimen temperature

Thickness (mm)	Local Ave.(ms)	Fitted Value(ms)	Error (ms)^2	Pure Error(ms)^2	Lack-of-fit (ms)^2	Calc. Error(ms)^2
0.5	0.1032	0.10299	0.000221	0.000221	2.127 x 10^{-7}	0.000221
1	0.1216	0.1227	7.32x 10^{-5}	6.72x 10^{-5}	6.05x 10^{-6}	7.33x 10^{-5}
1.5	0.136	0.1334	2.98 x 10^{-4}	3.0x 10^{-4}	2.6x 10^{-5}	3.26x 10^{-4}
2	0.1416	0.1434	1.234x 10^{-4}	1.07 x 10^{-4}	1.62x 10^{-5}	1.23 x 10^{-4}
2.5	0.1572	0.155	7.6x 10^{-5}	5.28x 10^{-5}	2.324x 10^{-5}	7.6 x 10^{-5}
3	0.17	0.1679	3.0x 10^{-5}	8.0 x 10^{-6}	2.20x 10^{-5}	3.0x 10^{-5}

The lowest maximum least square error (0.0003 (ms)^2), defined as the sum of pure error and the lack-of-fit was found to be minimal in the 4th polynomial.

A plot of the times of crossing in milliseconds versus specimen thicknesses in millimeters at 30 ^{0}C, for the indicated sample times, is presented in figure 7.5. An error band of ±0.005 ms is observed from the data from the averaged

Table 7.6: Calculated statistical data for the fitted 4 th polynomial that describes the relationship between the TOC and varying specimen thickness at a common specimen temperature

Thickness (mm)	Local Ave.(ms)	Fitted Value(ms)	Error $(ms)^2$	MSE $(ms)^2$	Standard Dev.(ms)	LOF Dev.(ms)
0.5	0.1032	0.10299	2.21x 10^{-5}	4.42 x 10^{-5}	6.64 x 10^{-3}	0.2 x 10^{-3}
1	0.1216	0.1227	7.32x 10^{-5}	1.46 x 10^{-5}	3.83 x 10^{-3}	1.1x 10^{-3}
1.5	0.136	0.1334	2.98 x 10^{-4}	5.97 x 10^{-5}	7.73 x 10^{-3}	2.3 x 10^{-3}
2	0.1416	0.1434	1.234x 10^{-4}	2.47 x 10^{-5}	4.97 x 10^{-3}	1.8 x 10^{-3}
2.5	0.1572	0.155	7.6x 10^{-5}	1.52 x 10^{-5}	3.9 x 10^{-3}	2.2 x 10^{-3}
3	0.17	0.1679	3.0x 10^{-5}	0.6 x 10^{-5}	2.45 x 10^{-3}	2.1 x 10^{-3}

relatioship. This means that for any value of the specimen thickness, the time of crossing will be within ± 0.005 ms of the fitted 4^{th} polynomial value.

In table 7.6 statistical data referred to as Lack-of-fit deviation (LOF Dev.)is included. This value is defined in this study as the deviation of the local average from the fitted value.

- LOF Deviation = $\sqrt{(LOF))/5}$

Considering that in a single data collection activity, a considerable number of TOC points at various times within the pickup coil signal are available, one can work with a local average. In the analysis of data that follows, a local average is always used together with the fitted value. It is noted that the deviation of the local average from the fitted value is approximately 2 μs for the thicknesses that are considered. The value of the TOC that is subsquently used in this study is the local average at the considered specimen thickness.

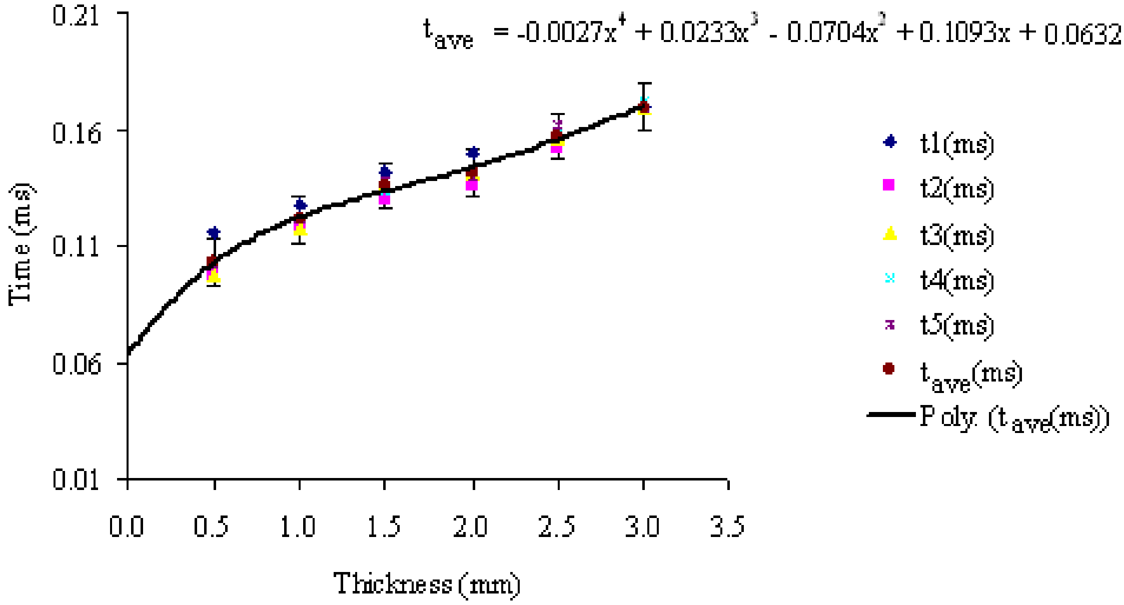

Figure 7.5: Time of crossing versus specimen thickness.

Table 7.7: Simulation results showing the relationship between the TOC (ms) for different thicknesses at a common temperature

Thickness (mm)	25 ^0C	50 ^0C	100 ^0C	150 ^0C
0.5	0.0965	0.0925	0.0875	0.0845
1	0.1165	0.1115	0.1055	0.1005
1.5	0.1285	0.1225	0.1155	0.1105
2	0.1355	0.1305	0.1225	0.1175
2.5	0.1415	0.1355	0.1275	0.1215
3	0.1455	0.1395	0.1315	0.1255
3.5	0.1495	0.1425	0.1345	0.1285
4	0.1505	0.1455	0.1365	0.1305

The relationship between the time of crossing for various thicknesses at a common temperature was established by taking thicknesses of the specimen at a common temperature varied between 0.5 mm and 4 mm in steps of 0.5 mm. Table 7.7 summarises results from the simulations and figure 7.6 shows the relationships at 25 ^{o}C, 50 ^{0}C, 100 ^{0}C and 150 ^{0}C together with the curves that give the best fit. All the curves show a 4^{th} order polynomial (see figure 7.6).

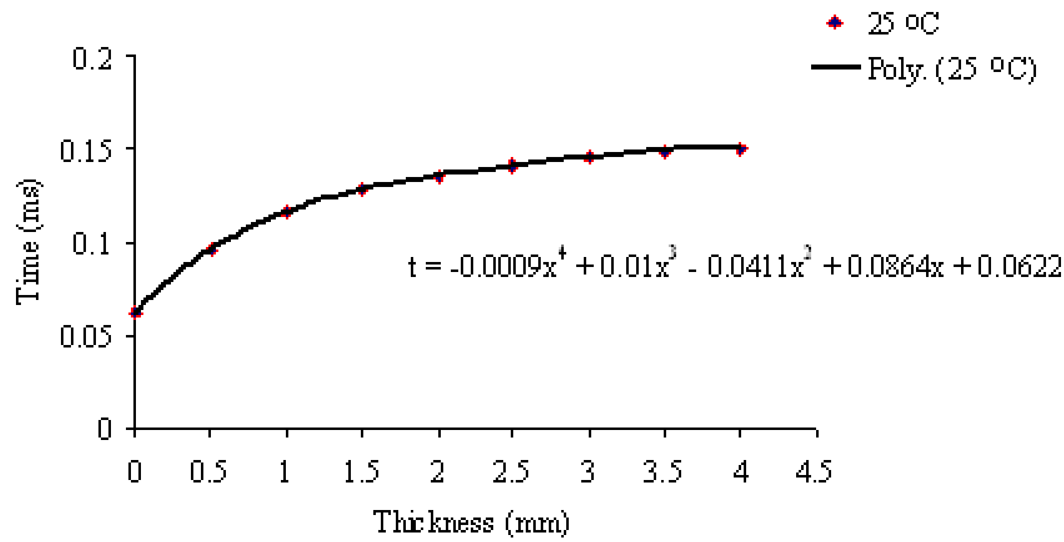

(a)

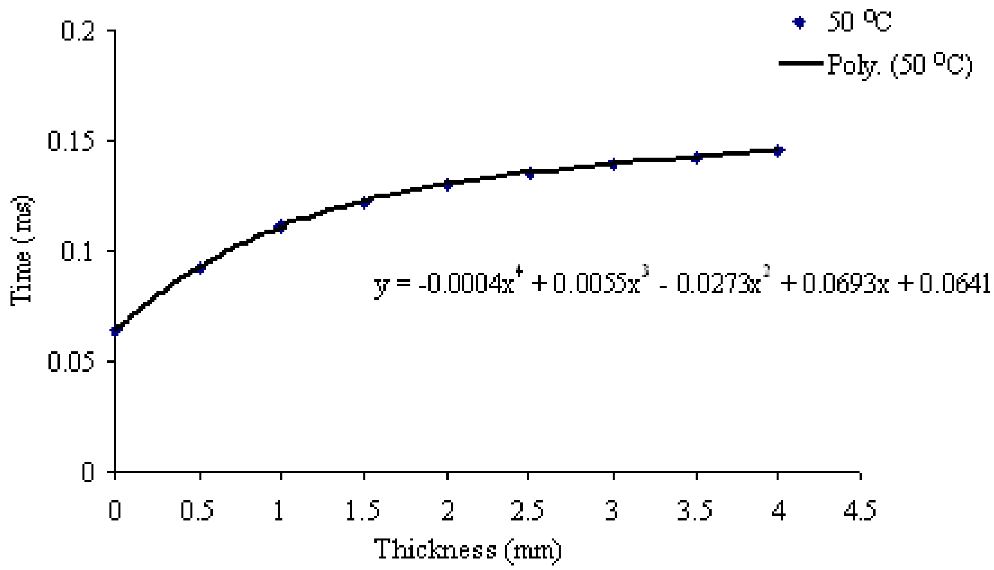

(b)

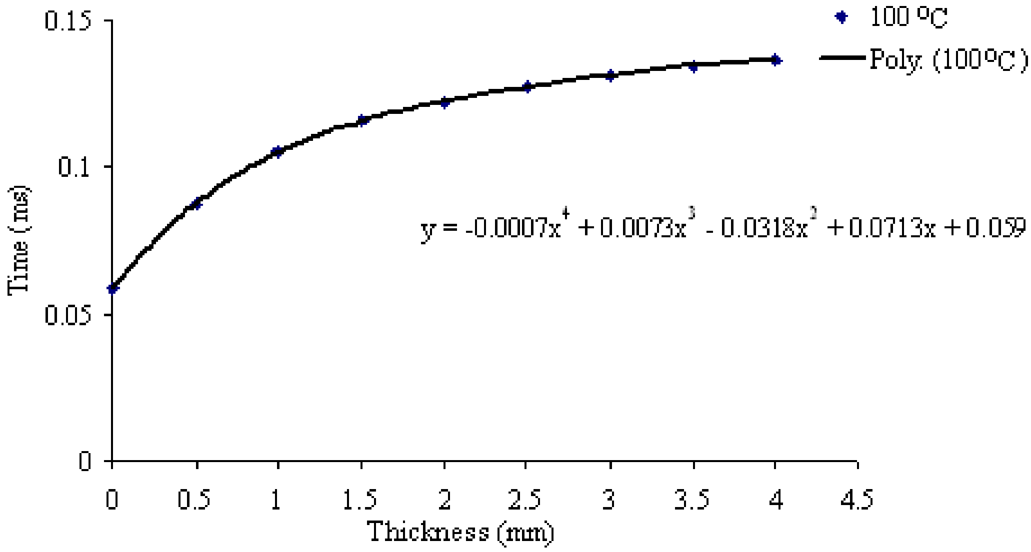

(c)

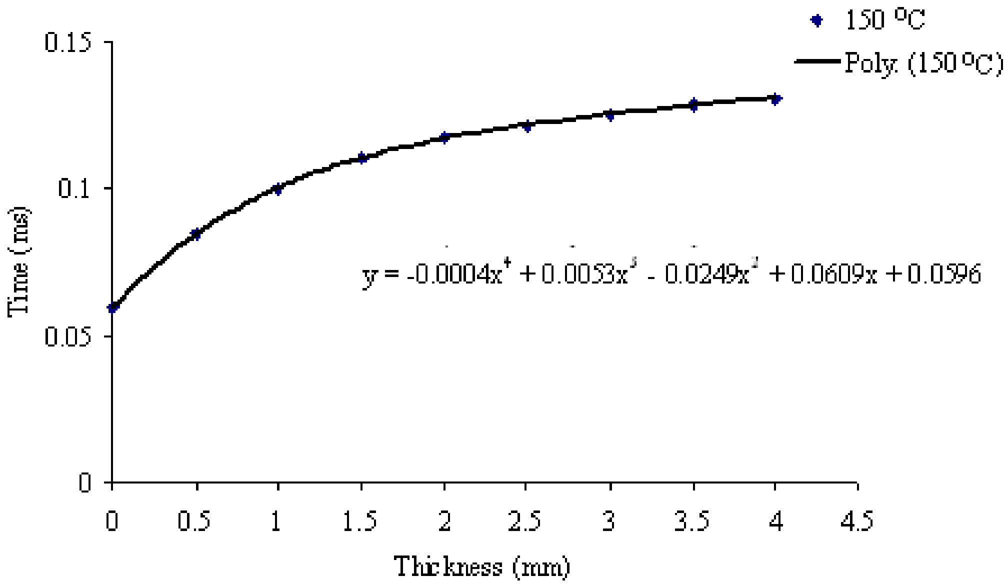

Figure 7.6: Best fit for TOC versus specimen thicknesses at indicated specimen temperatures.

Simulations on varying signal amplification factors were carried out to establish whether signal amplification would affect the time of crossing. Results are presented in figure 7.7 and they show that the amplification factor does not affect the time of crossing. For the indicated amplification factors, all the curves cross the zero line at the same time (0.2 ms).

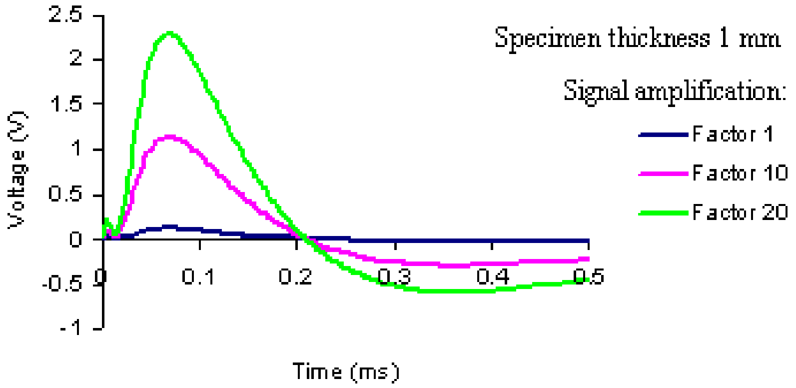

Figure 7.7: Time of crossing for varying signal amplification factor.

7.3 Simulation for a three point profile gauging system

In order to make a conclusive assessment of the system, simulations were carried out for the three point system. Differences in specimen thickness of up to 5 μm were considered.

7.3.1 Profile at a nominal thickness

Table 7.8 presents results from simulations for the TOC at a nominal thicknesses h_o of 2 mm and 2.5 mm. Small variations of 4 μm and 5 μm about the nominal thickness are chosen to investigate profile accuracies for a crown definition of 0.2%.

Table 7.8: TOC (ms) at small thickness variations about nominal thicknesses of 2 mm and 2.5 mm for the indicated specimen temperatures

Thickness (mm)	25 ^0C	50 ^0C	100 ^0C	125 ^0C
1.996	0.1345	0.12983	0.12200	0.11871
2.000	0.13462	0.12988	0.12204	0.11876
2.004	0.13467	0.12993	0.12209	0.11880
2.495	0.14018	0.13522	0.12701	0.12356
2.500	0.14023	0.13526	0.12705	0.12360
2.505	0.14028	0.13531	0.12709	0.12364

It is observed that for small changes of 5 μm at a nominal thickness of 2.5 mm, there is a small change in the TOC of up $\pm$0.06 μs at all specimen temperature considered and for small changes of 4 μm at a nominal thickness of 2.0 mm, there is a small change in the TOC of up $\pm$0.05 μs

7.4 Summary and conclusion

The results from the experiments carried out to investigate effects of temperature and thickness changes in an aluminium specimen on the PEC system signal have been presented in this chapter. In order to make a conclusive assessment of the system, simulations of the three point system, used for quality control in aluminium hot rolling mills, were carried out for variations in specimen thickness of up to 5 μm. Observations made from experiments and simulations reported on in this chapter are summarised here:

- Changes in temperature of a specimen affect the locus of the received signal.
- A crossing point was observed for varying specimen temperatures of upto 100 ^{0}C at a common specimen thickness. This is referred to as the Temperature Point of Crossing (TPC) in this study.
- The TPC increased as the thickness of the specimen increased.
- The locus received in the presence of a specimen always crossed that

received without the specimen at a time referred to, in this study, as the time of crossing (TOC).

- The time of crossing (TOC) was observed to be the same for a common thickness for temperatures below 100 ^{0}C and it increases with increasing specimen thickness.

- An error band of ±0.005 ms is observed from the data taken at an ambient temperature of 30 ^{0}C for specimen thickness varying between 0.5 mm and 3 mm.

- The relationship between the TOC and specimen thickness is a 4^{th} order polynomial for results from both experiments and simulations.

- It is noted that the deviation of the local average from the fitted value is approximately 2 μs for the thicknesses that are considered.

- For small changes of 5 μm at a nominal thickness of 2.5 mm, there is a small change in the TOC of up ±0.06 μs at all specimen temperature considered and for small changes of 4 μm at a nominal thickness of 2.0 mm, there is a small change in the TOC of up ±0.05 μs

The value of the TOC that is subsquently used in this study is the local average at the considered specimen thickness. In chapter 8 a report on the analysis of the findings from the experiments and simulations is given. This process leads to a method of isolating profile from the effects of specimen temperature changes.

Chapter 8

ANALYSIS OF RESULTS

Results from experiments and simulations presented in chapter 5, 6 and 7 show that various changes in the aluminium specimen and the PEC system affect the signal received from the probe. The received signal is affected by system and specimen parameters such as lift-off, specimen thickness and temperature, coil sizes, wire sizes etc. In this chapter, observations made from the investigative experiments and simulations are analysed to establish possible procedures of using the received signals to isolate a profile from other system parameters.

8.1 Introduction

Researchers have investigated pulsed eddy currents for various applications. Effects of thickness and conductivity of a specimen together with probe lift-off distances on the received signal have been reported (see chapter 2). The application in this study adds in two other parameters that are not well documented for PEC application:

- Temperature of the specimen and
- Relative motion between the specimen and the probe.

Findings regarding relative motion between the probe and the specimen are reported in Appendix A. From these investigations, a quasi-static estimation was adapted for the model.

A summary of the observations made in preceding chapters, on the effects of specimen temperature on the PEC signal, is given below:

- Changes in temperature of a specimen affect the locus of the received signal.
- A crossing point (referred to as Temperature crossing point (TCP)) was observed for varying specimen temperatures at a common specimen thickness for temperatures of upto 100 ^{o}C.
- The TCP happens at an earlier time in the PEC signal period for thinner materials than it does for thicker materials.
- The locus of the signal received in the presence of a specimen always crosses the locus of the signal received in the absence of a specimen.
- This time referred to as the time of crossing (TOC) happens at different times depending on specimen conditions.
- Experiments presented in chapter 7 showed that the TOC for a specimen with a common thickness happens at the same time for temperatures below 100 ^{o}C.
- Observations made on the signal above 150 ^{o}C ceased to follow trends observed at lower specimen temperatures.

It was also observed, from experiments and simulations that:

- Thinner aluminium specimen attenuate the PEC signal more than thicker ones.
- Thinner specimens manifest earlier TOC than thicker specimens despite temperature changes.

This consistent change in TOC as the specimen thickness increases is investigated further to suggest a way of separating specimen temperature effects from those due to thickness changes in the specimen.

8.2 Extracting thickness from a temperature varying specimen

As reported in chapter 7, the relationship between specimen thickness and TOC, at a specimen temperature of 30 ^{o}C, is a 4^{th} polynomial. Figure 8.1 shows data from experiments conducted at 30 ^{o}C plotted on the same graph with simulated data at the indicated temperatures and thicknesses. It is observed that the simulated data at 25 ^{o}C and data from experiments at 30 ^{o}C, can be fitted with a 4^{th} polynomial with the expression:

$$t = -0.00088x^4 + 0.0094x^3 - 0.039x^2 + 0.084x + 0.063 \tag{8.1}$$

where t is time and x is thickness.

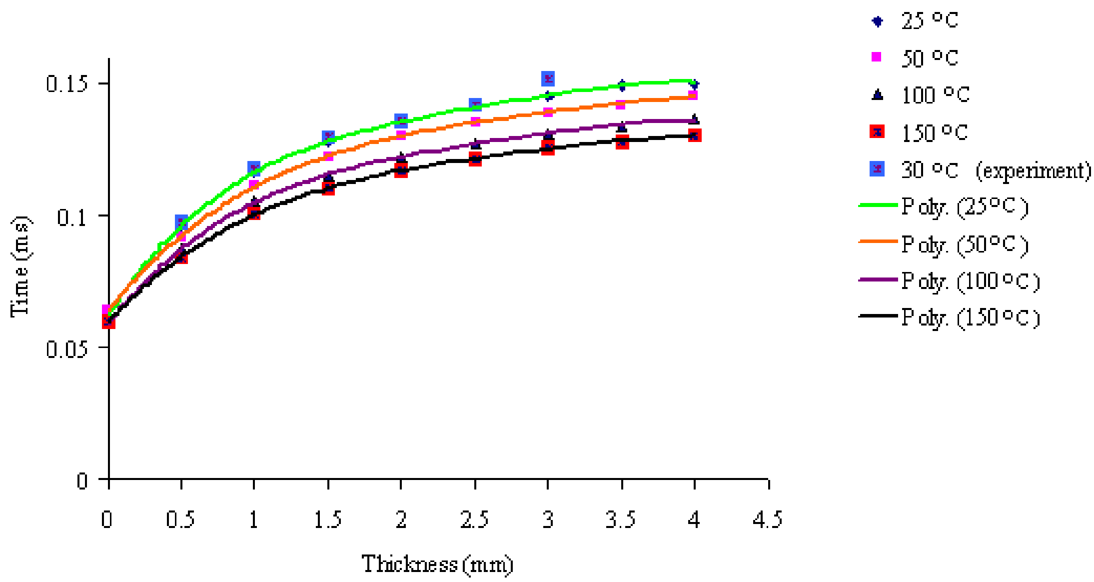

Figure 8.1: Simulated and experiment data for TOC versus specimen thicknesses at indicated specimen temperatures.

This relationship is nonlinear. However, to make profile measurement, small changes about a nominal thickness need to be measured. The next step is to linearization equation 8.1 for small changes about a nominal thickness x_o, of the specimen.

8.2.1 Profile definition related to small changes in specimen thickness

For the purposes of this analysis, we look at the three point definition of profile in hot rolling mills (see section 1.2). Equation 1.1 and 1.2 repeated here as equations 8.2 and 8.3 give a review of the definition of profile.

$$h_{crown} = \frac{[h_o - (h_e^+ + h_e^-)/2]100\%}{h_o} \tag{8.2}$$

$$h_{wedge} = \frac{(h_e^+ - h_e^-)100\%}{h_o} \tag{8.3}$$

where:

- h_o is the thickness at strip center line (mill center line)
- h_e^+ is the thickness at nominal distances x_o more than 100 mm from the drive edge.
- h_e^- is the thickness at nominal distances x_o more than 100 mm from the operator edge.
- h_{wedge} is percentage wedge
- h_{crown} is percentage crown

Acceptable profile definition requires thickness differences as small as 4 μm. By linearising the relationship between small changes in thickness and small changes in TOC at the centre line thickness h_o, profile is defined for the monitored sheet dimensions.

At a point (x_o, t_o) on any curve in figure 8.1 a small change in time, $\triangle t$, due to a small change in thickness, $\triangle x$, is expressed below as:

$$\triangle x = x - x_o \tag{8.4}$$

$$\triangle t = t - t_o \tag{8.5}$$

$$\triangle t = \left(\frac{dt(x)}{dx}\right)_{x_o} \triangle x \tag{8.6}$$

Equation 8.6 when applied to equation 8.1 yields a small change in TOC, $\triangle t$, as a function of a small change in specimen thickness, $\triangle x$, at a nominal thickness x_o.

$$\triangle t = (-0.00352x_o^3 + 0.0282x_o^2 - 0.078x_o + 0.084)\triangle x \tag{8.7}$$

and

$$\triangle x = \triangle t/(-0.00352x_o^3 + 0.0282x_o^2 - 0.078x_o + 0.084) \tag{8.8}$$

This is a linear relationship for small change in TOC and specimen thickness at a specific point on the non linear relationship.

8.2.2 Extending the expressions to profile definition

The symbol x is replaced by h. For a three point definition of the profile, the crown expressed in terms of small changes about the nominal thickness h_o (see equation 8.3), $h_e^+ = h_o + \triangle h_e^+$ and $h_e^- = h_o + \triangle h_e^-$.

$$h_{crown} = \frac{[h_o - (h_o + \triangle h_e^+ + h_o + \triangle h_e^-)/2]100\%}{h_o} \tag{8.9}$$

Crown expressed in terms of small changes about h_o gives:

$$h_{crown} = \frac{[-(\triangle h_e^+ + \triangle h_e^-)/2]100\%}{h_o} \tag{8.10}$$

Using equation 8.8 and substituting for $\triangle h_e^+$ and $\triangle h_e^-$

$$h_{crown} = \frac{[-(\triangle t_e^+ + \triangle t_e^-)/2]100\%}{h_o(-0.00352h_o^3 + 0.0282h_o^2 - 0.078h_o + 0.084)} \tag{8.11}$$

The expression of the wedge as a function of small changes about the nominal thickness is derived with the same approach used for the crown and for small changes in profile thicknesses, equation 8.2 becomes:

$$h_{wedge} = \frac{(\triangle h_e^+ - \triangle h_e^-)100\%}{h_o} \tag{8.12}$$

$$h_{wedge} = \frac{[\triangle t_e^+ - \triangle t_e^-]100\%}{h_o(-0.00352h_o^3 + 0.0282h_o^2 - 0.078h_o + 0.084)} \tag{8.13}$$

8.3 The three point profile gauging system

To extend the analysis to samples with differences in thicknesses of less than 0.1 mm, the results obtained from the simulations carried out in chapter 7 are used. Other observations made on the curves presented in figure 8.1 include:

- The TOC for a given thickness is highest at the lowest temperature.
- For thicknesses between 1 mm and 4 mm, the curves' loci are approximately parallel to each other implying similar gradients at a given thickness for the different temperatures indicated on the plot.

Also results from experiment show that:

- For specimen temperatures up to 100 ^{o}C, the value of the TOC was observed to be the same for a common thickness despite the difference in specimen temperature.

- The TOC increases with increasing specimen thickness and the trend at 30 ^{o}C is similar to the trend for the simulated data at 25 ^{o}C.

The trends observed from experiments and simulations are used in the processing of the signal received from the PEC system. In the next section, values of crown and wedge determined using the observed trend are discussed.

8.3.1 Signal processing

In order to process the signal recieved from the PEC system, an expression between the TOC and the specimen thickness is established at ambient temperature is used. This section investigates the errors introduced by the use of the same equation for other specimen temperatures. Small variations about the nominal thickness would have a linear expression as explained earlier (section 8.2). Using the equation obtained from experiments carried out at an ambient temperature of 30 ^{o}C, profile is defined by calculating the crown and wedge for simulated results of varying specimen thickness (2 mm and 2.5 mm) at varying specimen temperatures (25 ^{o}C, 50 ^{o}C, 100 ^{o}C and 125 ^{o}C). The expression for the curve is given in equation 8.1. Let $y = t$,the TOC and $x = h$, a thickness at a point in the gauged profile.

$$t = -0.00088h^4 + 0.0094h^3 - 0.039h^2 + 0.0864h + 0.063 \tag{8.14}$$

In this section, the simulation results presented in chapter 7 are used to calculate crown and wedge. Table 7.6 presents the results for the TOC at a nominal thickness h_o of 2 mm and 2.5 mm. Small variations of 4 μm and 5 μm about the nominal thickness are chosen to investigate profile accuracies for a crown definition of 0.2%.

8.3.2 Crown

The small changes in time are derived from table 7.6 and are presented in table 8.1.

Table 8.1: Changes in TOC (ms) at small thickness variations about nominal thicknesses (mm) of 2 mm and 2.5 mm for the indicated specimen temperatures

Thickness (mm)	Nominal (mm)	25 ^oC	50 ^oC	100 ^oC	125 ^oC
1.996	2	-0.00005	-0.00005	-0.00004	-0.00005
2.004	2	0.00005	0.00005	0.00005	0.00004
2.495	2.5	-0.00005	-0.00004	-0.00004	-0.00004
2.505	2.5	0.00005	0.00005	0.00004	0.00004

For the nominal thicknesses of 2 mm and 2.5 mm, consider the thicknesses at the operator side h_e^- and the drive side h_e^+ to be 2.004 mm and 2.505 mm respectively. Using results recorded in table 8.1 for the small changes in TOC, $\triangle t_e^-$ and $\triangle t_e^+$, the crown, h_{crown}, can be processed fom the received PEC signals using equation 8.11. The results are presented in table 8.2.

Table 8.2: The percentage crown caculate from small changes in TOC (ms) due to small thickness variations about nominal thicknesses (mm) of 2 mm and 2.5 mm for the indicated specimen temperatures

h_e^- (mm)	h_e^+ (mm)	Nominal (mm)	25 ^oC	50 ^oC	100 ^oC	125 ^oC
2.004	2.004	2	-0.19778%	-0.19778%	-0.19778%	-0.15825%
2.505	2.505	2.5	-0.19512%	-0.19512%	-0.1561%	-0.1561%

The processed crown definitions give a negative crown of ≈ -0.2% for all conditions with a maximum error 0.04%.

Using the same considerations for thicknesses at the operator side and the drive side of 1.996 and 2.495 mm at a nominal thickness ess of 2 and 2.5 mm for all considered temperatures, the percentage crowns are presented in table 8.3.

All processed crown definitions give a positive crown of ≈ 0.2% for all conditions with a maximum error 0.04%.

Table 8.3: The percentage crown caculate from small changes in TOC (ms) due to small thickness variations about nominal thicknesses of 2 mm and 2.5 mm for the indicated specimen temperatures

h_e^- (mm)	h_e^+ (mm)	Nominal (mm)	25 ^oC	50 ^oC	100 ^oC	125 ^oC
1.996	1.996	2	-0.19778%	-0.19778%	-0.15825%	-0.19778%
2.495	2.495	2.5	-0.19512%	-0.1561%	-0.1561%	-0.1561%

8.3.3 Wedge

For wedge definition, the small changes in time are again obtained from table 8.1. For a wedge of 0.2%, the thickness at the operator side, h_e^-, and at the drive side, h_e^+, can be chosen to be 2.505 mm and 2.500 mm respectively at a nominal thickness of 2.5 mm. At a nominal thickness of 2 mm, h_e^- and h_e^+ is chosen as 2.004 and 2.000 mm respectively. Wedge is calculated using equation 8.13. The results for the wedge definitions derived from the TOC for the considered conditions are presented in table 8.4.

Table 8.4: The percentage wedge caculate from small changes in TOC (ms) due to small thickness variations about nominal thicknesses of 2 mm and 2.5 mm for the indicated specimen temperatures

h_e^+ (mm)	h_e^- (mm)	Nominal (mm)	25 ^oC	50 ^oC	100 ^oC	125 ^oC
2.004	2.000	2	-0.19778%	-0.19778%	-0.19778%	-0.15823%
2.505	2.500	2.5	-0.19512%	-0.1561%	-0.1561%	-0.1561%

The processed wedge definitions also give a wedge of $\approx 0.2\%$ for all conditions with a maximum error 0.04%.

8.4 Summary and Conclusion

An analysis of results reported from simulations and experiments has been presented in this chapter. A possible process of extracting changes in specimen thickness from changes in other specimen parameters has been explored. Variation in specimen temperatures have been circumvented for the profile application since small changes about a nominal thickness are being considered.

An equation determined at a low temperature of 30 ^{o}C has successfully been used to extract values of profile from the PEC signal at a higher temperatures. By linearising the expression small changes in thickness at a common temperature are echoed in the time of crossing. The changes in the time of crossing are used to extract profile from the signal collected at the pickup coil. For nominal specimen thicknesses of 2 mm and 2.5 mm the wedge and crown were procesed to be $\approx 0.2\%$ for the temperatures considered with a maximum error of $\pm 0.04\%$

It can be concluded that a calibration can be carried out at room temperature to obtain an equation for the relationship between the point of crossing and changes in the specimen thickness. This equation can then be used to process the signals received from the PEC system to determine profile definition values for crown and wedge at temperatures other than ambient for small variations in profile thicknesses of up to 4 μm.

In the next chapter, findings, limitations and recommendations presented are given. Further research is also suggested.

Chapter 9

CONCLUSION

9.1 Introduction

An investigation of Pulsed Eddy Currents for the purpose of establishing possible application of this phenomenon to profile gauging in Aluminium Hot Rolling mills has been carried out in this study. This chapter summarises findings and implications of the study. It includes limitations of the study and suggestions for further research are also presented.

9.2 Findings

The study made on the PEC system presented show that:

- The movement of the alumnium sheet at varying speed does not affect the pulsed eddy current signal and so a quasi-static approximation could be adopted for the system model that was used to extend the study by simulations.
- Characterising the aluminium sheet as resistance and inductance proved to be a good estimate of the specimen and it was possible to carry out

a simulation study for samples that could not be readily emulated for experiments.

- Low frequencies showed interferences and high frequencies did not allow the establishment of steady state. A frequency of 1 kHz was adopted for experiments and simulations as a compromise between the two extremes.
- Different coil sizes give different signal loci and choice of coil dimensions is import in an application.
- A lower voltage source can be used to achieve the same results as a higher voltage source. This was proved by experimenting with amplification factors.
- It can be said from the presented study that pulsed eddy currents (PEC) system show a good sensitivity. A 1 μm change in specimen thickness gives a 3 μV change in the PEC signal.
- There is a temperature point of crossing (TPC) observed for PEC signals obtained when the probe is placed on a specimen of a specific thickness, at a constant liftoff distance and varying specimen temperatures.
- This TPC increases with increasing specimen thickness: for the coil used in the investigations, this happened at 0.132 ms for a thickness of 1 mm, at 0.154 ms for a thickness of 2 mm and at 0.166 ms for a thickness of 3 mm.
- A time of crossing (TOC) is observed between the PEC signal received without a specimen present and that received in the presence of a specimen and was used in the process of determining the profile.
- This TOC increases with incresing specimen thickness and is not affected by signal amplification.
- A relationship between the TOC and the specimen thickness was obtained for different specimen temperatures. Each one of these expressions was a 4^{th} order polynomial.
- An equation relating this TOC and the thickness of the specimen at 30 ^{o}C was used to calculate values of percentage crown and wedge using a three point system for other temperatures by linearising the expression

at the nominal thickness. The calculated crown agreed well with the expected crown for the specified changes in profile with an acurracy of ±0.04%. This suggests that effects of temperature can be separated from those of thickness.

9.3 Implications of the findings

The implications of the outcome of the study include:

- A PEC system can be developed to separate thicknesses of up to 4 microns and profile definition made within accuracies of ±0.04%.
- Low frequency interferences can be eliminated by raising the source frequency to about 1 kHZ.
- Frequencies of the system must be limited to allow steady state conditions to be established in the PEC signal in order to assess effects of thickness on the signal. A source frequency 1.5 kHz did not allow the establishment of steady state condition.
- Interferences brought about by electronic amplification can be eliminated by using software amplification.
- Time of crossing was used to extract profile form the received PEC signals minimising effects due to changes in specimen temperatures with an accuracy of ±0.04% for crown and wedge definitions of 0.2%.
- In this method, the equation relating time of crossing to changes in specimen thickness at ambient temperature is the basis for the calibration of the profile gauging system.
- Choice of coil dimensions is important for an application.

9.4 Limitation of the study

While it was possible to carry out an extensive simulation study, experiments were not as extensive because of the following factors:

- Resources available could not allow for the accurate development of samples with variations less than a tenth of a millimeter. These variations were investigated using the validated simulation environment developed for this study.
- The data collection unit available could not reach sampling times of less than a microsecond.
- Formers available were limited in dimensions.
- Wire sizes are standardized and one had to keep within the available standards.

However, for the purpose of the study, the data collected allowed for an adequate assessment of the PEC technique for profile gauging in aluminium hot rolling mills. The simulation environment developed extended the investigation to thickness differences of up to 4 μm.

9.5 Recommendations

Further investigation would require more extensive experiments. To overcome the limitations of the study, the following is recommended.

- experiments to be carried out on precisely prepared samples with the appropriate variations in thicknesses.
- a data collection system with a higher sampling rate to be sourced.
- Increase variations in probe formers

9.5.1 Development of the profile gauging system

The proposed system has been investigated and extraction of profile has been made possible by processing the signal using the procedures described in chapter 8. Acurracies within ±0.04% were observed. The following are recommendation on what should be considered in the process of developing a gauging system.

- Probe dimensions should be investigated to arrive at the most sensitive probe for the application.
- Signal amplification can be achieved by use of software manipulations to eliminate interferences brought in by electronic circuitry.
- Data collection system with high sampling rates should be used to ensure good resolution.
- Mechanical procedures should be investigated to eliminate lift-off effects.
- Probe should be shielded from magnetic interferences from each other and from near by equipment.

9.6 Conclusion

Pulsed Eddy Currents have been investigated to establish possible application for profile gauging in Aluminium Hot Rolling Mills. Experiments together with simulations studies carried out using an environment developed for the study were the tools used for the investigation. Implications derived from the findings of the study have been used to make recommendations and suggestions for further investigations. A profile within accuracies of ±0.04% at differences in thickness of up to 4 μm, could be determined from the study. This gives an indication that profile can be gauged using PEC to within the specified requirements for the finishing gauge suitable for the needs at Hulett Aluminium in Pietermaritsburg, South Africa.

In the process of the investigation, effects of specimen temperature changes on the PEC signal were observed to have a temperature crossing point (TPC). At this point the loci of the signals received at different specimen temperatures, with the specimen kept at the same thickness, crossed each other. The time at which the crossing point happened increased with increasing specimen thickness.

Expressions characterising the specimen as resistance and inductance were derived in the processes of modelling the PEC system. These expressions lead to simulation results that correlated with results from experiments. This confirms that Eddy currents can be modelled effectively using lumped parameters.

To determine the profile a time of crossing (TOC), which was defined as the time the locus of the PEC signal received without a specimen present crosses that of the signal received in the presence of a specimen, was used. The study suggests that a relationship between the TOC and varying specimen thickness, determined at ambient temperature, could be used to calculate the percentage profile defined for quality assurance. From the study, it can be concluded that PEC could be a good candidate for profile gauging in Aluminium Hot Rolling Mills for very small changes in thickness about a nominal thickness.

References

[1] Brian Wallace. Pulsed Eddy Current Non-destructive testing technique. Technical report, National Research Council: Institute for Aerospace Research, Ottaw, Canada, 1997. Physics Co-op Work Term Report.

[2] IRT. Introduction to strip profile, shape and flatness, Lecture 10, 1999. International Rolling Technology Course.

[3] A. Young. Profile and shape. Technical report, Comalco rolled Product, November 1993. Process Technology Education, Level 1.

[4] T. Heidemeyer. Process control systems. Technical report, Hulett Aluminium Rolled Products (Pty) Ltd, Hulett Aluminium, Pietermaritzburg, RSA, August 1998.

[5] Profile Measurement. Technical report, Hulett Aluminium Rolled Products (Pty) Ltd, Hulett Aluminium, Pietermaritzburg, RSA, 2002. Hulett Aluminium Hotline.

[6] IRT. Profile control strategies, Lecture 20, 1999. International Rolling Technology Course.

[7] R. B. Cresdee, W. J. Edwards, and P. J. Thomas. 'An Advanced model for flatness and profile prediction in hot rolling'. *Bell Labs Technical Journal*, 68(10):41–51, 1998.

[8] Thickness and Profile Measurement, Multi-channel /X-ray. Technical report, Hulett Aluminium Rolled Products (Pty), Hulett Aluminium, Pietermaritzburg RSA., 2004. Technical Specifications A02-24-005n1e.

[9] J. H. Lamble. *Principles and practice of Non- destructive Testing*. London Heywood and Company Ltd, London U.K., 1962.

[10] R. Halmshaw. *Non-desructive testing.* Metallurgy and Material Science, Edward Arnold, 1987.

[11] D. E. Caro, J. A. McDonell, and B. M. Spicer. *An introduction to Atomic and Nuclear physics.* Modern Physics, Edward Arnold, Bedford square London, 3^{rd} edition, 1978.

[12] C. Burnett. Sensor development report. Technical report, Thermo Radimetrie Washington, Washington,USA, December 2001.

[13] G. J. Gibbon. Investigation of measurement from x-ray thickness gauges at Hulett Aluminium Hot line at Camps Drift. Technical report, Hulett Aluminium Rolled Products (Pty) Ltd, Hulett Aluminium, Pietermaritzburg RSA., November 2001.

[14] Radiometrie RM 215 X-Ray Flat Strip Thickness Gauge. Technical report, visited February 2007. `http://www.thermo.com/ethermo/CMA/PDFs/Product/ProductPDF_21390.pdf`.

[15] Oryx. Laser thickness gauge. Technical report, Oryx systems Inc., visited February 2007. `http://www.oryxsystems.com/laser_thickness.htm`.

[16] J. P. Bentley. *Principles of Measurement Systems*, pages 404–408. Longman Scientific and Technical, Essex, England, 3^{rd} edition, 1995.

[17] Checkline. Precision instruments for quality. Technical report, Checkline by electromatic, visited February 2007. `http://www.ultrasonicthicknessgauges.com/`.

[18] A. Krawcyzyk and J. A. Tegopoulos. *Numerical Modelling of Eddy Currents*, pages 1–42. Clarendon Press-oxford, 1993.

[19] D. L. Waidelich. Pulsed Eddy Currents. *'Research Techniques in Nondestructive Testing, Academic press'*, pages 383–416, 1970.

[20] CAN/CGSB. Advanced Manual for Eddy Current Test Methods. Technical report, Canadian General Standards Board, Canada, 1986. CAN/CGSB-48. 14-M86.

[21] E. Kreyszig. *Advanced Engineering Mathematics*, pages 431–485. Wiley International Edition, New York, USA, second edition, 1967.

[22] C. Tia, J. H. Rose, and J. C. Moulder. Thickness and conductivity of metallic layers from pulsed eddy current measurements. *Review of scientific Instruments*, 67(11):3965–3972, November 1996.

[23] J.A. Bieber, C. Tia, and J. C. Moulder. Quantitative assessment of corrosion in aircraft structures using scanning Pulsed Eddy Current. *Review of progress in quantitative Non-destructive Evaluation*, 17:315–322, 1998.

[24] ABB. Unique thickness gauging technology for strip production. Technical report, ABB, visited February 2007. `http://www.sovereign-publications.com/abb-pressductor.htm`.

[25] S. Giguere, B. A. Lepine, and J. M. S. Dubios. Pulsed Eddy Current Technology: Characterizing material Loss with Gap and lift-off Variation. *Research in Non detructive Evaluation*, 13:119–129, November 2001.

[26] J. R. S. Giguere and J. M. S. Dubios. Pulsed Eddy Current: Finding corrosion independently of transducer lift-off. *Review of progress in QNDE*, 19:449–456, 2002.

[27] R. A. Serway and J. W. Jewett. *Physics for scientists and Engineers, with modern physics*, pages 967–1002. Thomson Brooks/Cole, New York, USA, 6^{th} edition, 2000.

[28] N. Mohan, T. M. Undeland, and W. P. Robbins. *Power Electronics, Converters, Applications and Designs*. John Wiley and Sons, Inc, New York, USA, 2^{nd} edition, 1995.

[29] D. L. Waidelech and C. R. Lahmeyer. The testing of thick sheets of metal using Pulsed Eddy Currents. Technical report, University of Missouri Colombia, Missouri 65211, USA, 1979.

[30] H. Knoepfel. *Pulsed High magnetic Fields*, pages 290–386. North-Holland Publishing Company, London, UK, 1970.

[31] W. W. Ward and J. C. Moulder. Low frequency, Pulsed Eddy Currents for deep Penetration. *Review of progress in quantitative Non-destructive Evaluation*, 17:291–298, 1998.

[32] W. Podney. Electromagnetic Microscope for low frequency, Pulsed Eddy Current Evaluation of Airframes. *Review of progress in Quantitative Non-destructive Evaluation*, 17:1017–1024, 1998.

[33] J. H. V. Lefebvre and J. M. S. Dubois. Lift-off Point of Intercept (LOI) Behaviour. 31^{st} *Review of progress in QNDE*, 17, Summer 2001.

[34] D. L. Waidelich and S. C. Huang. The use of Crossing Points in Pulsed Eddy Currents. *Materials Evaluation*, pages 20–24, January 1972.

[35] C. J. Renken. Theory and some application of pulsed current fields to the problem of Non-Destructive Testing. *Progress in Applied Materials Research*, 6:239–269, 1964.

[36] J. A. Bieher, C. Tai, and J. C. Moulder. Time Gating of Pulsed Eddy Currents signals for defects characterization and discrimination in aircraft lap-joints. *Review of progress in quantitative Non-destructive Evaluation*, 16:1915–1921, 1997.

[37] J. R. S. Giguere, B. A. Lepine, and J. M. S. Dubios. Detection of cracks beneath rivets via pulsed eddy current technique. *Review of Progress in QNDE*, 21:1968–1975, 2003.

[38] B. A. Lepine, J. R. S. Giguere, D. S. Forsyth, A. Chahbaz, and J. M. S. Dubios. Interpretetion of pulsed eddy current signals for locating and quantifying metal loss in skin lap splices. *Review of Progress in QNDE*, 21:415–422, 2003.

[39] M. S. Safizadeh, B. A. Lepine, D. S. Forsyth, and A. Fahr. Time frequency analysis of pulsed Eddy Current signals. *Journal of Nondestructive Evaluation*, 20(2):73–87, June 2001.

[40] L. J. Stankovic. On the realization of the polynomial Wigner-Ville Distribution for multicomponent signals. *IEEE Signal processing letter*, 5(7):157–159, July 1998.

[41] J. Grman. Application of wavelet transformation in Eddy Current testing. *Measurement science review*, 1(1):21–24, 2001.

[42] R. K. Young. *Wavelet theory and its application.* Kluwer Academic publishers, 1993.

[43] P. Addison. The little wave with the big future. *Physics world*, pages 35–39, 2004.

[44] A. Grossmann, R. Kronland-Martinet, and Morlet. Reading and Understanding Continuous Wavelet Transforms. In *Proceedings of the international conference on Wavelets Time frequency methods and phase space*, Marseille, France, December 1987.

[45] I. Daubechies. Orthonormal Bases of Wavelets with Finite Support - connection with discrete filters. In *Proceedings of the international conference on Wavelets Time frequency methods and phase space*, Marseille, France, December 1987.

[46] R.Polikar. Series of tutorials to wavelet transform. Technical report, Technology and Quality Control Center, visited June 2011. `http://users.rowan.edu/~polikar/wavelets/wtpart1.html`.

[47] F. Thollon and N. Burais. Modeling and characterization of Pulsed Eddy Currents - Application to Non destructive Testing in Riveted Assemblies used in aeronoutics. *Electric and Magnetic fields, edited by Nicolet A and Belmans R*, pages 261–264, September 1995.

[48] C. J. Renkin. The use of a Personal computer to extract information from Pulsed Eddy Current tests. *Materials Evaluation*, 59(3):362–366, 2001.

[49] J. Bowler and M. Johnson. Pulsed Eddy Current Response to a conducting Half-space. *IEEE Transaction on Magnetics*, 33(3):2258–2264, May 1997.

[50] R. Ludwig and X. Dai. Numerical and Analytical Modeling of Pulsed Eddy Currents in a Conducting Half-Space. *Transaction on Magnetics*, 26(1):299–307, January 1990.

[51] O. Biro and K. Preis. On the use of the Magnetic Vector potential in the Finite Element Analysis of Three- Dimensional Eddy Currents. *Transaction on Magnetics*, 25(4):3145–3159, July 1989.

[52] U. Patel and D. Rodger. Finite element Modeling of Pulsed Eddy Currents for Non- destructive Testing. *IEEE Transaction on Magnetics*, 32(3):1593–1596, July 1996.

[53] B.A. Auld and J. C. Moulder. Review of Advances in Qualitative Eddy Current Nondestructive Evaluation. *Journal of Nondestructive Evaluation*, 18(1):3–36, March 1999.

[54] W. G. Hurley and M. C. Duffy. Calculation of Self and Mutual impedances in Planar Magnetic Structures. *IEEE Transaction on Magnetics*, 31(4):2416–2422, July 1995.

[55] Jack Chessa. Programing the Finite Element Method with Matlab. Technical report, visited July 2011 2002. `http://www.math.purdue.edu/~zcai/math615/matlab_fem.pdf`.

[56] Finite Element Method. Technical report, visited July 2011. `http://en.wikipedia.org/wiki/Finite_element_method`.

[57] James Doyle. *Modern Experimental Stress Analysis: completing the solution of partially specified problems*, pages 11–82. John Wiley and Sons, Ltd, 2004.

[58] E. Kreyszig. *Advanced Engineering Mathematics*, pages 149–154. Wiley International Edition, New York, USA, second edition, 1967.

[59] Daniels A. R. *Introduction to Electrical Machines*. The Macmillan press LTD, Great Britain, 1^{st} edition, 1979.

[60] X. Dai, R. Ludwig, and R. Palanisamy. Numerical simulation of Pulsed Eddy-Current Non-destructive Testing Phenomena. *Transactions on Magnetics*, 26(6):3089–3096, November 1990.

[61] J. L. Rasolonjanahary, F. Thollon, and N. Burais. Study of Eddy Currents Non Destructive Testing System in Riveted Assemblies. *Transactions on Magnetics*, 32(3):1585–1588, November 1996.

[62] B. Angelle and J. C. Sabonnadiere. Numerical Solution of 3D Magnetic field problem using Boundary Integral Equations. *IEEE Transactions on Magnetics*, Mag-16(5):1089–1091, September 1980.

[63] R. Palanisamy and W. Lord. Predication of Eddy Current probe Signal Trajectories. *IEEE Transactions on Magnetics*, Mag-16(5):1083–1085, September 1980.

[64] R. J. Smith. *Circuits, Devices and Systems*, pages 221–222. John Wiley and Sons,INC, New York, USA, 1966.

[65] I. S. Grant and W. R. Philips. *Electromagnetism*, pages 232–233. John Wiley and Sons Ltd, New York, USA, 1978.

[66] Undeland T. M. Mohan N. and Robbins W. P. *Power Electronics, Converters, Applications and Designs*, pages 831–857. John Wiley and Sons,Inc, New York, USA, 2^{nd} edition, 1995.

[67] E. Kreyszig. *Advanced Engineering Mathematics*, pages 192–234. Wiley International Edition, New York, USA, second edition, 1967.

[68] R. A. Serway and J. W. Jewett. *Physics for scientists and Engineers, with modern physics*, pages 926–966. Thomson Brooks/Cole, New York, USA, 6^{th} edition, 2000.

[69] I. S. Grant and W. R. Philips. *Electromagnetism*, pages 149–153. John Wiley and Sons Ltd, New York, USA, 1978.

[70] Serway R. A. and Jewett J. W. *Physics for scientists and Engineers, with modern physics*, pages 894–1032. Thomson Brooks/Cole, New York, USA, 6^{th} edition, 2000.

[71] A. M. Watson, P. G. Lund, and J. D. Todd. *Engineering tables and data*. Chapman and Hall, 1972.

[72] Undeland T. M. Mohan N. and Robbins W. P. *Power Electronics, Converters, Applications and Designs*. John Wiley and Sons,Inc, New York, USA, 2^{nd} edition, 1995.

[73] R. L. Stoll. *The Analysis of Eddy Currents*, pages 4–9. Clarendon Press-Oxford, London, England, 1974.

[74] R. A. Serway and J. W. Jewett. *Physics for scientists and Engineers, with modern physics*, pages 831–857. Thomson Brooks/Cole, New York, USA, 6^{th} edition, 2000.

[75] Bentley J. P. *Principles of Measurement Systems*, pages 135–139. Longman Scientific and Technical, Essex, England, 3^{rd} edition, 1995.

[76] F. C. Moon. *Magneto-solid mechanics*. Wiley, New York, USA, 1984.

[77] Rudra and Pratap. *Getting started with Matlab* **7**. Oxford University Press, New york, USA, 2006.

[78] Matlab. *Learning Matlab* **7**. The MathsWork, Inc., July 2004. Matlab and Simulink Student version.

[79] Simulink. *Learning Simulink.* The MathsWork, Inc., July 2004. Matlab and Simulink Student version.

[80] Bentley J. P. *Principles of Measurement Systems*, pages 43–50. Longman Scientific and Technical, Essex, England, 3^{rd} edition, 1995.

[81] Keithley. Keithley Series 2400 Source Meter line. Technical report, visited August 2007. http://www.keithley.com/products/currentvoltage/path=2400/Documents#4.

[82] Bentley J. P. *Principles of Measurement Systems*, pages 95–110. Longman Scientific and Technical, Essex, England, 3^{rd} edition, 1995.

[83] Regression Analysis. Technical report, visited July 2011. http://en.wikipedia.org/wiki/Regression_analysis.

[84] Lack-of-fit. Technical report, visited July 2011. http://en.wikipedia.org/wiki/Lack-of-fit_sum_of_squares.

[85] Measurement analysis. Technical report, visited July 2011. http://alignment.hep.brandeis.edu/Lab/Measurement.html.

[86] Engineering statistics hand book . Technical report, visited July 2011. http://www.itl.nist.gov/div898/handbook/index.htm.

Appendix A

Experiments carried out for varying specimen speeds with the probe held stationary

A.1 Introduction

In this section, an analysis of the effects of the moving body on the received pickup coil signal in a pulsed eddy current (PEC) system is carried out. A literature review on the subject of motion and eddy currents is given. Experiments were setup to give results from a pickup coil of stationary probe supplied by a specified voltage source at a specified frequency, on a specimen that was moving at different speeds. Two source amplitudes and two source frequencies are investigated. An analysis of results is made and a conclusion is given.

A.2 Eddy currents in moving media

The majority of eddy current applications involve moving media. Eddy currents can be induced in a conducting medium due to relative motion between the magnetic field lines and the medium or due to time varying magnetic fields.

In the rolling mill application, it was important to understand and separate the eddy currents induced due to relative motion between the probe and the medium and those induced due to a time varying magnetic field in order to manipulate effects due to relative motion in the received PEC system signal. The electromotive force (emf) E_s induced in the medium has two terms; that due to relative motion and that due to time varying magnetic fields. These are expressed in equation A.1.

$$E_s(t) = -A_s cos\theta \frac{dB_x(t)}{dt} + \mu v L B_x \tag{A.1}$$

The two mechanisms of induction are summarized as:

- Eddy currents induced by time-varying excitation and represented by the term $\frac{\partial H}{\partial t}$ or $\frac{\partial B}{\partial t}$
- Eddy currents induced by motion and represented by the term $curl(v \times H)$ or $curl(v \times B)$

Under certain conditions, one of the mechanisms prevails over the other. Moon [76] uses a magnetic Reynolds number R_m to evaluate the type of eddy currents that dominate (see equation A.2)

$$R_m = \sigma \mu L v \tag{A.2}$$

where L is the characteristic length of the body in contact with the magnetic field lines, σ and μ are the conductivity and the permeability of the body and v is the relative velocity between the body and the field. If R_m is small the eddy currents induced by time-varying excitation prevails while for large values of R_m, the effects of motion dominate. When R_m is of the order unity neither of the two effects can be ignored [76]. To verify the effects of motion on the signal received from the PEC system, experiments were conducted.

A.3 Experiments and Results

The setup in figure 5.1 was used with a specimen having a length of 1000 mm, a width of 250 mm and a thickness of 3 mm. The probe dimensions are summarized in the table below.

Table A.1: Measured values and calculated values for the reflection probe used in this study

	Drive coil	Pickup coil
Wire diameter (mm)	0.18	0.18
Inner radius (mm)	6.35	4.25
Outer radius (mm)	8.75	6.35
Resistance (Ω)	17.6	10.9
Inductance (mH)	1.56	0.53
Coil length (mm)	9	9
Lift-off (mm)	1	1
Wire length (m)	25	15
Number of turns	530	464

The whole setup was modelled as three networks that interact with each other obeying the laws of electromagnetism (see figure 3.3). The aim of the experiment was to compare signals received at the pickup coil network output resistance R_{out} when the specimen speed is varied while the probe is kept stationary. To begin with, voltage readings were recorded across the pickup coil circuit output resistance R_{out} with the coil and the specimen kept stationary. Then observations were made on the same signal with the specimen moving at speeds between 0 mm and 150 mm per second. The probe placed above the specimen was held stationary at the built-in lift-off thickness of 1 mm. The signal from the pickup circuit for each speed was recorded and stored for further processing. Figures A.1, A.2 and A.3 show graphical results of the experiments under varied conditions as explained for each figure.

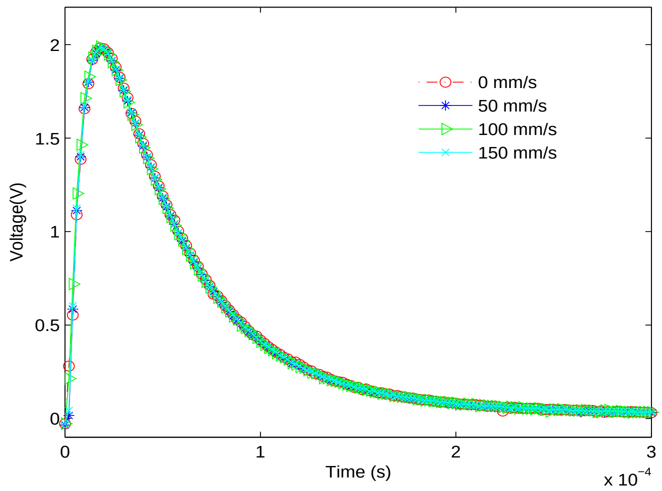

Figure A.1: Pickup signals recorded for varying specimen speed below a stationary probe supplied by a 20 volt peak to peak source at 1 kHz.

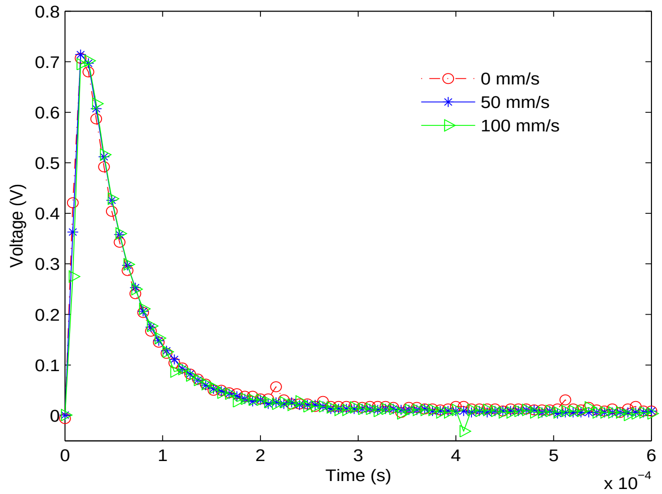

Figure A.2: Pickup signals recorded for varying specimen speed below a stationary probe supplied by a 10 volt peak to peak source at 100 Hz.

A.4 Analysis

The magnetic Reynolds number R_m [76] is used to evaluate the type of eddy currents that should dominate (see equation A.1). The characteristic length L of the specimen in contact with the primary field is the same as the inner radius of the drive coil and is 6.35 mm (see table A.1) and the maximum velocity of

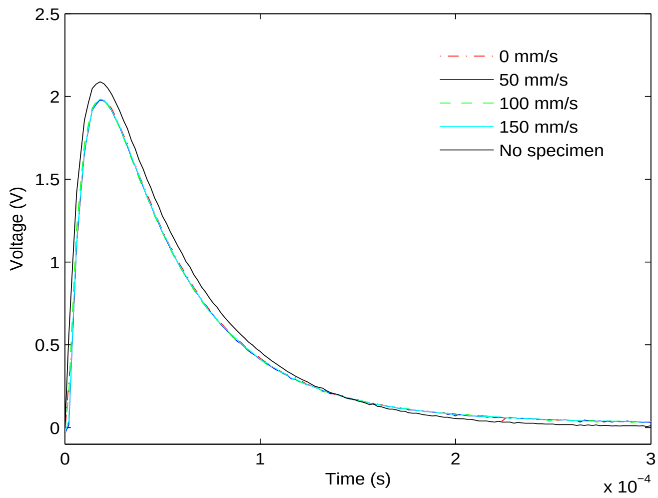

Figure A.3: Pickup signals recorded for varying specimen speed below a stationary probe supplied by a 20 volt peak to peak source at 1 kHz together with that received from the probe with no specimen present.

the tested specimen is 1.6 m/s (section 1.1). R_m for an aluminium specimen with a resistivity and a permeability of 18.8×10^{-9} and 4×10^{-7} is of the order 10^{-2}. This value is much smaller than unity. The eddy currents induced by time-varying excitation should prevail over those induced by motion. The experimental result agree with predictions made using the magnetic Reynolds number.

A.5 Conclusion

Results agreed with the prediction that there should be non or minimal effects on the received signal due to specimen movement. It is concluded at this point that the eddy currents induced in the specimen are predominantly due to the time varying magnetic flux and not due to the relative speed between the specimen and the probe. A quasi-static approximation was assumed for the model.

Appendix B

The factor k_f

B.1 Introduction

To predict the number of turns in the drive coil and the pickup coil was part of the development of the PEC system model presented in chapter 3 of this report. It was observed that the number of conductors that fitted in the solenoid cross-sectional area constituted the number of turns that made up the solenoid winding. However, the conductor had a circular cross-sectional area and there was part of the solenoid cross sectional area that could not be occupied by the conductors. A factor k_f was used to account for this phenomenon. It was estimated by taking the ratio of the turn value determined at the time of winding $N_{det.}$ to the calculated turn value $N_{cal.}$, to determine the actual number of turns (equation B.1).

$$K_f = \frac{N_{det.}}{N_{cal.}} \tag{B.1}$$

A study was setup to investigate the effect of wire diameters on the said factor. A range of values were determined for wire sizes ranging from diameter d of 0.35 mm to 1.5 mm fitted in a similar circular cross sectional area.

B.2 Experiments and results

In order to estimated the number of turns that occupy a given area, an investigation that involved the study of various cylindrical wire sizes fitted in a cylindrical volume with a diameter of 6 mm was carried out. The cross-sectional area, A, of the cylindrical volume was 28.27 mm^2.

The factor was determined as the ratio of the number of wires with a cross sectional area a that fitted practically N_{det} to that which was calculated to fit N_{cal} (equation B.1). The value for the number of wires that would fill the volume cross-sectional area was calculated with the assumption that the sum of cross-sectional areas of the wires covers the cross-sectional area of the volume. Equations B.2 gives the value of the calculated number of wires N_{cal} that would fit.

When determining the number of wires that would fit practically in the same area, care had to be taken to pack the cylindrical volume as tightly as possible. Loosely packing the volume resulted in a lower number of wires that practically fitted the area.

The value of the factor k_f was determined using equation B.1 (see table B.1).

$$N_{cal1} = \frac{A}{a_1} \tag{B.2}$$

Table B.1: Results for the factor k_f observed for different wire diameters

Wire diameter d (mm)	Wire X-sectional area, a (mm^2)	(N_{det})	(N_{cal})	Factor k_f
1.5	1.76	10	16	0.625
0.85	0.567	35	50	0.702
0.5	0.196	105	144	0.729
0.35	10.096	226	294	0.769

B.3 Conclusion

Practical results show that the calculated value of the number of wires expected in an area is always greater than that which fits practically. The factor k_f is a fraction used to correct this difference. This factor increases in value as the wire size decreases. The thinner the wire that forms the winding, the higher the factor. However, the looseness with which the cylindrical area was packed resulted in the reduction of the number of wires that were packed in the circular area. k_f was used as a fitting factor in the PEC system environment to make an initial fit of experimental data and simulated data for a probe in the absence of a specimen (see chapter 5). Subsequent simulations for the same probe were carried out, in this study of the PEC system, with the same value of k_f.

Appendix C

Matlab and Simulink simulation environment

C.1 Introduction

The mathematical expressions developed for the pulsed eddy current system in chapter 3 of this report were converted into an interactive model using Matlab and Simulink [77, 78, 79]. In this appendix, example combinations of blocks used in the development of the simulation environment are presented. Figures C.1 to C.6 show the blocks in decreasing hierarchy of the various subsystems of the environment. Transfer functions, differential blocks, gain blocks addition and subtraction blocks together with primary and secondary souces were interconnected to make possible the simulation environment

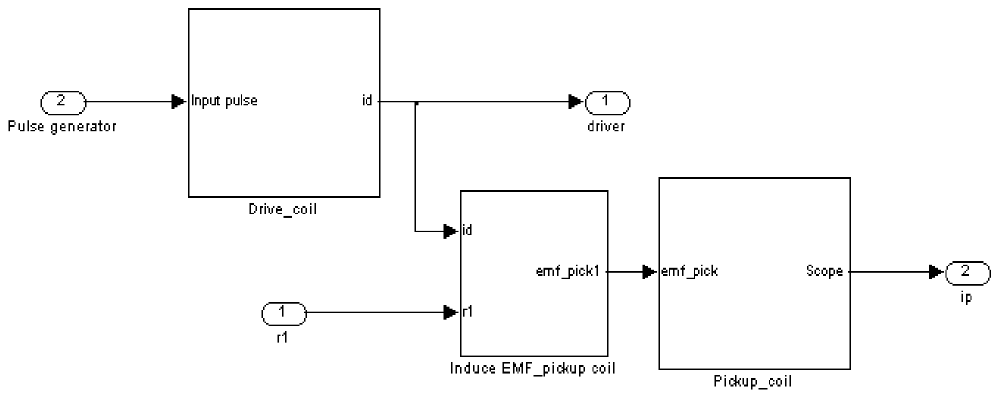

Figure C.1: Blocks representing the probe without any specimen effects.

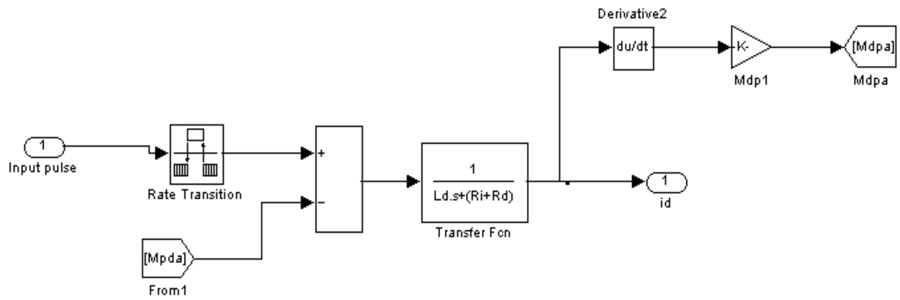

Figure C.2: Blocks representing the drive coil network.

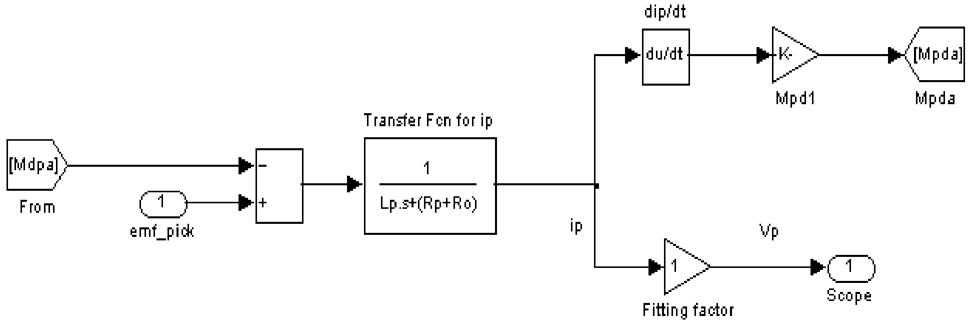

Figure C.3: Blocks representing liftoff and wobble.

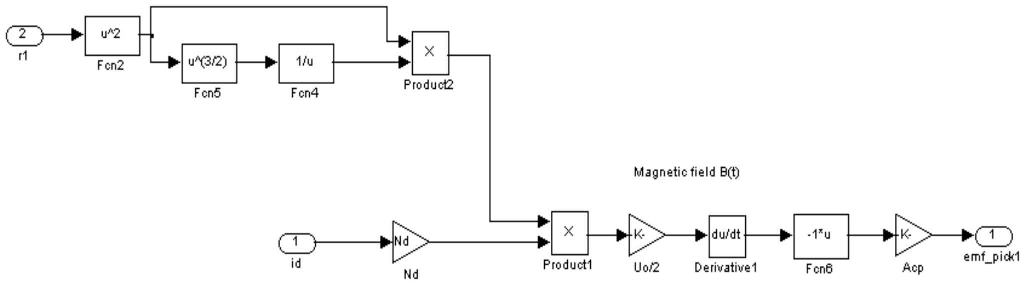

Figure C.4: Blocks representing the pickup coil induced electromotive force.

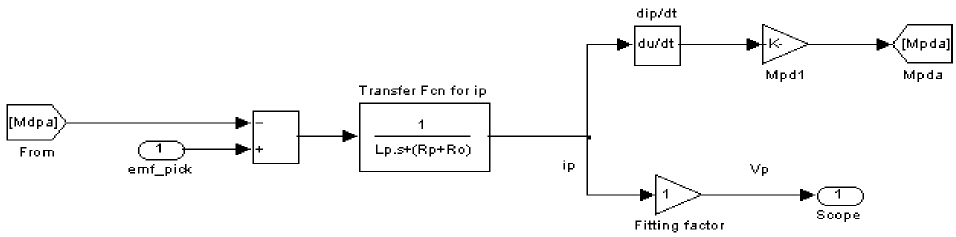

Figure C.5: Blocks representing the pickup coil network

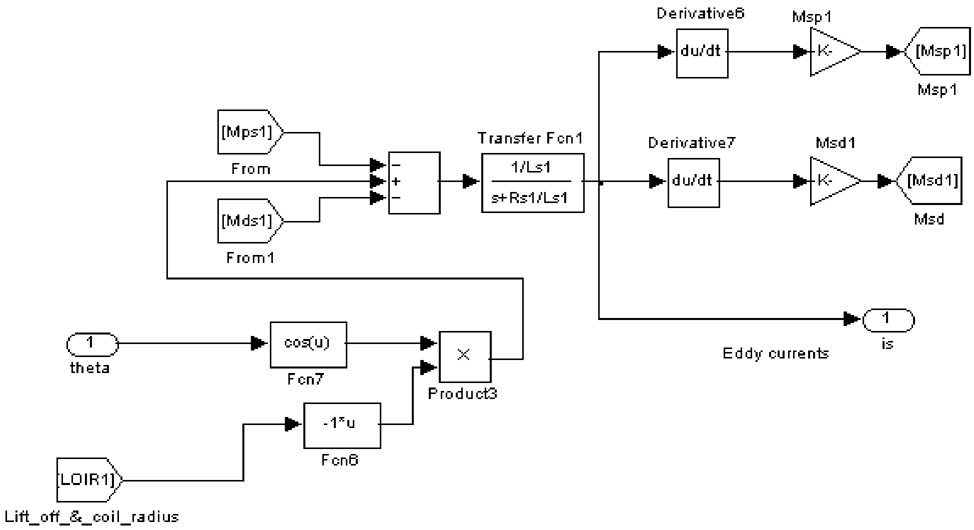

Figure C.6: Blocks representing the specimen network.

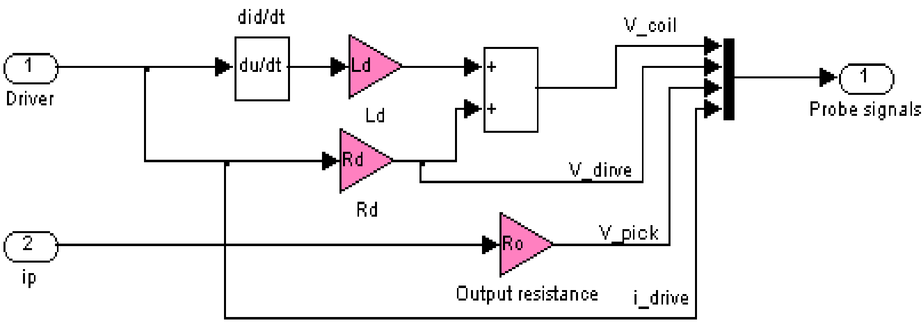

Figure C.7: Blocks representing the probe signals.

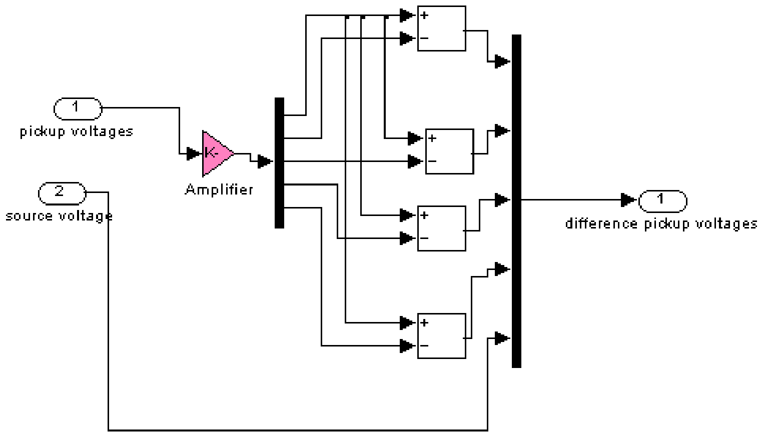

Figure C.8: Blocks representing the beginning of signal processing. The time of crossing is observed from the section.

Varying the parameters in the model resulted in the possibility of simulating various scenarios of the investigated PEC system.

C.2 Matlab m-file program listing

The parameters used by the simulation environment described in section C.1 were provided by the Matlab m-file listing given below. The % symbol is used before a brief explanation for each parameter. The values of the parameters are picked up by the Simulink model from the work space and the results from the model are saved in the Matlab workspace for further processing. Four specimens at a time were used in the simulations.

% solenoid parameters(dimensions in m)
ldg=9.5e-3; %solenoid length for the drive coil
lpg=9.5e-3; %solenoid length for the pickup coil
r1=6.35e-3; %innner radius drive coil
r3=4.25e-3; %innner radius pickup coil
r2=8.75e-3; %outer radius drive coil

```
r4=6.35e-3; %outer radius pickup coil
%outer radius pick coil
d=0.18e-3;%wire diameter
%increasing kf increases time constant but decreases amplitude of the
%pickup signal
kfd=0.785; %fill factor drive coil
kfp=0.791; %fill factor pickup coil
Pdp=17.2e-9%resistivity of copper(solenoid wire)
alpha1=4.3e-3 % temperature coefficient of copper
T=25 %Coil temperature
Pd=Pdp*(1+alpha1*(T-20)); %resistivity of copper(solenoid wire)
Pp=Pdp*(1+alpha1*(T-20)); %resistivity of copper(solenoid wire)
Pos=26.5e-9; %resistivity of Aluminium specimen
Uo=pi*4e-7; %free space permeability.
Us=Uo%specimen permeability.
Ud=Uo%drive coil permeability.
Up=Uo%pickup coil permeability.
%varied Specimen thickness
y1=1e-3;
y2=2e-3;
y3=3e-3;
y4=4e-3;


%lift-off
x=1e-3;
x1=1e-3;
x2=1e-3;
x3=1e-3;
ad=pi*(d2̂)/4;%cross-sectional area of solenoid wire
ap=ad
ad1=pi*((d+.02e-3)2̂)/4;%cross-sectional area of solenoid wire %with insulation included.
ap1=ad1
Ad=ldg*(r2-r1); %cross-sectional area of solenoid coil-drive.
Ap=lpg*(r4-r3); %cross-sectional area of solenoid coil-pickup.
```

```
Aed=(r2-r1)*y1; %cross sectional area cut by eddy currents
Acd=pi*r12̂; %cross sectional area of core material (drive coil).
Acs=pi*r12̂; %area cut by primary magnetic field in specimen.
Acp=pi*r32̂; %cross sectional area of core material (pickup coil).

r0=(r1*r2)0̂.5; %Geometric mean radius of eddy current ring
led= 2*pi*r0; %eddy current path length

Nd=kfd*ldg*(r2-r1)/ad1 %Number of solenoid turns-drive coil
Np=kfp*lpg*(r4-r3)/ap1 %Number of solenoid turns-pickup coil
ld=Nd*pi*(r1+r2) %length of solenoid wire drive coil.
lp=Np*pi*(r3+r4) %length of solenoid wire pickup coil.
Pos=26.5e-9;%specimen resistivity(aluminium) at 20 degrees centigrade. alpha=4.2e-
3;%Temperature coefficient of aluminium.
%specimen temperature in degrees celcius
T1=100
T2=100
T3=100
T4=100

%duty cycle
fs=1000 %Hz
Ts=1/fs %seconds
t=Ts/2
%specimen resistivity at temperature T
Ps4=Pos*(1+alpha*(T4-20))
Ps1=Pos*(1+alpha*(T1-20))
Ps2=Pos*(1+alpha*(T2-20))
Ps3=Pos*(1+alpha*(T3-20))

%Skin depth
delta1=sqrt((Ps1*4*t)/Us)
```

```
delta2=((Ps2*4*t)/Us)0̂.5
delta3=sqrt((Ps3*4*t)/Us)
delta4=sqrt((4*t*Ps4)/Us)
%resistance
Rd=Pd*ld/ad %Drive coil
Rp=Pp*lp/ap %Pickup coil
% specimen eddy current ring
Rs4=Ps4*led/(delta4*(exp(y4/delta4)-1)*r0*log(r2/r1))
Rs1=Ps1*led/(delta1*(exp(y1/delta1)-1)*r0*log(r2/r1))
Rs2=Ps2*led/(delta2*(exp(y2/delta2)-1)*r0*log(r2/r1))
Rs3=Ps3*led/(delta3*(exp(y3/delta3)-1)*r0*log(r2/r1))
%inductances
Ld=1*(Uo*Nd2̂*pi*r12̂)/(2*(ldg+(r2-r1)))
Lp=1*(Uo*Np2̂*pi*r32̂)/(2*(ldg+(r4-r3)))
Ls1=1*Us*pi*r12̂/((delta1*(exp(y1/delta1)-1)+(r0*log(r2/r1))))
Ls2=1*Us*pi*r12̂/((delta2*(exp(y2/delta2)-1)+(r0*log(r2/r1))))
Ls3=1*Us*pi*r12̂/((delta3*(exp(y3/delta3)-1)+(r0*log(r2/r1))))
Ls4=1*Us*(pi*r12̂)/((delta4*(exp(y4/delta4)-1)+(r0*log(r2/r1))))
%Capacitance
Cd=1.2e-14;
Cp=1.2e-14;
%Mutual inductances
%Increasing Kds increases amplitude while
%increasing Kps decreases amplitude
Kds=0.155;
Kps=0.095;


%Increasing Kdp increases amplitude and increases time constant
Kdp=0.69;
%Mutual inductances
Mds1=Kds*(Ls1*Ld)0̂.5;
Msd1=Mds1;
Mds2=Kds*(Ls2*Ld)0̂.5;
Msd2=Mds2;
Mds3=Kds*(Ls3*Ld)0̂.5;
```

```
Msd3=Mds3;
Mds4=Kds*(Ls4*Ld)0̂.5;
Msd4=Mds4;
Mps1=Kps*(Ls1*Lp)0̂.5;
Msp1=Mps1;
Mps2=Kps*(Ls2*Lp)0̂.5;
Msp2=Mps2;
Mps3=Kps*(Ls3*Lp)0̂.5;
Msp3=Mps3;
Mps4=Kps*(Ls4*Lp)0̂.5;
Msp4=Mps4; Mdp1=Kdp*(Ld*Lp)0̂.5;
Mpd1=Mdp1;
Mdp2=Mdp1;
Mpd2=Mdp2;
Mdp3=Mdp1;
Mpd3=Mdp3;
Mdp4=Mdp1;
Mpd4=Mdp4;
Mds4=Kds*(Ls4*Ld)0̂.5;
Msd4=Mds4;
Mps4=Kps*(Ls4*Lp)0̂.5;
Msp4=Mps4;
Mdp4=Mdp1;
Mpd4=Mdp4;
%external resistance values
Ro=14.7 %pickup coil output resistance
Rdo=0 % drive coil added resistance
Ri=50 % internal resistance of source generator


%wabble
theta=0;
% TIME CONTANTS
Td= Ld/Rd % drive coil
Tp=Lp/Rp % pickup coil
%specimen time constants
```

Ts4=Ls4/Rs4

Ts1=Ls1/Rs1

Ts2=Ls2/Rs2

Ts3=Ls3/Rs3